

# Hadronic structure on the light-front VIII. Light scalar and vector mesons

Wei-Yang Liu,<sup>\*</sup> Edward Shuryak,<sup>†</sup> and Ismail Zahed<sup>‡</sup>  
*Center for Nuclear Theory, Department of Physics and Astronomy,  
Stony Brook University, Stony Brook, New York 11794-3800, USA*

We use the QCD instanton vacuum model to discuss the emergence of the light scalar and vector mesons on the light front. We take into account both the instanton and anti-instanton single and molecular interactions on the light quarks, in the form of non-local effective interactions. Although the molecular induced interactions are suppressed by a power of the packing fraction, they are still sufficient to bind the vector mesons, while keeping most of the scalar spectrum relatively unchanged. We explicitly derive the light front distribution amplitudes (DAs) and partonic functions (PDFs) for the scalar and vector mesons, and compare them after pertinent QCD evolution, to the available empirical and lattice measured counterparts. The Dirac electric form factors for both the pion and rho meson are derived, and shown to compare well with current data.

## I. INTRODUCTION

Parton distribution functions (PDFs) are used to assess most processes at high energy, whenever factorisation holds. They are important for the description of inclusive and exclusive processes alike, and play an essential role in precision measurements at the current Large Hadron Collider (LHC).

The PDFs capture the longitudinal distribution of partons (quarks and gluons) in a given hadron in the light front frame, at a given resolution. These uni-modular distributions are inherently non-perturbative and light-like. The leading twist PDFs are currently accessible from experiments through pertinent parametrizations [1], or using lattice simulations following the LaMET procedure [2, 3] or some variations [4, 5].

The determination of the PDFs whether empirically or through numerical simulations, does not provide a comprehensive understanding of their content for physicists, nor on the basic mechanism(s) at the origin of their composition. For that, an understanding of the QCD vacuum at some preferably low resolution is required.

At low resolution, detailed cooled lattice configurations show that the QCD vacuum is populated by instantons and anti-instantons [6]. Their effects in the formation of both the scalar and vector mesons on the light front, will be the main subject of this paper. Some essential aspects of this vacuum, are cap-

tured by the instanton vacuum model, which allows for a semi-classical description based on a drastically reduced set of gauge configurations [7–11].

However, the QCD instanton vacuum is inherently space-like, and is more naturally formulated in Euclidean space. In a recent series of work [12–16], two of us have shown that some of the non-perturbative aspects of the QCD instanton vacuum, can be exported to the light front via an analytical continuation not in the fields but in the boost parameter. The results are a variety of central and spin dependent potentials on the light front, that provide for the emergence of a non-perturbative constituent quark type model. Similar approaches more rooted in phenomenology, have been also suggested in [5, 17–37].

On the light front, hadrons at low resolution are described by their lowest constituent quark and gluon Fock components. The underlying non-perturbative gluonic content is mostly packaged in the emerging constituent mass and effective interactions between the constituents, following mostly from the spontaneous breaking of chiral symmetry [12–16]. However, the description of the emerging Goldstone modes (pions and kaons) requires special care on the light front, but otherwise parallels the description in the rest frame [13, 38].

Another important subtlety of the light front formulation is the apparent breaking of  $SO(1,3)$  to  $SO(1,2)$ , following from the use of the infinite momentum frame. We will address this issue analysing the formation of the low-lying vector mesons in the QCD instanton vacuum. On the light front, the longitudinal and transverse vector mesons follow from different constitutive equations, with apparently different characteristics. The purpose of this work is

<sup>\*</sup> wei-yang.liu@stonybrook.edu

<sup>†</sup> edward.shuryak@stonybrook.edu

<sup>‡</sup> ismail.zahed@stonybrook.edu

two-fold: first, we will follow up on our suggestion in [12], that the light vector mesons in the QCD instanton vacuum receive sizable contributions from the instanton-anti-instanton molecular configurations; second we will explicitly show that despite the explicit breaking of Lorentz symmetry on the light front, the rest frame  $SO(1,3)$  symmetric vector spectra and decay constants are recovered dynamically. For completeness, we note that a number of phenomenological studies of the light mesons, have been carried by many using the covariant formulation in [39–44], relativistic equal-time formulation in [45–48], and variants of the light cone formulation in [36, 49–53].

The organization of the paper is as follows. In section II we briefly review the emergent 't Hooft non-local fermionic interactions in the two-flavor QCD instanton vacuum, induced by both the single instantons and anti-instantons, and the instanton-anti-instanton molecules. The latters are chirality preserving and contribute in leading order in the vector channels. In section III we show how these emerging interactions yield to the spontaneous breaking of chiral symmetry, and a running constituent quark mass. In section IV we construct the pertinent light front Hamiltonian using the book-keeping in  $1/N_c$  and the diluteness of the QCD instanton vacuum. The bound states equations in the scalar and vector channels are made explicit, and solved. We also show how these solutions are related to covariant formulations. In section V, all scalar and vector light front wavefunctions in the QCD instanton vacuum with non-local interactions are detailed. In section VI we derive the parton distribution functions for the scalar and vector mesons, and analyze their partonic content both for the unpolarized and polarized states. In section VII the meson distribution amplitudes are dis-

cussed, and the results compared to existing empirical measurements, and current lattice simulations. In section VIII we use the light front wavefunctions, to derive the electromagnetic form factors for the pion and rho and omega mesons. The results are compared to the available measurements and lattice results. Our conclusions are in section IX. A number of Appendices are included to complement some of the derivations.

## II. GENERALIZED 'T HOOFT INDUCED INTERACTIONS

The QCD vacuum at low resolution, is populated by mostly topologically active instantons and anti-instantons, Euclidean tunneling configurations between vacua with different topological charges [11] (and references therein). Light quarks scattering through these topological configurations develop zero modes with fixed handedness. For instance, a massless left handed quark going tunneling through an instanton, can emerge as a right-handed massless quark, with the handedness flipped through an anti-instanton.

For a single quark species, this mechanism is at the origin of the explicit breaking of  $U_A(1)$  symmetry. For many light quark species this mechanism can account for the dual breaking of the  $U_A(1)$  (explicitly) and chiral symmetry (spontaneously). This is manifested through the emergent multi-flavored interactions, between the light quarks zero modes.

### A. Local approximation

In the non-interacting instanton vacuum, these multi-flavored interactions are the well-known 't Hooft determinantal interactions. In the local approximation where the instanton size is taking to zero, the induced interactions from single instantons plus anti-instantons give

$$\mathcal{L}_I = \frac{G_I}{8(N_c^2 - 1)} \left\{ \frac{2N_c - 1}{2N_c} [(\bar{\psi}\psi)^2 - (\bar{\psi}\tau^a\psi)^2 - (\bar{\psi}i\gamma^5\psi)^2 + (\bar{\psi}i\gamma^5\tau^a\psi)^2] + \frac{1}{4N_c} [(\bar{\psi}\sigma_{\mu\nu}\psi)^2 - (\bar{\psi}\sigma_{\mu\nu}\tau^a\psi)^2] \right\} \quad (1)$$

which are seen to mix  $LR$  chiralities. The effective coupling

$$G_I = \int d\rho n(\rho) \rho^{N_f} (2\pi\rho)^{2N_f} = \frac{n_{I+\bar{I}}}{2} (4\pi^2\rho^3)^{N_f} \left( \frac{1}{m^*\rho} \right)^{N_f} \quad (2)$$

is fixed by the mean-instanton density

$$\frac{n_{I+\bar{I}}}{2} = \int d\rho n(\rho) \prod_{f=1}^{N_f} (m_f^*\rho) \quad (3)$$

with  $m_f^*$  the induced determinantal mass [54]. At low resolution, the instanton distribution is sharply peaked around the average instanton size  $\rho \approx 0.31$  fm, with a mean density  $n_{I+\bar{I}} \sim 1 \text{ fm}^{-4}$ .

In the interacting instanton vacuum, additional multi-flavor interactions are expected. Given the

diluteness of the tunneling processes in the QCD vacuum at low resolution, the natural interactions are molecular in the form of binary instanton-anti-instanton configurations. When maximally locked in color, they induce flavor mixing interactions of the form [55]

$$\begin{aligned} \mathcal{L}_{I\bar{I}} = G_{I\bar{I}} & \left\{ \frac{1}{N_c(N_c - 1)} [(\bar{\psi}\gamma^\mu\psi)^2 + (\bar{\psi}\gamma^\mu\gamma^5\psi)^2] - \frac{N_c - 2}{N_c(N_c^2 - 1)} [(\bar{\psi}\gamma^\mu\psi)^2 - (\bar{\psi}\gamma^\mu\gamma^5\psi)^2] \right. \\ & + \frac{2N_c - 1}{N_c(N_c^2 - 1)} [(\bar{\psi}\psi)^2 + (\bar{\psi}\tau^a\psi)^2 + (\bar{\psi}i\gamma^5\psi)^2 + (\bar{\psi}i\gamma^5\tau^a\psi)^2] \\ & \left. - \frac{1}{2N_c(N_c - 1)} [(\bar{\psi}\gamma^\mu\psi)^2 + (\bar{\psi}\tau^a\gamma^\mu\psi)^2 + (\bar{\psi}\gamma^\mu\gamma^5\psi)^2 + (\bar{\psi}\tau^a\gamma^\mu\gamma^5\psi)^2] \right\} \end{aligned} \quad (4)$$

which are  $LL$  and  $RR$  chirality preserving, in contrast to (1). The effective molecule-induced coupling is defined as

$$G_{I\bar{I}} = \int d\rho_I d\rho_{\bar{I}} \int dud^4R \frac{1}{8T_{I\bar{I}}^2} (4\pi^2\rho_I^2)(4\pi^2\rho_{\bar{I}}^2)n(\rho_I)n(\rho_{\bar{I}})T_{I\bar{I}}(u, R)^{2N_f}\rho_I^{N_f}\rho_{\bar{I}}^{N_f} \quad (5)$$

Here  $R = z_I - z_{\bar{I}}$  is the relative molecular separation,  $u_\mu = \frac{1}{2i}\text{tr}(U_{\bar{I}}\tau_\mu^+U_I^\dagger)$  is the relative molecular orientation with the locked color with  $\tau_\mu^+ = (\vec{\tau}, -i)$ , and  $T_{I\bar{I}}$  is the hopping quark matrix. (5) is readily understood as the unquenched tunneling density for a molecular configuration, whereby a pair of quark lines is removed by the division  $T_{I\bar{I}}^2$  to account for the induced 4-Fermi interaction. The strength of the induced molecular coupling  $G_{I\bar{I}}$  to the single coupling  $G_I$  is

$$G_{I\bar{I}} = \frac{G_I^2}{128\pi^4\rho^2}\xi \quad (6)$$

where the dimensionless and positive hopping pa-

rameter is defined as

$$\xi = \frac{1}{\rho^4} \int dud^4R [\rho T_{I\bar{I}}(u, R)]^{2N_f-2} \quad (7)$$

In summary, we will use the effective action

$$\mathcal{L} = \bar{\psi}(i\cancel{D} - m)\psi + \mathcal{L}_I + \mathcal{L}_{I\bar{I}} \quad (8)$$

to describe light quark interactions in the QCD vacuum at low resolution. The smallness of the density  $n_{I+\bar{I}}$  allows us to consider the complex many-body dynamics, by organizing it around the dilute limit. Throughout, we will use the  $1/N_c$  counting for book-keeping, with  $n_{I+\bar{I}} \sim N_c$  and both  $G_I$  and  $G_{I,\bar{I}}$  of the same order in  $1/N_c$ , but with a parametrically small ratio  $G_{I\bar{I}}/G_I$  from the diluteness. With this in mind, the leading contributions in  $1/N_c$  in (8) are

$$\begin{aligned} \mathcal{L}_I &= \frac{G_I}{8N_c^2} [(\bar{\psi}\psi)^2 - (\bar{\psi}\tau^a\psi)^2 - (\bar{\psi}i\gamma^5\psi)^2 + (\bar{\psi}i\gamma^5\tau^a\psi)^2] \\ \mathcal{L}_{I\bar{I}} &= \frac{G_{I\bar{I}}}{2N_c^2} \left[ 4 [(\bar{\psi}\psi)^2 + (\bar{\psi}\tau^a\psi)^2 + (\bar{\psi}i\gamma^5\psi)^2 + (\bar{\psi}i\gamma^5\tau^a\psi)^2] \right. \\ & \quad \left. - [(\bar{\psi}\gamma^\mu\psi)^2 + (\bar{\psi}\tau^a\gamma^\mu\psi)^2 - 3(\bar{\psi}\gamma^\mu\gamma^5\psi)^2 + (\bar{\psi}\tau^a\gamma^\mu\gamma^5\psi)^2] \right] \end{aligned} \quad (9)$$

The induced 't Hooft interaction  $\mathcal{L}_I$  does not op-

erate in the light vector channels, but the molec-

ular induced interaction  $\mathcal{L}_{II}$  does. The molecular interaction is equally attractive in the scalar  $\sigma, a_0$  and pseudoscalar  $\pi, \eta'$  channels. Since the instanton molecules are topologically neutral, the molecular

interaction are  $U(1)_A$  symmetric. Note that this Lagrangian predicts no splitting between the isoscalar ( $\omega$ ) and isovector ( $\rho$ ) vector channels.

For later use, we rewrite (8) in leading order in  $1/N_c$  as

$$\begin{aligned} \mathcal{L} = & \bar{\psi}(i\partial - M)\psi + \frac{G_\sigma}{2}(\bar{\psi}\psi)^2 + \frac{G_{a_0}}{2}(\bar{\psi}\tau^a\psi)^2 + \frac{G_{\eta'}}{2}(\bar{\psi}i\gamma^5\psi)^2 + \frac{G_\pi}{2}(\bar{\psi}i\gamma^5\tau^a\psi)^2 \\ & - \frac{G_\omega}{2}(\bar{\psi}\gamma_\mu\psi)^2 - \frac{G_\rho}{2}(\bar{\psi}\gamma_\mu\tau^a\psi)^2 - \frac{G_{f_1}}{2}(\bar{\psi}\gamma_\mu\gamma^5\psi)^2 - \frac{G_{a_1}}{2}(\bar{\psi}\gamma_\mu\gamma^5\tau^a\psi)^2 \end{aligned} \quad (10)$$

with the effective couplings

$$\begin{array}{llll} G_\sigma = G_S & G_{a_0} = -G_S + 8G_V & G_\pi = G_S & G_{\eta'} = -G_S + 8G_V \\ G_\omega = G_V & G_\rho = G_V & G_{a_1} = G_V & G_{f_1} = -3G_V \end{array}$$

where  $G_S = \frac{G_I}{4N_c^2} + \frac{4G_{II}}{N_c^2}$  and  $G_V = \frac{G_{II}}{N_c^2}$  from the QCD instanton vacuum.

### B. Non-local approximation

Each instanton and anti-instanton configuration carries a finite size, which is fixed on average to be around  $\frac{1}{3}$  fm. This size is not small in comparison to the size of the light hadrons and cannot be ignored. More importantly, this size fixes the UV scale and provides for a natural cut-off both in Euclidean or light front signature. Finite size instantons yield finite size zero modes, and therefore non-local effective interactions between the light quarks. The net

effect is captured by the substitution

$$\psi(x) \rightarrow \sqrt{\mathcal{F}(i\partial)}\psi(x) \quad (11)$$

in the local approximation. Here  $\mathcal{F}(i\partial)$  is the zero mode profile, that acts as a form factor. In singular gauge its form is more user friendly in momentum space

$$\mathcal{F}(k) = \left[ (zF'(z))^2 \right] \Big|_{z=\frac{k\rho}{2}} \quad (12)$$

where  $F(z) = I_0(z)K_0(z) - I_1(z)K_1(z)$  are spherical Bessel functions, and  $k = \sqrt{k^2}$  is the Euclidean 4-momentum. Inserting (11) into (8) yields the non-local form of the effective action in the QCD instanton vacuum in leading order in  $1/N_c$

$$\begin{aligned} \mathcal{L} = & \bar{\psi}[i\partial - M(k)]\psi + \frac{G_S}{2}(\bar{\psi}\sqrt{\mathcal{F}(i\partial)}\sqrt{\mathcal{F}(i\partial)}\psi)^2 - \frac{G_S}{2}(\bar{\psi}\sqrt{\mathcal{F}(i\partial)}\tau^a\sqrt{\mathcal{F}(i\partial)}\psi)^2 \\ & - \frac{G_S}{2}(\bar{\psi}\sqrt{\mathcal{F}(i\partial)}i\gamma^5\sqrt{\mathcal{F}(i\partial)}\psi)^2 + \frac{G_S}{2}(\bar{\psi}\sqrt{\mathcal{F}(i\partial)}i\gamma^5\tau^a\sqrt{\mathcal{F}(i\partial)}\psi)^2 - \frac{G_V}{2}(\bar{\psi}\sqrt{\mathcal{F}(i\partial)}\gamma_\mu\sqrt{\mathcal{F}(i\partial)}\psi)^2 \\ & - \frac{G_V}{2}(\bar{\psi}\sqrt{\mathcal{F}(i\partial)}\gamma_\mu\tau^a\sqrt{\mathcal{F}(i\partial)}\psi)^2 + \frac{3G_V}{2}(\bar{\psi}\sqrt{\mathcal{F}(i\partial)}\gamma_\mu\gamma^5\sqrt{\mathcal{F}(i\partial)}\psi)^2 - \frac{G_V}{2}(\bar{\psi}\sqrt{\mathcal{F}(i\partial)}\gamma_\mu\gamma^5\tau^a\sqrt{\mathcal{F}(i\partial)}\psi)^2 \end{aligned} \quad (13)$$

### III. GAP EQUATION IN QCD INSTANTON VACUUM

Before analysing (13) in the light front frame, we briefly discuss the bulk vacuum properties following from (13) in the center of mass frame. In leading

order in  $1/N_c$  or mean-field approximation, the light quarks develop a running constituent mass

$$M(k) = m + 2g_S\mathcal{F}(k) \int \frac{d^4q}{(2\pi)^4} \frac{4M(q)}{q^2 + M^2(q)} \mathcal{F}(q) \quad (14)$$

where  $g_S = N_c G_S$  is the coupling strength for the isosinglet scalar channel in 't-Hooft Lagrangian. In

the same approximation, the chiral quark condensate is

$$\langle \bar{\psi}\psi \rangle = - \int \frac{d^4 k}{(2\pi)^4} \text{Tr} S(k) = -2N_c \int \frac{d^4 k}{(2\pi)^4} \frac{4M(k)}{k^2 + M^2(k)} \mathcal{F}(k) \quad (15)$$

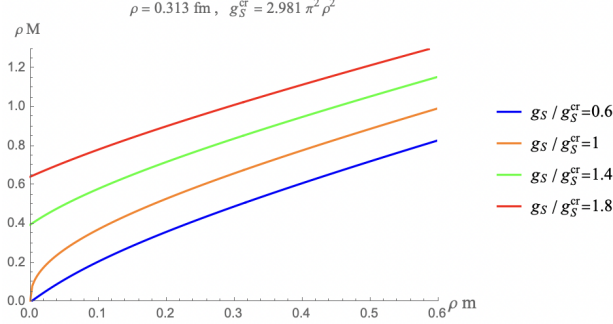


FIG. 1: Constituent mass as a function of the current mass with different scalar couplings  $g_S$ , for a fixed instanton size  $\rho = 0.31$  fm.

In the low momentum limit ( $k \ll 1/\rho$ ),  $M(k) \sim M\mathcal{F}(k)$  with  $M$  the zero-momentum constituent mass, (14) and (15) simplify

$$\frac{m}{M} = 1 - 8g_S \int \frac{d^4 k}{(2\pi)^4} \frac{\mathcal{F}^2(k)}{k^2 + M^2} \quad (16)$$

with  $M = m - G_S \langle \bar{\psi}\psi \rangle$ . We have approximated the running quark mass  $M(k)$  in the loop integration in both (14) and (15), by its zero momentum limit. This is numerically justified by the cut-off form factor  $\mathcal{F}(k)$  with a range of about the inverse instanton size  $1/\rho$ .

More explicitly,

$$\frac{m}{M} = 1 - \frac{4g_S}{\pi^2 \rho^2} \int_0^\infty dz \frac{z^3}{z^2 + \frac{\rho^2 M^2}{4}} (zF'(z))^4 \quad (17)$$

with  $M$  fixed by the scalar 't Hooft coupling strength  $g_S$  for fixed  $\rho$ . In the chiral limit, the constituent mass is nonzero only when the scalar coupling is

stronger than the critical coupling  $g_S^{\text{cr}}$ , which is set by

$$g_S^{\text{cr}} = 2\pi^2 \rho^2 \left[ 8 \int_0^\infty dz z (zF'(z))^4 \right]^{-1} \approx 2.981 \pi^2 \rho^2 \quad (18)$$

The small size expansion reduces the solution of the gap equation back to the point interaction limit,

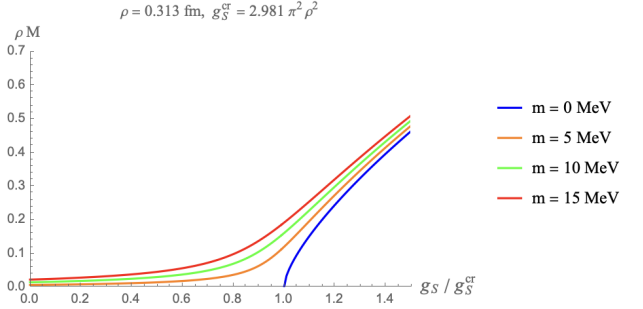


FIG. 2: Constituent quark mass versus the scalar coupling  $g_S$ .

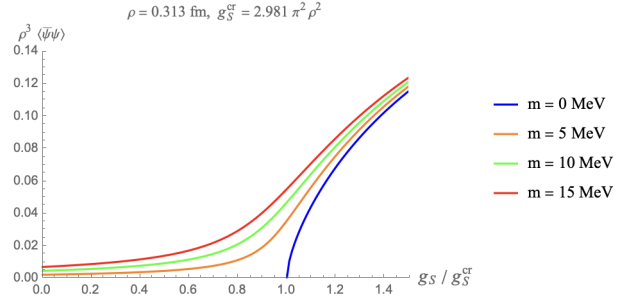


FIG. 3: Quark condensate as a function of the scalar coupling  $g_S$ .

with both the quadratic  $1/\rho$  and logarithmic dependence in  $1/\rho$ ,

$$\frac{m}{M} = 1 - \frac{g_S}{2\pi^2 \rho^2} \left[ 8 \int_0^\infty dz z (zF'(z))^4 + \rho^2 M^2 \ln \rho^2 M^2 + \mathcal{O}(\rho^2 M^2) \right] \quad (19)$$

This is to be compared to the cut-off scheme in

the zero size limit, where the instanton size  $\rho$  in the

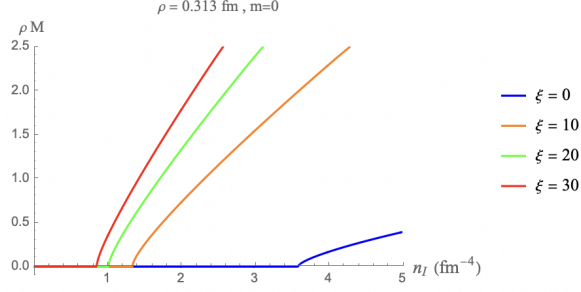


FIG. 4: Quark constituent mass in chiral limit as a function of instanton density in the presence of different  $\xi$

QCD instanton vacuum provides a natural cut-off. Similarly, we have for the chiral quark condensate

$$\rho^3 \langle \bar{\psi}\psi \rangle = -\frac{4N_c}{\pi^2} \rho M \int_0^\infty dz \frac{z^3}{z^2 + \frac{\rho^2 M^2}{4}} z (z F'(z))^2 \quad (20)$$

In the standard 2-flavor QCD instanton vacuum with  $\rho \approx (636\text{MeV})^{-1}$ ,  $g_S^{\text{cr}}$  is approximately  $72.64 \text{ GeV}^{-2}$ . In Fig. 1 we show the the constituent mass versus the current quark mass in units of the instanton size, for different scalar couplings  $g_S/g_S^{\text{cr}}$ . In Fig. 2 the constituent mass is shown versus  $g_S/g_S^{\text{cr}}$  for different current quark masses, with a clear onset of the spontaneously broken chiral phase. In Fig. 3 we show the chiral condensate versus  $g_S/g_S^{\text{cr}}$  for different current quark masses.

The effect of the instanton molecular contributions with  $G_{I\bar{I}} \neq 0$  but parametrically small in comparison to  $G_I$ , is seen to enhance the on-set of the spontaneous breaking of chiral symmetry. This is readily seen by noting that (18) is now changed to

$$\frac{G_I}{4N_c} \left( 1 + \frac{G_I}{8\pi^2 \rho^2 N_c} \xi \right) \geq g_S^{\text{cr}} \approx 2.981 \pi^2 \rho^2 \quad (21)$$

with the positive hopping parameter  $\xi$  given in (7). In Fig. 4 we show the constituent quark mass versus the instanton density, for increasing values of the hopping parameter, in the chiral limit. The larger  $\xi$ , the smaller the instanton density required for the onset of chiral symmetry breaking. This effect is also illustrated in Fig. 5, where we show that a lower in-

stanton density is needed for a fixed scalar coupling in the presence of the molecular component.

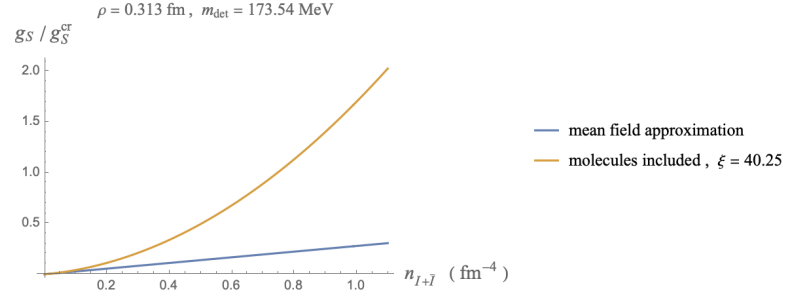


FIG. 5: The effective coupling  $g_S$  in  $\sigma$  channel as a function of instanton density.

#### IV. LIGHT FRONT FORMALISM OF NON-LOCAL 'T HOOFT LAGRANGIAN

On the light front, the spontaneous breaking of chiral symmetry in QCD follows from the emergent 't Hooft induced interactions, when the the constrained part of the fermion field is eliminated [38]. This observation was initially made in the context of the NJL model in [56–58]. The projected fermion field along the light front, yields a good plus bad component, with the latter non-propagating or constrained. The elimination of the non-propagating degrees of freedom induces the resummation of the multi-fermion interactions in terms of the good component. These interactions account for the spontaneous breaking of chiral symmetry on the light front through tadpoles.

More specifically, the fermionic constraint can be organized in  $1/N_c$

$$\psi \rightarrow \psi_+ + \frac{\gamma^+}{2} \frac{-i}{\partial_-} (i\gamma_\perp^i \partial_i - M) \psi_+ + \mathcal{O}(G_S, G_V) \quad (22)$$

to render it manageable. The pair of fermion bilinears are of order  $\mathcal{O}(\sqrt{N_c})$ , compensating the  $\mathcal{O}(1/N_c)$  contribution from the 't Hooft coupling  $G_S = g_S/N_c$  and  $G_V = g_V/N_c$ . In leading order, the interactions on the light front are of order  $N_c^0$ . The light front effective theory follows from the integration of the bad component to the same order,

$$\mathcal{L} \rightarrow \bar{\psi}(i\partial - M)\psi - V(x) \quad (23)$$

with the local kernels (zero size instantons) after integration

$$V(x) = V^\sigma(x) + V^{a_0}(x) + V^\pi(x) + V^{\eta'}(x) + V^\omega(x) + V^\rho(x) + V^{a_1}(x) + V^{f_1}(x) \quad (24)$$

**isoscalar  $\sigma$  channel:**

$$V^\sigma(x) = -\frac{G_\sigma}{2} \bar{\psi}\psi \frac{1}{1 + G_\sigma \left\langle \bar{\psi}\gamma^+ \frac{-i}{\partial_-} \psi \right\rangle} \bar{\psi}\psi \quad (25)$$

**isovector scalar channel:**

$$V^{a_0}(x) = -\frac{G_{a_0}}{2} \bar{\psi}\tau^a\psi \frac{1}{1 + G_{a_0} \left\langle \bar{\psi}\gamma^+ \frac{-i}{\partial_-} \psi \right\rangle} \bar{\psi}\tau^a\psi \quad (26)$$

**pion channel:**

$$V^\pi(x) = -\frac{G_\pi}{2} \left( \bar{\psi}i\gamma^5\tau^a\psi + iG_{a_1} \left\langle \bar{\psi} \frac{-i}{\partial_-} \psi \right\rangle \bar{\psi}\gamma^+\gamma^5\tau^a\psi \right) \frac{1}{1 + G_\pi \left\langle \bar{\psi}\gamma^+ \frac{-i}{\partial_-} \psi \right\rangle} \left( \bar{\psi}i\gamma^5\tau^a\psi + iG_{a_1} \left\langle \bar{\psi} \frac{-i}{\partial_-} \psi \right\rangle \bar{\psi}\gamma^+\gamma^5\tau^a\psi \right) \quad (27)$$

**$\eta'$  meson channel:**

$$V^{\eta'}(x) = -\frac{G_{\eta'}}{2} \left( \bar{\psi}i\gamma^5\psi + iG_{f_1} \left\langle \bar{\psi} \frac{-i}{\partial_-} \psi \right\rangle \bar{\psi}\gamma^+\gamma^5\psi \right) \frac{1}{1 + G_{\eta'} \left\langle \bar{\psi}\gamma^+ \frac{-i}{\partial_-} \psi \right\rangle} \left( \bar{\psi}i\gamma^5\psi + iG_{f_1} \left\langle \bar{\psi} \frac{-i}{\partial_-} \psi \right\rangle \bar{\psi}\gamma^+\gamma^5\psi \right) \quad (28)$$

**isoscalar vector channel:**

$$V^\omega(x) = \frac{G_\omega}{2} \bar{\psi}\gamma_\perp^i\psi \frac{1}{1 + G_\omega \left\langle \bar{\psi}\gamma^+ \frac{-i}{\partial_-} \psi \right\rangle} \bar{\psi}\gamma_{i\perp}\psi + G_\omega \bar{\psi}\gamma^+\psi \left[ \bar{\psi}\gamma^-\psi + G_\omega \left\langle \bar{\psi}\gamma^- \frac{-i}{\partial_-} \psi \right\rangle \bar{\psi}\gamma^+\psi \right] \quad (29)$$

**$\rho$  meson channel:**

$$V^\rho(x) = \frac{G_\rho}{2} \bar{\psi}\gamma_\perp^i\tau^a\psi \frac{1}{1 + G_\rho \left\langle \bar{\psi}\gamma^+ \frac{-i}{\partial_-} \psi \right\rangle} \bar{\psi}\gamma_{i\perp}\tau^a\psi + G_\rho \bar{\psi}\gamma^+\tau^a\psi \left[ \bar{\psi}\gamma^-\tau^a\psi + G_\rho \left\langle \bar{\psi}\gamma^- \frac{-i}{\partial_-} \psi \right\rangle \bar{\psi}\gamma^+\tau^a\psi \right] \quad (30)$$

**isovector axial vector channel:**

$$V^{a_1}(x) = \frac{G_{a_1}}{2} \bar{\psi}\gamma_\perp^i\gamma^5\tau^a\psi \frac{1}{1 + G_{a_1} \left\langle \bar{\psi}\gamma^+ \frac{-i}{\partial_-} \psi \right\rangle} \bar{\psi}\gamma_{i\perp}\gamma^5\tau^a\psi + G_{a_1} \bar{\psi}\gamma^+\gamma^5\tau^a\psi \left[ \bar{\psi}\gamma^-\gamma^5\tau^a\psi + G_{a_1} \left\langle \bar{\psi}\gamma^- \frac{-i}{\partial_-} \psi \right\rangle \bar{\psi}\gamma^+\gamma^5\tau^a\psi \right] \quad (31)$$

**isoscalar axial vector channel:**

$$V^{f_1}(x) = \frac{G_{f_1}}{2} \bar{\psi}\gamma_\perp^i\gamma^5\psi \frac{1}{1 + G_{f_1} \left\langle \bar{\psi}\gamma^+ \frac{-i}{\partial_-} \psi \right\rangle} \bar{\psi}\gamma_{i\perp}\gamma^5\psi + G_{f_1} \bar{\psi}\gamma^+\gamma^5\psi \left[ \bar{\psi}\gamma^-\gamma^5\psi + G_{f_1} \left\langle \bar{\psi}\gamma^- \frac{-i}{\partial_-} \psi \right\rangle \bar{\psi}\gamma^+\gamma^5\psi \right] \quad (32)$$

For finite size instantons, the tadpole contributions in the emerging non-local kernels follow from

the substitutions

$$\left\langle \bar{\psi}\gamma^+ \frac{-i}{\partial_-} \psi \right\rangle \rightarrow \left\langle \bar{\psi}\mathcal{F}(i\partial)\gamma^+ \frac{-i}{\partial_-} \mathcal{F}(i\partial)\psi \right\rangle \quad (33)$$

$$\left\langle \bar{\psi} \frac{-i}{\partial_-} \psi \right\rangle \rightarrow \left\langle \bar{\psi}\mathcal{F}(i\partial) \frac{-i}{\partial_-} \mathcal{F}(i\partial)\psi \right\rangle \quad (34)$$

$$\left\langle \bar{\psi}\gamma^- \frac{-i}{\partial_-} \psi \right\rangle \rightarrow \left\langle \bar{\psi}\mathcal{F}(i\partial)\gamma^- \frac{-i}{\partial_-} \mathcal{F}(i\partial)\psi \right\rangle \quad (35)$$

which amount to the loop integrations in momentum space

---

$$\frac{1}{2N_c} \left\langle \bar{\psi} \mathcal{F}(i\partial) \gamma^+ \frac{-i}{\partial_-} [\mathcal{F}(i\partial) \psi] \right\rangle \rightarrow w_+(P^+) = \int \frac{dk^+ d^2 k_\perp}{(2\pi)^3} \frac{\epsilon(k^+)}{P^+ - k^+} \mathcal{F}(k) \mathcal{F}(P - k) \quad (36)$$

$$\frac{1}{2N_c} \left\langle \bar{\psi} \mathcal{F}(i\partial) \frac{-i}{\partial_-} [\mathcal{F}(i\partial) \psi] \right\rangle \rightarrow w_0(P^+) = \int \frac{dk^+ d^2 k_\perp}{(2\pi)^3} \frac{M \epsilon(k^+)}{k^+ (P^+ - k^+)} \mathcal{F}(k) \mathcal{F}(P - k) \quad (37)$$

$$\frac{1}{2N_c} \left\langle \bar{\psi} \mathcal{F}(i\partial) \gamma^- \frac{-i}{\partial_-} [\mathcal{F}(i\partial) \psi] \right\rangle \rightarrow w_-(P^+) = \int \frac{dk^+ d^2 k_\perp}{(2\pi)^3} \frac{(k_\perp^2 + M^2) \epsilon(k^+)}{2(k^+)^2 (P^+ - k^+)} \mathcal{F}(k) \mathcal{F}(P - k) \quad (38)$$


---

The fermionic tadpole functions  $w_\pm(P^+)$  are even in  $P^+$ , while  $w_0(P^+)$  are odd in  $P^+$ .

tions, follows from the effective action (30) in the form

### A. Light front Hamiltonian

The emergent light front Hamiltonian for the QCD instanton vacuum with molecular contribu-

---

$$\begin{aligned} P^- = & \int [d^3 k]_+ \int [d^3 q]_+ \frac{k_\perp^2 + M^2}{2k^+} \bar{\psi}(k) \gamma^+ \psi(q) (2\pi)^3 \delta_+^3(k - q) \\ & + \int [d^3 k]_+ \int [d^3 q]_+ \int [d^3 p]_+ \int [d^3 l]_+ (2\pi)^3 \delta_+^3(p + k - q - l) \sqrt{\mathcal{F}(k) \mathcal{F}(q) \mathcal{F}(p) \mathcal{F}(l)} V(k, q, p, l) \end{aligned} \quad (39)$$

with the short hand notations

$$\int [d^3 k]_+ = \int \frac{dk^+ d^2 k_\perp}{(2\pi)^3 2k^+} \epsilon(k^+) \quad \delta_+^3(k) = \delta(k^+) \delta^2(k_\perp) \quad (40)$$

The interaction kernel in (IV A) is given by

$$V(k, q, p, l) = \sum_{s_1, s'_1, s_2, s'_2} \mathcal{V}_{s_1, s_2, s'_1, s'_2}(k, q, p, l) b_{s_1}^\dagger(k) c_{s_2}^\dagger(q) c_{s'_2}(p) b_{s'_1}(l) \quad (41)$$

with the transition amplitude  $\mathcal{V}_{s_1, s_2, s'_1, s'_2}(k, q, p, l)$  summing over the eight meson channels,

$$\begin{aligned} \mathcal{V}_{s_1, s_2, s'_1, s'_2}(k, q, p, l) = & \mathcal{V}_{s_1, s_2, s'_1, s'_2}^\sigma(k, q, p, l) + \mathcal{V}_{s_1, s_2, s'_1, s'_2}^{\eta'}(k, q, p, l) + \mathcal{V}_{s_1, s_2, s'_1, s'_2}^\pi(k, q, p, l) + \mathcal{V}_{s_1, s_2, s'_1, s'_2}^{a_0}(k, q, p, l) \\ & + \mathcal{V}_{s_1, s_2, s'_1, s'_2}^\omega(k, q, p, l) + \mathcal{V}_{s_1, s_2, s'_1, s'_2}^\rho(k, q, p, l) + \mathcal{V}_{s_1, s_2, s'_1, s'_2}^{a_1}(k, q, p, l) + \mathcal{V}_{s_1, s_2, s'_1, s'_2}^{f_1}(k, q, p, l) \end{aligned} \quad (42)$$

**isoscalar scalar  $\sigma$  channel:**

$$\mathcal{V}_{s_1, s_2, s'_1, s'_2}^\sigma(k, q, p, l) = - \frac{g_\sigma}{N_c} \frac{1}{1 + 2g_\sigma w_+(P^+)} \bar{u}_{s_1}(k) v_{s_2}(q) \bar{v}_{s'_2}(l) u_{s'_1}(p) \quad (43)$$

**isovector scalar  $a_0$  channel:**

$$\mathcal{V}_{s_1, s_2, s'_1, s'_2}^{a_0}(k, q, p, l) = - \frac{g_{a_0}}{N_c} \frac{1}{1 + 2g_{a_0} w_+(P^+)} \bar{u}_{s_1}(k) \tau^a v_{s_2}(q) \bar{v}_{s'_2}(l) \tau^a u_{s'_1}(p) \quad (44)$$



**pion channel:**

$$\begin{aligned}\mathcal{V}_{s_1, s_2, s'_1, s'_2}^\pi(k, q, p, l) = & -\frac{g_\pi}{N_c} \frac{1}{1 + 2g_\pi w_+(P^+)} \\ & \times [\bar{u}_{s_1}(k) i\gamma^5 \tau^a v_{s_2}(q) + 2ig_{a_1} w_0(P^+) \bar{u}_{s_1}(k) \gamma^+ \gamma^5 \tau^a v_{s_2}(q)] \\ & \times [\bar{v}_{s'_2}(l) i\gamma^5 \tau^a u_{s'_1}(p) - 2ig_{a_1} w_0(P^+) \bar{v}_{s'_2}(l) \gamma^+ \gamma^5 \tau^a u_{s'_1}(p)]\end{aligned}\quad (45)$$

**$\eta'$  meson channel:**

$$\begin{aligned}\mathcal{V}_{s_1, s_2, s'_1, s'_2}^{\eta'}(k, q, p, l) = & -\frac{g_{\eta'}}{N_c} \frac{1}{1 + 2g_{\eta'} w_+(P^+)} \\ & \times [\bar{u}_{s_1}(k) i\gamma^5 v_{s_2}(q) + 2ig_{f_1} w_0(P^+) \bar{u}_{s_1}(k) \gamma^+ \gamma^5 v_{s_2}(q)] \\ & \times [\bar{v}_{s'_2}(l) i\gamma^5 u_{s'_1}(p) - 2ig_{f_1} w_0(P^+) \bar{v}_{s'_2}(l) \gamma^+ \gamma^5 u_{s'_1}(p)]\end{aligned}\quad (46)$$

**isoscalar vector channel:**

$$\begin{aligned}\mathcal{V}_{s_1, s_2, s'_1, s'_2}^\omega(k, q, p, l) = & \frac{g_\omega}{N_c} \frac{1}{1 + 2g_\omega w_+(P^+)} \bar{u}_{s_1}(k) \gamma_\perp^i v_{s_2}(q) \bar{v}_{s'_2}(l) \gamma_{i\perp} u_{s'_1}(p) \\ & + \frac{g_\omega}{N_c} \bar{u}_{s_1}(k) \gamma^+ v_{s_2}(q) [\bar{v}_{s'_2}(l) \gamma^- u_{s'_1}(p) + 2g_\omega w_-(P^+) \bar{v}_{s'_2}(l) \gamma^+ u_{s'_1}(p)] \\ & + \frac{g_\omega}{N_c} [\bar{u}_{s_1}(k) \gamma^- v_{s_2}(q) + 2g_\omega w_-(P^+) \bar{u}_{s_1}(k) \gamma^+ v_{s_2}(q)] \bar{v}_{s'_2}(l) \gamma^+ u_{s'_1}(p)\end{aligned}\quad (47)$$

**$\rho$  meson channel:**

$$\begin{aligned}\mathcal{V}_{s_1, s_2, s'_1, s'_2}^\rho(k, q, p, l) = & \frac{g_\rho}{N_c} \frac{1}{1 + 2g_\rho w_+(P^+)} \bar{u}_{s_1}(k) \gamma_\perp^i \tau^a v_{s_2}(q) \bar{v}_{s'_2}(l) \gamma_{i\perp} \tau^a u_{s'_1}(p) \\ & + \frac{g_\rho}{N_c} \bar{u}_{s_1}(k) \gamma^+ \tau^a v_{s_2}(q) [\bar{v}_{s'_2}(l) \gamma^- \tau^a u_{s'_1}(p) + 2g_\rho w_-(P^+) \bar{v}_{s'_2}(l) \gamma^+ \tau^a u_{s'_1}(p)] \\ & + \frac{g_\rho}{N_c} [\bar{u}_{s_1}(k) \gamma^- \tau^a v_{s_2}(q) + 2g_\rho w_-(P^+) \bar{u}_{s_1}(k) \gamma^+ \tau^a v_{s_2}(q)] \bar{v}_{s'_2}(l) \gamma^+ \tau^a u_{s'_1}(p)\end{aligned}\quad (48)$$

**isotriplet axial vector channel:**

$$\begin{aligned}\mathcal{V}_{s_1, s_2, s'_1, s'_2}^{a_1}(k, q, p, l) = & \frac{g_{a_1}}{N_c} \frac{1}{1 + 2g_{a_1} w_+(P^+)} \bar{u}_{s_1}(k) \gamma_\perp^i \gamma^5 \tau^a v_{s_2}(q) \bar{v}_{s'_2}(l) \gamma_{i\perp} \gamma^5 \tau^a u_{s'_1}(p) \\ & + \frac{g_{a_1}}{N_c} \bar{u}_{s_1}(k) \gamma^+ \gamma^5 \tau^a v_{s_2}(q) [\bar{v}_{s'_2}(l) \gamma^- \gamma^5 \tau^a u_{s'_1}(p) + 2g_{a_1} w_-(P^+) \bar{v}_{s'_2}(l) \gamma^+ \gamma^5 \tau^a u_{s'_1}(p)] \\ & + \frac{g_{a_1}}{N_c} [\bar{u}_{s_1}(k) \gamma^- \gamma^5 \tau^a v_{s_2}(q) + 2g_{a_1} w_-(P^+) \bar{u}_{s_1}(k) \gamma^+ \gamma^5 \tau^a v_{s_2}(q)] \bar{v}_{s'_2}(l) \gamma^+ \gamma^5 \tau^a u_{s'_1}(p)\end{aligned}\quad (49)$$

**isoscalar axial vector channel:**

$$\begin{aligned}\mathcal{V}_{s_1, s_2, s'_1, s'_2}^{f_1}(k, q, p, l) = & \frac{g_{f_1}}{N_c} \frac{1}{1 + 2g_{f_1} w_+(P^+)} \bar{u}_{s_1}(k) \gamma_\perp^i \gamma^5 v_{s_2}(q) \bar{v}_{s'_2}(l) \gamma_{i\perp} \gamma^5 u_{s'_1}(p) \\ & + \frac{g_{f_1}}{N_c} \bar{u}_{s_1}(k) \gamma^+ \gamma^5 v_{s_2}(q) [\bar{v}_{s'_2}(l) \gamma^- \gamma^5 u_{s'_1}(p) + 2g_{f_1} w_-(P^+) \bar{v}_{s'_2}(l) \gamma^+ \gamma^5 u_{s'_1}(p)] \\ & + \frac{g_{f_1}}{N_c} [\bar{u}_{s_1}(k) \gamma^- \gamma^5 v_{s_2}(q) + 2g_{f_1} w_-(P^+) \bar{u}_{s_1}(k) \gamma^+ \gamma^5 v_{s_2}(q)] \bar{v}_{s'_2}(l) \gamma^- \gamma^5 u_{s'_1}(p)\end{aligned}\quad (50)$$

where  $g_X = N_c G_X$ .

## B. Bound state equations

The light scalar and vector eigenstates to the light front hamiltonian (IV A), can be formally sought in the following form

$$|\text{Meson } X, \lambda, P\rangle = \int_0^1 \frac{dx}{\sqrt{2x\bar{x}}} \int \frac{d^2 k_\perp}{(2\pi)^3} \sum_{s_1, s_2} \Phi_X^\lambda(x, k_\perp, s_1, s_2) b_{s_1}^\dagger(k) c_{s_2}^\dagger(P-k) |0\rangle \quad (51)$$

with  $\lambda = \pm$  (transverse) and  $\lambda = 0$  (longitudinal) polarisations of the X-vector mesons. The polarisation label is absent for the X-scalar mesons. In the QCD instanton vacuum, the pertinent eigen-equation for the X-meson on the light front is

$$m_X^2 \Phi_X^\lambda(x, k_\perp, s_1, s_2) = \frac{k_\perp^2 + M^2}{x\bar{x}} \Phi_X^\lambda(x, k_\perp, s_1, s_2) + \frac{1}{\sqrt{2x\bar{x}}} \sqrt{\mathcal{F}(k)\mathcal{F}(P-k)} \int_0^1 \frac{dy}{\sqrt{2y\bar{y}}} \int \frac{d^2 q_\perp}{(2\pi)^3} \sum_{s,s'} \mathcal{V}_{s_1, s_2, s, s'}(k, P-k, q, P-q) \Phi_X^\lambda(y, q_\perp, s, s') \sqrt{\mathcal{F}(q)\mathcal{F}(P-q)} \quad (52)$$

using the  $1/N_c$  book-keeping.

Throughout, we will be mostly interested in the vector (spin-1) mesons, as the scalar (spin-0) mesons were already discussed in [38], to which we refer for further details. Here, the scalars are kept solely for the purpose of comparison to the vector results. Also, the diluteness of the instanton tunneling rate in the QCD vacuum yields a parametrically small

$G_V/G_S$  ratio, with minor changes in the vacuum parameters as we discussed earlier. Hence, only the leading contribution in  $G_V$  in the bound state problem will be kept. As a result, the (pseudo)scalar-axial-vector mixing of order  $G_V/G_S$  will be ignored. With this in mind, we now detail the interaction kernels for the scalar and vector channels, and their corresponding bound state equations.

### 1. Scalar channels

$$\sum_{s,s'} \mathcal{V}_{s,s',s_1,s_2}^\sigma(q, q', k, k') \Phi_\sigma(y, q_\perp, s, s') = -\frac{4g_\sigma}{1+2g_\sigma w_+(P^+)} \left( \frac{q_\perp^2 + (y-\bar{y})^2 M^2}{y\bar{y}} \right) \phi_\sigma(y, q_\perp) \bar{u}_{s_1}(k) v_{s_2}(k') \quad (53)$$

$$\sum_{s,s'} \mathcal{V}_{s,s',s_1,s_2}^{a_0}(q, q', k, k') \Phi_{a_0}(y, q_\perp, s, s') = -\frac{4g_{a_0}}{1+2g_{a_0} w_+(P^+)} \left( \frac{q_\perp^2 + (y-\bar{y})^2 M^2}{y\bar{y}} \right) \phi_{a_0}(y, q_\perp) \bar{u}_{s_1}(k) \tau^a v_{s_2}(k') \quad (54)$$

where  $g_\sigma = g_S$  and  $g_{a_0} = -g_S + 8g_V$

### 2. Pseudoscalar channels

$$\sum_{s,s'} \mathcal{V}_{s,s',s_1,s_2}^\pi(q, q', k, k') \Phi_\pi(y, q_\perp, s, s') = -\frac{4g_\pi}{1+2g_\pi w_+(P^+)} \left( \frac{q_\perp^2 + M^2}{y\bar{y}} \right) \phi_\pi(y, q_\perp) \bar{u}_{s_1}(k) i\gamma^5 \tau^a v_{s_2}(k') \quad (55)$$

$$\sum_{s,s'} \mathcal{V}_{s,s',s_1,s_2}^{\eta'}(q, q', k, k') \Phi_{\eta'}(y, q_\perp, s, s') = -\frac{4g_{\eta'}}{1+2g_{\eta'} w_+(P^+)} \left( \frac{q_\perp^2 + M^2}{y\bar{y}} \right) \phi_{\eta'}(y, q_\perp) \bar{u}_{s_1}(k) i\gamma^5 v_{s_2}(k') \quad (56)$$

with  $g_\sigma = g_S$  and  $g_{a_0} = -g_S + 8g_V$ .

### 3. Vector channels

**transverse polarization states:**

$$\sum_{s,s'} \mathcal{V}_{s_1,s_2,s,s'}^\omega(k, k', q, q') \Phi_\omega^\pm(y, q_\perp, s, s') = -\frac{4g_\omega}{1+2g_\omega w_+(P^+)} \left( \frac{q_\perp^2 + M^2 - 2y\bar{y}q_\perp^2}{y\bar{y}} \right) \phi_\omega(y, q_\perp) \epsilon_i^\pm(P) \bar{u}_{s_1}(k) \gamma_\perp^i v_{s_2}(k') \quad (57)$$

$$\sum_{s,s'} \mathcal{V}_{s_1,s_2,s,s'}^\rho(k,k',q,q') \Phi_\rho^\pm(y,q_\perp,s,s') = -\frac{4g_\rho}{1+2g_\rho w_+(P^+)} \left( \frac{q_\perp^2 + M^2 - 2y\bar{y}q_\perp^2}{y\bar{y}} \right) \phi_\rho(y,q_\perp) \epsilon_i^\pm(P) \bar{u}_{s_1}(k) \tau^a \gamma_\perp^i v_{s_2}(k') \quad (58)$$

**longitudinal polarization states:**

$$\begin{aligned} & \sum_{s,s'} \mathcal{V}_{s_1,s_2,s,s'}^\omega(k,k',q,q') \Phi_\omega^0(y,q_\perp,s,s') \\ &= -8g_\omega \left[ \frac{q_\perp^2 + M^2}{y\bar{y}} - 4g_\omega w_-(P^+)(P^+)^2 \right] y\bar{y} \left( 1 + \frac{q_\perp^2 + M^2}{m_\omega^2 y\bar{y}} \right) \phi_\omega(y,q_\perp) \left[ -\frac{m_\omega}{2P^+} \bar{u}_{s_1}(k) \gamma^+ v_{s_2}(P-k) \right] \\ & \quad - 8g_\omega \left[ \frac{k_\perp^2 + M^2}{x\bar{x}} - 4g_\omega w_-(P^+)(P^+)^2 \right] y\bar{y} \left( 1 + \frac{q_\perp^2 + M^2}{m_\omega^2 y\bar{y}} \right) \phi_\omega(y,q_\perp) \left[ -\frac{m_\omega}{2P^+} \bar{u}_{s_1}(k) \gamma^+ v_{s_2}(P-k) \right] \end{aligned} \quad (59)$$

$$\begin{aligned} & \sum_{s,s'} \mathcal{V}_{s_1,s_2,s,s'}^\rho(k,k',q,q') \Phi_\rho^0(y,q_\perp,s,s') \\ &= -8g_\rho \left[ \frac{q_\perp^2 + M^2}{y\bar{y}} - 4g_\rho w_-(P^+)(P^+)^2 \right] y\bar{y} \left( 1 + \frac{q_\perp^2 + M^2}{m_\rho^2 y\bar{y}} \right) \phi_\rho(y,q_\perp) \left[ -\frac{m_\rho}{2P^+} \bar{u}_{s_1}(k) \gamma^+ \tau^a v_{s_2}(P-k) \right] \\ & \quad - 8g_\rho \left[ \frac{k_\perp^2 + M^2}{x\bar{x}} - 4g_\rho w_-(P^+)(P^+)^2 \right] y\bar{y} \left( 1 + \frac{q_\perp^2 + M^2}{m_\rho^2 y\bar{y}} \right) \phi_\rho(y,q_\perp) \left[ -\frac{m_\rho}{2P^+} \bar{u}_{s_1}(k) \gamma^+ \tau^a v_{s_2}(P-k) \right] \end{aligned} \quad (60)$$

with  $g_\omega = g_\rho = g_V$ . The minus component of the spinor wave function can be traded for the plus component

$$\epsilon_0^\mu(P) \bar{u}_{s_1}(k) \gamma_\mu v_{s_2}(P-k) = -\frac{m_X}{2P^+} \left( 1 + \frac{k_\perp^2 + M^2}{m_X^2 x\bar{x}} \right) \bar{u}_{s_1}(k) \gamma^+ v_{s_2}(P-k) \quad (61)$$

thanks to the longitudinal Ward identity

$$\bar{u}_{s_1}(k) \gamma^- v_{s_2}(P-k) = -\frac{1}{(P^+)^2} \frac{k_\perp^2 + M^2}{2x\bar{x}} \bar{u}_{s_1}(k) \gamma^+ v_{s_2}(P-k) \quad (62)$$

On the light front, the longitudinal and transverse polarizations appear decoupled, yet underlying this is hidden Lorentz symmetry. This will be recovered below in details both in the spectrum and ensuing longitudinal wavefunctions.

#### 4. Bound state equations for each channel

**scalar channels:**

$$\begin{aligned} m_{\sigma,a_0}^2 \phi_{\sigma,a_0}(x,k_\perp) &= \frac{k_\perp^2 + M^2}{x\bar{x}} \phi_{\sigma,a_0}(x,k_\perp) \\ & \quad - \frac{4g_{\sigma,a_0}}{\sqrt{2x\bar{x}}} \frac{\sqrt{\mathcal{F}(k)\mathcal{F}(P-k)}}{1+2g_{\sigma,a_0}w_+(P^+)} \int \frac{dy}{\sqrt{2y\bar{y}}} \int \frac{d^2q_\perp}{(2\pi)^3} \left( \frac{q_\perp^2 + (y-\bar{y})^2 M^2}{y\bar{y}} \right) \phi_{\sigma,a_0}(y,q_\perp) \sqrt{\mathcal{F}(q)\mathcal{F}(P-q)} \end{aligned} \quad (63)$$

**pseudoscalar channels:**

$$\begin{aligned} m_{\pi,\eta'}^2 \phi_{\pi,\eta'}(x,k_\perp) &= \frac{k_\perp^2 + M^2}{x\bar{x}} \phi_{\pi,\eta'}(x,k_\perp) \\ & \quad - \frac{4g_{\pi,\eta'}}{\sqrt{2x\bar{x}}} \frac{\sqrt{\mathcal{F}(k)\mathcal{F}(P-k)}}{1+2g_{\pi,\eta'}w_+(P^+)} \int \frac{dy}{\sqrt{2y\bar{y}}} \int \frac{d^2q_\perp}{(2\pi)^3} \left( \frac{q_\perp^2 + M^2}{y\bar{y}} \right) \phi_{\pi,\eta'}(y,q_\perp) \sqrt{\mathcal{F}(q)\mathcal{F}(P-q)} \end{aligned} \quad (64)$$

**transverse vector channels:**

$$m_{\omega,\rho}^2 \phi_{\omega,\rho}(x, k_\perp) = \frac{k_\perp^2 + M^2}{x\bar{x}} \phi_{\omega,\rho}(x, k_\perp) - \frac{4g_{\omega,\rho}}{\sqrt{2x\bar{x}}} \frac{\sqrt{\mathcal{F}(k)\mathcal{F}(P-k)}}{1 + 2g_{\omega,\rho}w_+(P^+)} \int \frac{dy}{\sqrt{2y\bar{y}}} \int \frac{d^2q_\perp}{(2\pi)^3} \left( \frac{q_\perp^2 + M^2 - 2y\bar{y}q_\perp^2}{y\bar{y}} \right) \phi_{\omega,\rho}(y, q_\perp) \sqrt{\mathcal{F}(q)\mathcal{F}(P-q)} \quad (65)$$

**longitudinal vector channels:**

$$m_{\omega,\rho}^2 \phi_{\omega,\rho}(x, k_\perp) = \frac{k_\perp^2 + M^2}{x\bar{x}} \phi_{\omega,\rho}(x, k_\perp) - \frac{4g_{\omega,\rho}}{\sqrt{2x\bar{x}}} \sqrt{\mathcal{F}(k)\mathcal{F}(P-k)} \int \frac{dy}{\sqrt{2y\bar{y}}} \int \frac{d^2q_\perp}{(2\pi)^3} 4(q_\perp^2 + M^2) \phi_{\omega,\rho}(y, q_\perp) \sqrt{\mathcal{F}(q)\mathcal{F}(P-q)} \quad (66)$$

The derivation of the bound state equation for the longitudinal channel is more challenging, with the details given in Appendix B. The asymmetry between the longitudinal and transverse channels, reflect on the lack of manifest Lorentz symmetry on the light front. However, a closer analysis shows that the longitudinal and transverse mass eigenstates are equal, and that the longitudinal and transverse distribution amplitudes are tied by covariance.

### C. Meson Spectrum

The eigenvalues to the bound-state equations for each of the meson channel, determine the mass spectrum in the light front formalism. In fact, the eigenvalue problem can be recast into an integral equation for the mass spectrum. For this, we note that the tadpole function  $w_+(P^+)$  controlling the emergent vertices, can be recast as follows

$$\begin{aligned} w_+(P^+) &= \int \frac{dk^+ d^2k_\perp}{(2\pi)^3} \frac{\epsilon(k^+)}{P^+ - k^+} \mathcal{F}(k) \mathcal{F}(P-k) \\ &= \int_0^1 dx \int \frac{d^2k_\perp}{(2\pi)^3} \frac{2}{x} \mathcal{F}(k) \mathcal{F}(P-k) - \int \frac{dk^+ d^2k_\perp}{(2\pi)^3} \frac{\epsilon(k^+)}{k^+} \mathcal{F}(P-k) \mathcal{F}(k) \\ &\simeq \int_0^1 dx \int \frac{d^2k_\perp}{(2\pi)^3} \frac{2}{x} \mathcal{F}(k) \mathcal{F}(P-k) - \frac{1}{2g_S} \left(1 - \frac{m}{M}\right) \end{aligned} \quad (67)$$

where we used

$$\int \frac{dk^+ d^2k_\perp}{(2\pi)^3} \frac{\epsilon(k^+)}{k^+} [\mathcal{F}(k) \mathcal{F}(P-k)] \simeq \frac{1}{2g_S} \left(1 - \frac{m}{M}\right) \quad (68)$$

With this in mind, the eigenvalue equations (63-66) can be recast in the form of gap-like equations, much like the vacuum parameters discussed earlier. More specifically, we obtain

**scalar modes**

$$1 - \frac{g_{\sigma,a_0}}{g_S} \left(1 - \frac{m}{M}\right) = -2g_{\sigma,a_0} (m_{\sigma,a_0}^2 - 4M^2) \int_0^1 dx \int \frac{d^2k_\perp}{(2\pi)^3} \frac{1}{x\bar{x}m_{\sigma,a_0}^2 - (k_\perp^2 + M^2)} \mathcal{F}(k) \mathcal{F}(P-k) \quad (69)$$

**pseudoscalar modes**

$$1 - \frac{g_{\pi,\eta'}}{g_S} \left(1 - \frac{m}{M}\right) = -2g_{\pi,\eta'} m_{\pi,\eta'}^2 \int_0^1 dx \int \frac{d^2k_\perp}{(2\pi)^3} \frac{1}{x\bar{x}m_{\pi,\eta'}^2 - (k_\perp^2 + M^2)} \mathcal{F}(k) \mathcal{F}(P-k) \quad (70)$$

**transverse modes**

$$1 - \frac{g_{\omega,\rho}}{g_S} \left(1 - \frac{m}{M}\right) = -2g_{\omega,\rho} \int_0^1 dx \int \frac{d^2k_\perp}{(2\pi)^3} \frac{m_{\omega,\rho}^2 - 2k_\perp^2}{x\bar{x}m_{\omega,\rho}^2 - (k_\perp^2 + M^2)} \mathcal{F}(k) \mathcal{F}(P-k) \quad (71)$$

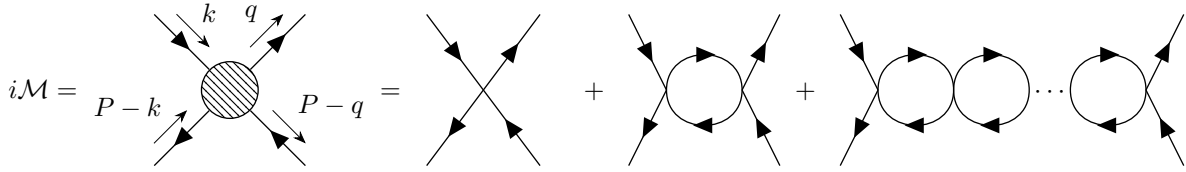
### longitudinal modes

$$1 = -8g_{\omega,\rho} \int_0^1 dx \int \frac{d^2 k_\perp}{(2\pi)^3} \frac{k_\perp^2 + M^2}{x\bar{x}m_{\omega,\rho}^2 - (k_\perp^2 + M^2)} \mathcal{F}(k)\mathcal{F}(P-k) \quad (72)$$

Despite the apparent difference between the longitudinal and transverse kernels, the mass solutions are the same.

### D. Meson spectrum in covariant formalism

For comparison, we now briefly derive the mass spectra for the light mesons in the covariant frame, by using the standard Bethe-Salpeter construction for bound states. Using the  $1/N_c$  book-keeping, we can resum the leading contributions to the 4-point function diagrammatically as follows



The diagrammatic rules follow from the effective action detailed in Sec. A. Since we are chiefly interested in mass eigenvalue equation for scalar and vector mesons in this covariant formulation, it is sufficient to note that the on-shell condition  $P^2 = m_X^2$  of the intermediate meson state  $X = \sigma, a_0, \omega, \rho, \eta', \pi$  is respectively,

$$\begin{aligned} 1 &= G_{\sigma,a_0} \Pi_{SS}(m_{\sigma,a_0}^2) \\ 1 &= G_{\omega,\rho} \Pi_{VV}(m_{\omega,\rho}^2) \\ 1 &= G_{\eta',\pi} \Pi_{PP}(m_{\eta',\pi}^2) \end{aligned} \quad (73)$$

where each vacuum polarization function is defined as

$$\begin{aligned} \Pi_{SS} &= 4N_c(P^2 - 4M^2)I_1(P^2) + 8N_c I_2(P^2) \\ \Pi_{PP} &= 4N_c P^2 I_1(P^2) + 8N_c I_2(P^2) \\ \Pi_{VV} &= \frac{8}{3}N_c(P^2 + 2M^2)I_1(P^2) + \frac{16}{3}N_c I_2(P^2) \end{aligned} \quad (74)$$

with the one-loop integrals

$$\begin{aligned} I_1(P^2) &= \int \frac{d^4 k}{(2\pi)^4} \frac{-i}{[(k - P/2)^2 - M^2][(k + P/2)^2 - M^2]} \mathcal{F}(k - P/2)\mathcal{F}(k + P/2) \\ I_2(P^2) &= \int \frac{d^4 k}{(2\pi)^4} \frac{i}{k^2 - M^2} \mathcal{F}(k)\mathcal{F}(P - k) \end{aligned} \quad (75)$$

(73) define implicitly the mass spectra in a covari-

ant frame. We note that in the pseudoscalar chan-

nel, the resummation of the vacuum polarization in the pion channel can receive additional contributions from  $\pi - a_1$  and  $\eta' - f_1$  mixing. However, these mixing contributions are suppressed in  $1/N_c$  or  $G_V/G_S$ , much like in the light front case. The interactions in the  $\sigma$ ,  $a_0$ ,  $\pi$ ,  $\eta'$ ,  $\omega$ , and  $\rho$  channels are attractive, and we expect binding for a given range of couplings.

The on-shell conditions (73) can be re-arranged by noting that

$$I_2(P^2) \simeq \int \frac{d^4k}{(2\pi)^4} \frac{i}{k^2 - M^2} \mathcal{F}^2(k) = \frac{1}{8g_S} \left(1 - \frac{m}{M}\right) \quad (76)$$

Inserting (76) into (75) and then in (73) yield the gap-like equations for the mass spectra in a covariant frame

$$\begin{aligned} 1 - \frac{g_{\sigma,a_0}}{g_\sigma} \left(1 - \frac{m}{M}\right) &= -4g_{\sigma,a_0}(m_{\sigma,a_0}^2 - 4M^2) \int \frac{d^4k}{(2\pi)^4} \frac{i}{(k^2 - M^2)[(P-k)^2 - M^2]} \mathcal{F}(k) \mathcal{F}(P-k) \\ 1 - \frac{g_{\pi,\eta'}}{g_\sigma} \left(1 - \frac{m}{M}\right) &= -4g_{\pi,\eta'} m_{\pi,\eta'}^2 \int \frac{d^4k}{(2\pi)^4} \frac{i}{(k^2 - M^2)[(P-k)^2 - M^2]} \mathcal{F}(k) \mathcal{F}(P-k) \\ 1 - \frac{2g_{\omega,\rho}}{3g_\sigma} \left(1 - \frac{m}{M}\right) &= -\frac{8}{3}g_{\omega,\rho}(m_{\omega,\rho}^2 + 2M^2) \int \frac{d^4k}{(2\pi)^4} \frac{i}{(k^2 - M^2)[(P-k)^2 - M^2]} \mathcal{F}(k) \mathcal{F}(P-k) \end{aligned} \quad (77)$$

### E. Connection to the light front

While in the light front formulation manifest Lorentz symmetry is irremediably lost, the mass spectra should be identical. To show this equivalence in our case, it is best to carry the integrations in (77) by splitting the measure  $d^4k \rightarrow dk^- dk^+ dk_\perp$ , and carrying first the  $k^-$ -integration in  $I_1(P^2)$

$$\int_{-\infty}^{\infty} \frac{dk^-}{2\pi} \frac{i}{(k^2 - M^2)[(P-k)^2 - M^2]} \mathcal{F}(k) \mathcal{F}(P-k) \Big|_{P^2=m_X^2} \rightarrow \frac{\theta(x\bar{x})}{2x\bar{x}P^+} \frac{1}{m_X^2 - \frac{k_\perp^2 + M^2}{x\bar{x}}} [zF'(z)]^4 \Big|_{z=\frac{\rho k_\perp}{2\lambda_X \sqrt{x\bar{x}}}} \quad (78)$$

This can be justified by doing the contour integral along  $k'^4 = \frac{-k^3 + ik^4}{\sqrt{2}}$  in Euclidean space. The parameter  $\lambda_X$  is of order 1, and can be determined by matching the integrals on both sides. They arise from the process of removing the spurious poles in the two-body non-local form factor, in the analytical continuation from Euclidean to Minkowski signature [59, 60]. Effectively, the parameter  $\lambda_X$  is a measure of the non-locality related to the finite-sized instanton vacuum with effective size cut-off  $\rho/\lambda_X$  which depends on the bound state mass  $m_X$ , con-

stituent mass  $M$  and instanton size  $\rho$ . We will use  $\lambda_S$  for the vertices emerging from single instantons, and  $\lambda_V$  for the vertices emerging from the molecules. Following [59, 60], we fix them empirically by the weak decay constants (see below)

$$\lambda_S = 2.464 \quad \lambda_V = 3.542 \quad (79)$$

Inserting (78) into (77) yields the same gap-like equations obtained in the light front, as expected. We now proceed to solve numerically these gap-like equations, to display the scalar and vector spectra.

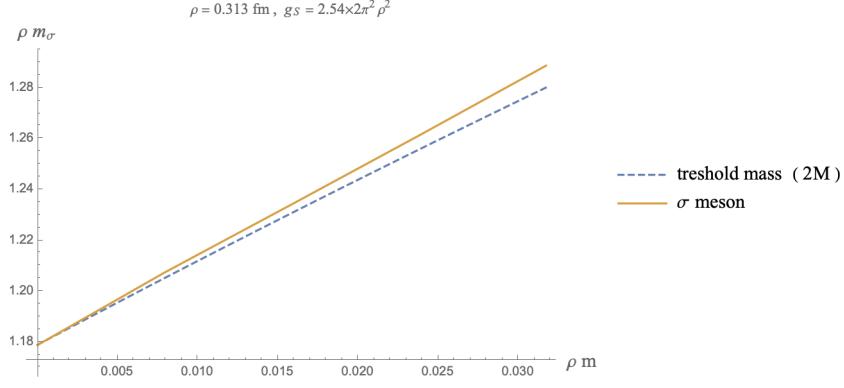


FIG. 6: Sigma mass versus the current quark mass solid-line. The dashed-line is the 2M threshold.

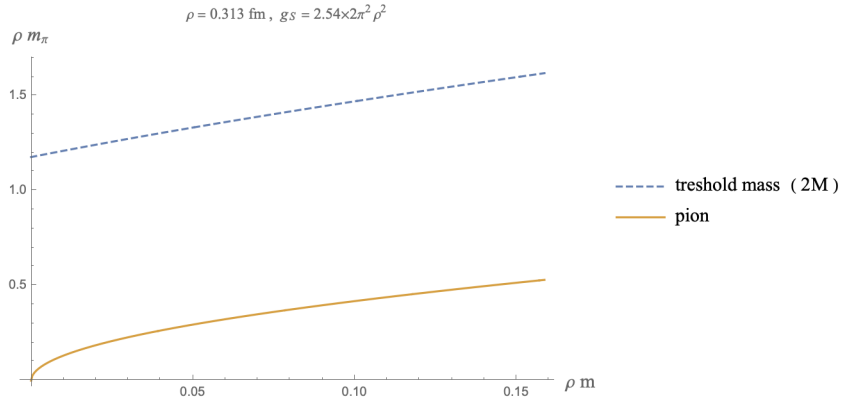


FIG. 7: Pion mass versus the current quark mass solid-line. The dashed-line is the 2M threshold.

### 1. Scalar sigma channel

$$\frac{m}{M} = \frac{g_S}{2\pi^2} (m_\sigma^2 - 4M^2) \int_0^1 dx \int_0^\infty dz \frac{z}{z^2 - \frac{\rho^2}{4\lambda_S} \left( m_\sigma^2 - \frac{M^2}{x\bar{x}} \right)} [zF'(z)]^4 \quad (80)$$

In Fig. 6 we show the sigma mass  $m_\sigma$  (solid-line) versus the current mass  $m$  for a fixed instanton size  $\rho = 0.31$  fm and scalar coupling, all in units of  $\rho$ . The dashed-line is the  $2M$  threshold. The  $\sigma$  meson is a threshold state in the chiral limit, and becomes unbound away from the chiral limit. For  $g_S = 2.54 \times 2\pi^2 \rho^2$ , the  $\sigma$  mass is  $m_\sigma = 2M = 743.1$  MeV in the chiral limit.

### 2. Pseudoscalar pion channel

$$\frac{m}{M} = \frac{g_S}{2\pi^2} m_\pi^2 \int_0^1 dx \int_0^\infty dz \frac{z}{z^2 - \frac{\rho^2}{4\lambda_S} \left( m_\pi^2 - \frac{M^2}{x\bar{x}} \right)} [zF'(z)]^4 \quad (81)$$

In Fig. 7 we show the pion mass  $m_\pi$  (solid-line) versus the current mass  $m$  for a fixed instanton size  $\rho = 0.31$  fm and scalar coupling, all in units of  $\rho$ . The dashed-line is the  $2M$  threshold. In comparison to the scalar

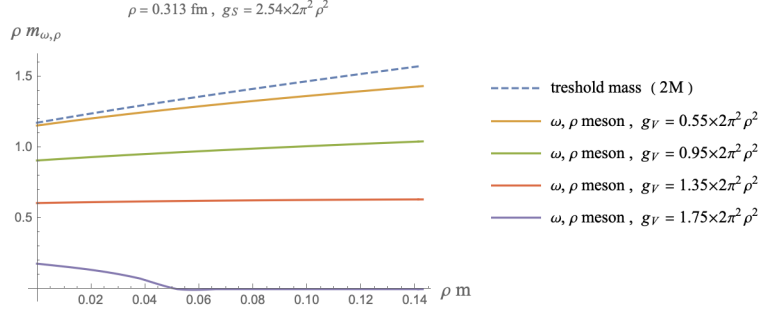


FIG. 8: Vector masses  $m_{\omega, \rho}$  versus the current quark mass in solid-lines, for different vector couplings  $g_V$ . The dashed line is the  $2M$  threshold in units of the instanton size  $\rho$ .

channel, the pion channel is strongly attractive in the QCD instanton vacuum. Flavor  $SU(2)$  symmetry guarantees  $g_\sigma = g_\pi = g_S$ . In particular, the chiral expansion of the pion mass eigenvalue or gap-like equation yields the Gell-Mann-Oakes-Renner (GOR) relation

$$m_\pi^2 = -\frac{2m}{f_\pi^2} \langle \bar{\psi}\psi \rangle \quad (82)$$

where the pion decay constant in chiral limit follows as

$$f_\pi = \frac{\sqrt{N_c} M}{\sqrt{2}\pi} \left[ \int_0^1 dx \int_0^\infty dk_\perp^2 \frac{1}{k_\perp^2 + M^2} \mathcal{F}(k) \mathcal{F}(P-k) \right]^{1/2} \quad (83)$$

### 3. Vector $\rho, \omega$ channels

Each of the longitudinal and transverse vector gap-like equations can be shown to yield the same masses for  $\rho, \omega$ . This is manifest if we use the spin averaged combination  $\frac{1}{3}[2 \times \text{Eq. (71)} + \text{Eq. (72)}]$ , with the result

$$1 - \frac{2g_V}{3g_S} \left(1 - \frac{m}{M}\right) = -\frac{4}{3}g_V(m_{\omega, \rho}^2 + 2M^2) \int_0^1 dx \int \frac{d^2 k_\perp}{(2\pi)^3} \frac{1}{x \bar{x} m_{\omega, \rho}^2 - (k_\perp^2 + M^2)} \mathcal{F}(k) \mathcal{F}(P-k) \quad (84)$$

This remarkably simple prescription, recovers the covariant gap-like equation for the vector mesons obtained in the covariant frame. With the explicit form factors, (84) is

$$1 - \frac{2g_V}{3g_S} \left(1 - \frac{m}{M}\right) = \frac{g_V}{3\pi^2} (m_{\omega, \rho}^2 + 2M^2) \int_0^1 dx \int_0^\infty dz \frac{z}{z^2 - \frac{\rho^2}{4\lambda_V^2} (m_{\omega, \rho}^2 - \frac{M^2}{x\bar{x}})} [zF'(z)]^4 \quad (85)$$

In Fig. 8, the vector masses are shown in solid-lines versus the current quark mass for different vector couplings  $g_V$ . The binding in the vector channels occur only for a finite range of  $g_V$ . In the chiral limit with a constituent mass  $M = 371.6$  MeV, the range is  $0.382 \times 2\pi^2 \rho^2 < g_V < 1.562 \times 2\pi^2 \rho^2$  as shown in Fig. 9.

## F. Physical mass spectrum

Our global results for the scalar and vector masses are summarized in the table

Model	$m_{\pi^0}$ (MeV)	$m_{\pi^\pm}$ (MeV)	$m_\omega$ (MeV)	$m_\rho$ (MeV)
ILM (this work)	135.0	135.0	780.0	780.0
PDG (exp)[61]	134.9766(6)	139.57018(35)	$782.65 \pm 0.12$	$775.26 \pm 0.25$

where the parameters in the emergent 't Hooft action are fixed as

$$\begin{aligned} g_S &= 2.540 \times 2\pi^2 \rho^2 = 126.17 \text{ GeV}^{-2} \\ g_V &= 0.531 \times 2\pi^2 \rho^2 = 26.37 \text{ GeV}^{-2} \end{aligned} \quad (86)$$



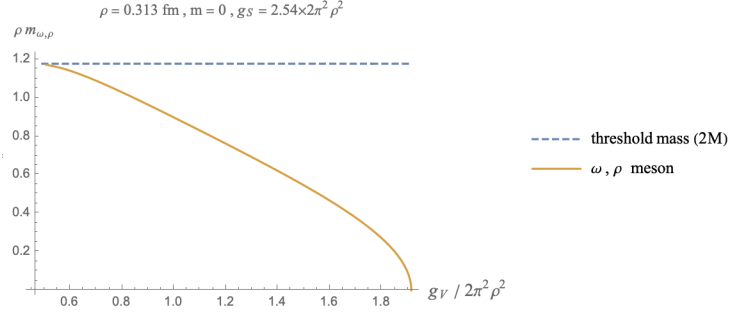


FIG. 9: Vector masses  $m_{\omega, \rho}$  versus the vector coupling as a solid-line, in units of the instanton size  $\rho$ . The dashed line is the  $2M$  threshold.

with the current quark mass  $m = 16.5$  MeV. This choice is commensurate with the standard  $\rho = 0.313$  fm and  $n_{I+\bar{I}} = 1 \text{ fm}^{-4}$  in the QCD instanton vacuum. The emergent constituent quark mass and the quark condensates are then

$$M = 398.2 \text{ MeV} \quad \langle \bar{\psi}\psi \rangle = (332.6 \text{ MeV})^3$$

The determinantal mass which is a measure of the light quark hopping between the instanton and anti-instanton, is found to be  $m_{det} \approx 173.54$  MeV, which is close to the value of 103 MeV in [12, 62]. The fixed parameters (86) translate to single and molecular induced couplings as

$$G_I = 248.34 \text{ GeV}^{-2} \quad G_{I\bar{I}} = 79.11 \text{ GeV}^{-2}$$

The dimensionless hopping parameter  $\xi = 40.25$  is

fixed by (6).

## V. LIGHT FRONT WAVE FUNCTIONS

The light front eigenstates (51) of the light front hamiltonian follows from (52). In leading order in  $1/N_c$ , only the leading quark-antiquark Fock component is retained. The eigenstates consist of a scalar wavefunction times a spin-dependent matrix element encoding the spin-flavor quantum numbers. The scalar wavefunction fixes the size of the pertinent meson, together with the strength of its effective coupling to the quark-antiquark pair. It is normalized to 1,

$$\int_0^1 dx \int \frac{d^2 k_\perp}{(2\pi)^3} \sum_{s_1, s_2} |\Phi_X^\lambda(x, k_\perp, s_1, s_2)|^2 = 1$$

### A. Light mesons light front wavefunctions

#### 1. scalar channels

$$\Phi_\sigma(x, k_\perp, s_1, s_2) = \frac{1}{\sqrt{N_c}} \left[ \frac{C_\sigma}{\sqrt{2x\bar{x}}(m_\sigma^2 - \frac{k_\perp^2 + M^2}{x\bar{x}})} \sqrt{\mathcal{F}(k) \mathcal{F}(P-k)} \right] \bar{u}_{s_1}(k) v_{s_2}(P-k) \quad (87)$$

$$\Phi_{a_0}(x, k_\perp, s_1, s_2) = \frac{1}{\sqrt{N_c}} \left[ \frac{C_{a_0}}{\sqrt{2x\bar{x}}(m_{a_0}^2 - \frac{k_\perp^2 + M^2}{x\bar{x}})} \sqrt{\mathcal{F}(k) \mathcal{F}(P-k)} \right] \bar{u}_{s_1}(k) \tau^a v_{s_2}(P-k) \quad (88)$$

The normalizations fix  $C_{\sigma,a_0}$  to

$$\begin{aligned}
C_{\sigma,a_0} &= - \left[ 2 \int_0^1 dx \int \frac{d^2 k_\perp}{(2\pi)^3} \frac{k_\perp^2 + (x - \bar{x})^2 M^2}{(x\bar{x}m_{\sigma,a_0}^2 - k_\perp^2 - M^2)^2} \mathcal{F}(k) \mathcal{F}(P - k) \right]^{-1/2} \\
&= - \sqrt{2}\pi \left[ \int_0^1 dx \int_0^\infty dz z \frac{x\bar{x}z^2 + \frac{\rho^2}{4\lambda_S^2}(x - \bar{x})^2 M^2}{\left(x\bar{x}z^2 - \frac{\rho^2}{4\lambda_S^2}(x\bar{x}m_{\sigma,a_0}^2 - M^2)\right)^2} (zF'(z))^4 \right]^{-1/2}
\end{aligned} \tag{89}$$

### 2. pseudoscalar channels

$$\Phi_{\eta'}(x, k_\perp, s_1, s_2) = \frac{1}{\sqrt{N_c}} \left[ \frac{C_{\eta'}}{\sqrt{2x\bar{x}(m_{\eta'}^2 - \frac{k_\perp^2 + M^2}{x\bar{x}})}} \sqrt{\mathcal{F}(k) \mathcal{F}(P - k)} \right] \bar{u}_{s_1}(k) i\gamma^5 v_{s_2}(P - k) \tag{90}$$

$$\Phi_\pi(x, k_\perp, s_1, s_2) = \frac{1}{\sqrt{N_c}} \left[ \frac{C_\pi}{\sqrt{2x\bar{x}(m_\pi^2 - \frac{k_\perp^2 + M^2}{x\bar{x}})}} \sqrt{\mathcal{F}(k) \mathcal{F}(P - k)} \right] \bar{u}_{s_1}(k) i\gamma^5 \tau^a v_{s_2}(P - k) \tag{91}$$

The normalizations fix  $C_{\pi,\eta'}$  to

$$\begin{aligned}
C_{\pi,\eta'} &= - \left[ 2 \int_0^1 dx \int \frac{d^2 k_\perp}{(2\pi)^3} \frac{k_\perp^2 + M^2}{(x\bar{x}m_{\pi,\eta'}^2 - k_\perp^2 - M^2)^2} \mathcal{F}(k) \mathcal{F}(P - k) \right]^{-1/2} \\
&= - \sqrt{2}\pi \left[ \int_0^1 dx \int_0^\infty dz z \frac{x\bar{x}z^2 + \frac{\rho^2 M^2}{4\lambda_S^2}}{\left(x\bar{x}z^2 - \frac{\rho^2}{4\lambda_S^2}(x\bar{x}m_{\pi,\eta'}^2 - M^2)\right)^2} (zF'(z))^4 \right]^{-1/2}
\end{aligned} \tag{92}$$

In chiral limit,  $C_\pi$  satisfies the Goldberger-Treiman relation.

$$\lim_{m_\pi \rightarrow 0} C_\pi = - \left[ 2 \int_0^1 dx \int \frac{d^2 k_\perp}{(2\pi)^3} \frac{1}{k_\perp^2 + M^2} \mathcal{F}(k) \mathcal{F}(P - k) \right]^{-1/2} = - \frac{\sqrt{2N_c}M}{f_\pi} \tag{93}$$

### 3. vector channels

$$\Phi_\omega^\lambda(x, k_\perp, s_1, s_2) = \frac{1}{\sqrt{N_c}} \left[ \frac{C_\omega}{\sqrt{2x\bar{x}(m_\omega^2 - \frac{k_\perp^2 + M^2}{x\bar{x}})}} \sqrt{\mathcal{F}(k) \mathcal{F}(P - k)} \right] \epsilon_\lambda^\mu(P) \bar{u}_{s_1}(k) \gamma_\mu v_{s_2}(P - k) \tag{94}$$

$$\Phi_\rho^\lambda(x, k_\perp, s_1, s_2) = \frac{1}{\sqrt{N_c}} \left[ \frac{C_\rho}{\sqrt{2x\bar{x}(m_\rho^2 - \frac{k_\perp^2 + M^2}{x\bar{x}})}} \sqrt{\mathcal{F}(k) \mathcal{F}(P - k)} \right] \epsilon_\lambda^\mu(P) \bar{u}_{s_1}(k) \gamma_\mu \tau^a v_{s_2}(P - k) \tag{95}$$

The normalization yields different transverse  $C_{\omega_T, \rho_T}$

$$\begin{aligned}
C_{\omega_T, \rho_T} &= \left[ 2 \int_0^1 dx \int \frac{d^2 k_\perp}{(2\pi)^3} \frac{k_\perp^2 + M^2 - 2x\bar{x}k_\perp^2}{(x\bar{x}m_{\omega,\rho}^2 - k_\perp^2 - M^2)^2} \mathcal{F}(k) \mathcal{F}(P - k) \right]^{-1/2} \\
&= \sqrt{2}\pi \left[ \int_0^1 dx \int_0^\infty dz x\bar{x}z \frac{(1 - 2x\bar{x})x\bar{x}z^2 + \frac{\rho^2 M^2}{4\lambda_V^2}}{\left(x\bar{x}z^2 - \frac{\rho^2}{4\lambda_V^2}(x\bar{x}m_{\omega,\rho}^2 - M^2)\right)^2} (zF'(z))^4 \right]^{-1/2}
\end{aligned} \tag{96}$$

and longitudinal  $C_{\omega_L, \rho_L}$

$$C_{\omega_L, \rho_L} = \left[ 2 \int_0^1 dx \int \frac{d^2 k_\perp}{(2\pi)^3} \left( \frac{1}{m_{\omega, \rho}^2} + \frac{4x\bar{x}(k_\perp^2 + M^2)}{(x\bar{x}m_{\omega, \rho}^2 - k_\perp^2 - M^2)^2} \right) \mathcal{F}(k)\mathcal{F}(P-k) \right]^{-1/2} \\ = \sqrt{2}\pi \left[ \int_0^1 dx \int_0^\infty dz x \bar{x} z \left( \frac{4\lambda_V^2}{\rho^2 m_{\omega, \rho}^2} + \frac{4x\bar{x} \left( x\bar{x}z^2 + \frac{\rho^2 M^2}{4\lambda_V^2} \right)}{\left( x\bar{x}z^2 - \frac{\rho^2}{4\lambda_V^2} (x\bar{x}m_{\omega, \rho}^2 - M^2) \right)^2} \right) (zF'(z))^4 \right]^{-1/2} \quad (97)$$

More specifically, the violation of the Lorentz covariance in the light front transverse and longitudinal constants, is captured by the identity

$$\frac{1}{3} \frac{1}{C_{\omega_L, \rho_L}^2} + \frac{2}{3} \frac{1}{C_{\omega_T, \rho_T}^2} = \frac{1}{C_{\omega, \rho}^2} \\ + \frac{2}{3m_{\omega, \rho}^2} \int_0^1 dx \int \frac{d^2 k_\perp}{(2\pi)^3} \mathcal{F}(k)\mathcal{F}(P-k) \quad (98)$$

which reflects on the irremediable loss of Lorentz symmetry on the light front. The spin average of the transverse and longitudinal constants is not equal to the covariant unpolarized constant  $C_{\omega, \rho}^2$ . The discrepancy is of order  $C_{\omega, \rho}^2/(2\pi^2 \rho^2 m_{\omega, \rho}^2)$ . Fortunately, our book-keeping in  $1/N_c$  suggests that

$$\frac{C_{\omega, \rho}^2}{g_{\omega, \rho} m_{\omega, \rho}^2} \sim \mathcal{O}(N_c^0)$$

as also observed in the context of effective models in [63, 64]. As a result, the difference (98) is controlled by the molecular coupling

$$\frac{1}{3} \frac{1}{C_{\omega_L, \rho_L}^2} + \frac{2}{3} \frac{1}{C_{\omega_T, \rho_T}^2} \simeq \frac{1}{C_{\omega, \rho}^2} \left[ 1 + \mathcal{O} \left( \frac{g_V}{2\pi^2 \rho^2} \right) \right] \quad (99)$$

which is parametrically subleading in the QCD instanton vacuum, thanks to its diluteness. Recall that only the leading contributions  $g_V/g_S$  were retained in our bound state analysis both on the light front and in the covariant frame.

To summarize, the normalization constants in the LFWFs from the QCD instanton vacuum are

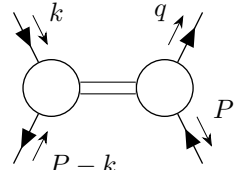
Model	$ C_\sigma $	$ C_\pi $	$ C_{\omega_T, \rho_T} $	$ C_{\omega_L, \rho_L} $	$ C_{\omega, \rho} $
ILM	4.264	7.391	2.420	2.285	2.426

In the last three column of the table,  $C_{\omega_T, \rho_T}$  and  $C_{\omega_L, \rho_L}$  follow from (96) and (97) using the light front analysis, while  $C_{\omega, \rho}$  follows from the covariant analysis (see below). The covariance-violating term

in (98) is numerically estimated to be  $7.734 \times 10^{-3}$  which is of order  $\mathcal{O} \left( \frac{g_V}{2\pi^2 \rho^2} \right)$ , hence parametrically small as we argued.

## B. Bound state wavefunctions in covariant frame

The light front wave functions can also be obtained from the covariant formalism. In this section, we will show that their derivation from the covariant frame, can be shown to agree with our derivation from the light front after a pertinent integration over the light front "energy". More specifically, in the covariant frame the Bethe-Salpeter (BS) wavefunctions are given by the residue of the 4-point Green's function, around the mass pole of each meson channel, or diagrammatically



$$= \frac{-i \sum_\lambda \Psi_\lambda(q; P) \Psi_\lambda^\dagger(k; P)}{P^2 - m_X^2} \quad (100)$$

In the scalar and pseudoscalar channels, the BS wavefunctions are given by

$$\begin{aligned} \Psi_\sigma(k; P) &= g_{\sigma qq} S(k) \sqrt{\mathcal{F}(k)} \sqrt{\mathcal{F}(P-k)} S(k-P) \\ \Psi_{a_0}(k; P) &= g_{a_0 qq} S(k) \sqrt{\mathcal{F}(k)} \tau^a \sqrt{\mathcal{F}(P-k)} S(k-P) \\ \Psi_{\eta'}(k; P) &= g_{\eta' qq} S(k) \sqrt{\mathcal{F}(k)} i\gamma^5 \sqrt{\mathcal{F}(P-k)} S(k-P) \\ \Psi_\pi(k; P) &= g_{\pi qq} S(k) \sqrt{\mathcal{F}(k)} i\gamma^5 \tau^a \sqrt{\mathcal{F}(P-k)} S(k-P) \end{aligned} \quad (101)$$

where  $S(k)$  is the quark propagator, while in the vector channels they are

$$\begin{aligned} \Psi_\omega(k; P) &= g_{\omega qq} \epsilon_\lambda^\mu(P) S(k) \sqrt{\mathcal{F}(k)} \gamma_\mu \sqrt{\mathcal{F}(P-k)} S(k-P) \\ \Psi_\rho(k; P) &= g_{\rho qq} \epsilon_\lambda^\mu(P) S(k) \sqrt{\mathcal{F}(k)} \gamma_\mu \tau^a \sqrt{\mathcal{F}(P-k)} S(k-P) \end{aligned} \quad (102)$$

The effective quark-meson couplings  $g_{Xqq}$  follow as

$$\begin{aligned} g_{\sigma,a_0qq}^2 &= \left( \frac{\partial \Pi_{SS}}{\partial P^2} \right)^{-1} \Big|_{P^2=m_{\sigma,a_0}^2} \\ g_{\pi,\eta'qq}^2 &= \left( \frac{\partial \Pi_{PP}}{\partial P^2} \right)^{-1} \Big|_{P^2=m_{\pi,\eta'}^2} \\ g_{\omega,\rho qq}^2 &= \left( \frac{\partial \Pi_{VV}}{\partial P^2} \right)^{-1} \Big|_{P^2=m_{\omega,\rho}^2} \end{aligned} \quad (103)$$

The light front wavefunctions can be extracted from the covariant BS wavefunctions, by integrating over the light front energy  $k^-$  of BS wavefunctions and projecting out the bounded quark spins

$$\frac{1}{\sqrt{2x\bar{x}}} \Phi_X(x, k_\perp, s_1, s_2) = iP^+ \int_{-\infty}^{\infty} \frac{dk^-}{2\pi} \frac{\bar{u}_{s_1} \gamma^+}{2k^+} \Psi_X(k; P) \frac{\gamma^+ v_{s_2}}{2(P^+ - k^+)} \Big|_{k^+=xP^+} \quad (104)$$

Alternatively, the integration of the BS kernel over the energy  $k^0$  yields the equal-time wavefunction.

In the covariant frame, the normalization constant of each light front wave functions  $C_X$  is related to the effective quark-meson couplings  $g_{Xqq}$  in (103) as

$$g_{Xqq} = -\frac{C_X}{\sqrt{N_c}} \quad (105)$$

Now we can compare the normalization constant de-

rived from the light front formalism and from the covariant formalism. In the latter, the normalization follows from (105). More specifically, in the scalar and pseudoscalar channels the normalization are readily shown to be the same. In the vector channels, the covariant normalization is the same for both longitudinal and transverse by Lorentz symmetry,

$$\begin{aligned} C_{\omega,\rho} &= \left[ \frac{4}{3} \int_0^1 dx \int \frac{d^2 k_\perp}{(2\pi)^3} \frac{k_\perp^2 + (1 + 2x\bar{x})M^2}{(x\bar{x}m_{\omega,\rho}^2 - k_\perp^2 - M^2)^2} \mathcal{F}(k) \mathcal{F}(P - k) \right]^{-1/2} \\ &= \sqrt{3}\pi \left[ \int_0^1 dx \int_0^\infty dz x \bar{x} z \frac{x\bar{x}z^2 + (1 + 2x\bar{x})\frac{\rho^2 M^2}{4\lambda_V^2}}{\left( x\bar{x}z^2 - \frac{\rho^2}{4\lambda_V^2} (x\bar{x}m_{\omega,\rho}^2 - M^2) \right)^2} (zF'(z))^4 \right]^{-1/2} \end{aligned} \quad (106)$$

Using (98) with  $g_V/g_S$  parametrically small, (106) yields

$$C_{\omega,\rho} \simeq C_{\omega_T,\rho_T} \simeq C_{\omega_L,\rho_L} \quad (107)$$

tions are related to the Fourier transform of these matrix elements, which can be calculated using the light front wavefunctions.

## VI. PARTON DISTRIBUTION FUNCTIONS

In general, the partonic structure in a hadron can be studied using pertinent hadronic matrix elements. In leading twist, the only non-trivial partonic structure functions for spin-0 hadrons, are the parton density distributions. For spin-1 hadrons, the other two distributions, helicity and transversity, contribute in leading twist. These distribution func-

### A. Twist-2 parton distribution functions

Throughout, we will mainly focus on the twist-2 partonic structure functions, including the parton density functions for both spin-0 and spin-1 mesons, as well as the spin distribution functions (helicity and transversity) inside the spin-1 hadronic bound states.

## 1. Parton density distributions

---

Parton density distributions are defined as

$$q_X^\lambda(x) = \int_{-\infty}^{\infty} \frac{d\xi^-}{4\pi} e^{ixP^+\xi^-} \langle P\lambda | \bar{\psi}(0) \gamma^+ W(0, \xi^-) \psi(\xi^-) | P\lambda \rangle = \int \frac{d^2 k_\perp}{(2\pi)^3} \sum_{s,s'} |\Phi_X^\lambda(x, k, s, s')|^2 \quad (108)$$

for quarks, and

$$\bar{q}_X^\lambda(x) = \int_{-\infty}^{\infty} \frac{d\xi^-}{4\pi} e^{-ixP^+\xi^-} \langle P\lambda | \bar{\psi}(0) \gamma^+ W(0, \xi^-) \psi(\xi^-) | P\lambda \rangle = \int \frac{d^2 k_\perp}{(2\pi)^3} \sum_{s,s'} |\Phi_X^\lambda(\bar{x}, k, s, s')|^2 \quad (109)$$


---

for the antiquarks, where

$$W(\xi^-, 0) = \exp \left[ -ig \int_0^{\xi^-} d\eta^- A^+(\eta^-) \right]$$

is a light-like gauge link. In the case of the meson PDFs, the quark and antiquark distributions are also

---

related by spin symmetry

$$\bar{q}_X(x) = q_X(x) = q_X(1-x) = \bar{q}_X(1-x).$$

For spin-1 meson, the quark distributions for different polarizations are related also by spin symmetry.

$$q_X^+(x) = q_X^-(x) = q_X^T(x) \quad q_X^0(x) = q_X^L(x)$$

### scalar channels

The  $\sigma$  PDF follows as

$$\begin{aligned} q_\sigma(x) &= 2C_\sigma^2 \int_0^1 dx \int \frac{d^2 k_\perp}{(2\pi)^3} \frac{k_\perp^2 + (x - \bar{x})^2 M^2}{(x\bar{x}m_\sigma^2 - k_\perp^2 - M^2)^2} \mathcal{F}(k) \mathcal{F}(P-k) \\ &= \frac{C_\sigma^2}{2\pi^2} x\bar{x} \int_0^\infty dz z \frac{x\bar{x}z^2 + (x - \bar{x})^2 \frac{\rho^2 M^2}{4\lambda_S^2}}{\left( x\bar{x}z^2 - \frac{\rho^2}{4\lambda_S^2} (x\bar{x}m_\sigma^2 - M^2) \right)^2} (zF'(z))^4 \end{aligned} \quad (110)$$

### pseudoscalar channels

The pion PDF follows as

$$\begin{aligned} q_{\pi,\eta'}(x) &= 2C_\pi^2 \int \frac{d^2 k_\perp}{(2\pi)^3} \frac{k_\perp^2 + M^2}{(x\bar{x}m_\pi^2 - k_\perp^2 - M^2)^2} \mathcal{F}(k) \mathcal{F}(P-k) \\ &= \frac{C_{\pi,\eta'}^2}{2\pi^2} x\bar{x} \int_0^\infty dz z \frac{x\bar{x}z^2 + \frac{\rho^2 M^2}{4\lambda_S^2}}{\left( x\bar{x}z^2 - \frac{\rho^2}{4\lambda_S^2} (x\bar{x}m_{\pi,\eta'}^2 - M^2) \right)^2} (zF'(z))^4 \end{aligned} \quad (111)$$

### vector channels

The vector PDF for the **transverse mode** can be evaluated as

$$q_{\omega,\rho}^T(x) = 2C_{\omega_T,\rho_T}^2 \int \frac{d^2 k_\perp}{(2\pi)^3} \frac{k_\perp^2 + M^2 - 2x\bar{x}k_\perp^2}{(x\bar{x}m_{\omega,\rho}^2 - k_\perp^2 - M^2)^2} \mathcal{F}(k) \mathcal{F}(P-k) \quad (112)$$

The PDF for the **longitudinal mode** can be evaluated as

$$q_{\omega,\rho}^L(x) = 2C_{\omega_L,\rho_L}^2 \int \frac{d^2 k_\perp}{(2\pi)^3} \left[ \frac{1}{m_{\omega,\rho}^2} + \frac{4x\bar{x}(k_\perp^2 + M^2)}{(x\bar{x}m_{\omega,\rho}^2 - k_\perp^2 - M^2)^2} \right] \mathcal{F}(k) \mathcal{F}(P-k) \quad (113)$$

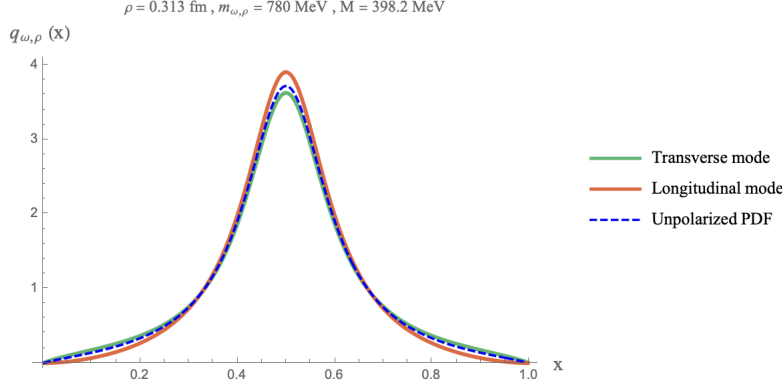


FIG. 10: Vector mesons PDFs versus parton- $x$ : transverse polarization (solid-green), longitudinal polarization (solid-red) and unpolarized (dashed-blue).

As we noted earlier, the difference between the longitudinal and transverse normalizations in QCD instanton vacuum on the light front is controlled by the ratio  $g_V/g_S$  which is parametrically small. Recall that in our book-keeping analysis in leading order in  $1/N_c$  only the leading  $g_V/g_S$  are also to be retained in the dilute limit. With this in mind, in the QCD instanton vacuum we obtain

$$q_{\omega, \rho}^T(x) \simeq \frac{C_{\omega, \rho}^2}{2\pi^2} x\bar{x} \int_0^\infty dz z \frac{(1 - 2x\bar{x})x\bar{x}z^2 + \frac{\rho^2 M^2}{4\lambda_V^2}}{\left(x\bar{x}z^2 - \frac{\rho^2}{4\lambda_X^2}(x\bar{x}m_{\omega, \rho}^2 - M^2)\right)^2} (zF'(z))^4 \quad (114)$$

$$q_{\omega, \rho}^L(x) \simeq \frac{C_{\omega, \rho}^2}{2\pi^2} x\bar{x} \int_0^\infty dz z \frac{4x\bar{x} \left(x\bar{x}z^2 + \frac{\rho^2 M^2}{4\lambda_V^2}\right)}{\left(x\bar{x}z^2 - \frac{\rho^2}{4\lambda_X^2}(x\bar{x}m_{\omega, \rho}^2 - M^2)\right)^2} (zF'(z))^4 + \mathcal{O}\left(\frac{g_V}{2\pi^2 \rho^2} x\bar{x}\right) \quad (115)$$

The polarization average over transverse mode and longitudinal mode yields the **unpolarized PDF**.

$$\begin{aligned} q_{\omega, \rho}(x) &= \frac{2}{3} q_{\omega, \rho}^T(x) + \frac{1}{3} q_{\omega, \rho}^L(x) \\ &\simeq \frac{4}{3} C_{\omega, \rho}^2 \int \frac{d^2 k_\perp}{(2\pi)^3} \frac{k_\perp^2 + (1 + 2x\bar{x})M^2}{(x\bar{x}m_{\omega, \rho}^2 - k_\perp^2 - M^2)^2} \mathcal{F}(k) \mathcal{F}(P - k) \\ &= \frac{C_{\omega, \rho}^2}{3\pi^2} x\bar{x} \int_0^\infty dz z \frac{x\bar{x}z^2 + (1 + 2x\bar{x})\frac{\rho^2 M^2}{4\lambda_V^2}}{\left(x\bar{x}z^2 - \frac{\rho^2}{4\lambda_X^2}(x\bar{x}m_{\omega, \rho}^2 - M^2)\right)^2} (zF'(z))^4 \end{aligned} \quad (116)$$

In Fig. 10 we show our results for the vector mesons PDFs versus  $x$ , in the QCD instanton vacuum for  $\rho = 0.313$  fm,  $m_{\omega, \rho} = 780$  MeV and a constituent mass  $M = 398.2$  MeV. The transverse PDF for the vectors is in solid-green, the longitudinal PDF for the vectors is in solid-red and the unpolarized PDF in dashed-blue. Note the small differences due to the parametrically small value of  $g_V/g_S$ , with the exception of the end-points for the longitudinal polarization. The unpolarized PDF is identical to that from the covariant analysis. In Fig. 11 we show the parton density functions versus parton- $x$ , for the sigma meson in solid-green, the pion in solid-blue and the rho meson in solid-red in the chiral limit. In this limit, the constituent mass is  $M = 372.3$  MeV.

## 2. Spin dependent parton distributions

For mesons with spin, we can also probe the parton distribution in a polarized hadron. In the case of spin-1 mesons, the spin dependent parton distribution can be described by the helicity distribution functions.

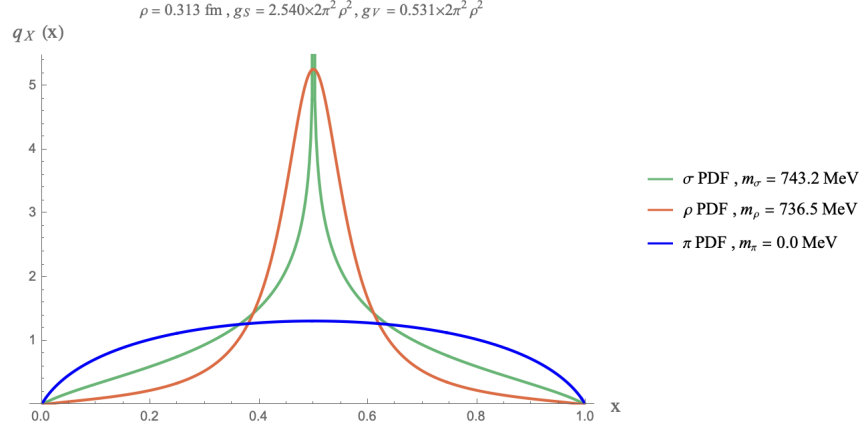


FIG. 11: Parton density functions in the chiral limit.

For quarks, the helicity distribution is given by

$$\Delta q_X^\lambda(x) = \int_{-\infty}^{\infty} \frac{d\xi^-}{4\pi} e^{ixP^+\xi^-} \langle P\lambda | \bar{\psi}(0) \gamma^+ \gamma^5 W(0, \xi^-) \psi(\xi^-) | P\lambda \rangle = \int \frac{d^2 k_\perp}{(2\pi)^3} \sum_{s,s'} s |\Phi_X^\lambda(x, k, s, s')|^2 \quad (117)$$

and for the antiquarks, it is given by

$$\Delta \bar{q}_X^\lambda(x) = \int_{-\infty}^{\infty} \frac{d\xi^-}{4\pi} e^{-ixP^+\xi^-} \langle P\lambda | \bar{\psi}(0) \gamma^+ \gamma^5 W(0, \xi^-) \psi(\xi^-) | P\lambda \rangle = \int \frac{d^2 k_\perp}{(2\pi)^3} \sum_{s,s'} s' |\Phi_X^\lambda(\bar{x}, k, s, s')|^2 \quad (118)$$

Charge symmetry implies that the helicity distributions for the quarks and antiquarks are tied

$$\Delta \bar{q}_X(x) = \Delta q_{\bar{X}}(x) = \Delta q_X(1-x) = \Delta \bar{q}_{\bar{X}}(1-x)$$

The quark helicity distributions for different polar-

izations are also related by spin symmetry,

$$\Delta q_X^+(x) = -\Delta q_X^-(x) \quad \Delta q_X^0(x) = 0$$

Due to the charge symmetry, the quark and antiquark should contribute to the meson helicity equally. Therefore, the helicity distribution in the longitudinal state is zero. Only the transverse modes have nontrivial helicity parton distribution, hence

$$\begin{aligned} \Delta q_{\omega,\rho}^\pm(x) &= \pm \frac{C_{\omega,\rho}^2}{2} \int \frac{d^2 k_\perp}{(2\pi)^3} \frac{xk_\perp^2 + M^2}{(x\bar{x}m_{\omega,\rho}^2 - k_\perp^2 - M^2)^2} \mathcal{F}(k) \mathcal{F}(P-k) \\ &= \pm \frac{C_{\omega,\rho}^2}{4\pi^2} \int_{\frac{\rho M}{2\lambda_M \sqrt{x\bar{x}}}}^{\infty} dz z \frac{xz^2 + \frac{\rho^2 M^2}{4x\lambda_M^2}}{\left(\frac{\rho^2 m_{\omega,\rho}^2}{4\lambda_M^2} - z^2\right)^2} (zF'(z))^4 \end{aligned} \quad (119)$$

The result satisfies the helicity sum rule,

$$\int_0^1 dx [\Delta q_{\omega,\rho}^\lambda(x) + \Delta q_{\omega,\rho}^\lambda(1-x)] = \lambda \quad (120)$$

As expected, the quark and antiquark contributes to

the meson helicity equally.

In Fig. 12 we show the parton helicity polarization in a vector meson with transverse polarization  $\lambda = +$  versus parton- $x$ , in the QCD instanton vac-

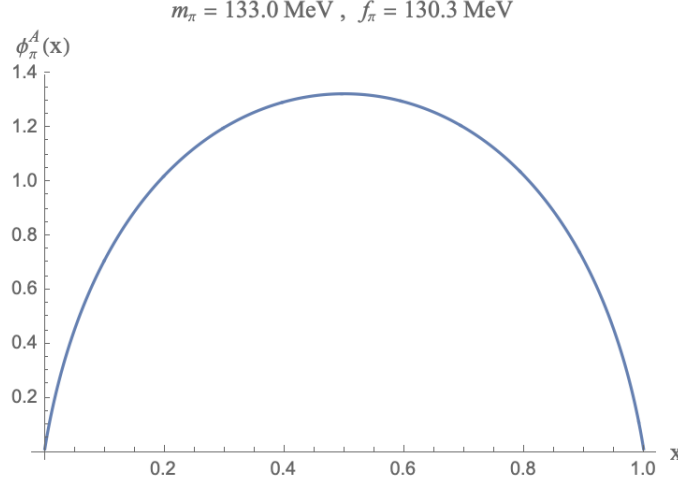


FIG. 13: The un-evolved pion DA versus parton- $x$  at low resolution, in the the QCD instanton vacuum.

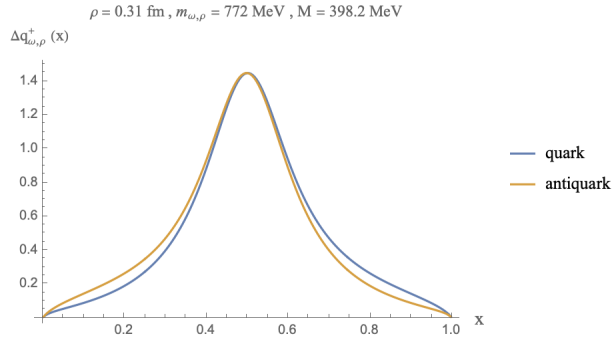


FIG. 12: Helicity distribution function for the quark (solid-blue) and the anti-quark (solid-brown) in a +polarized vector meson, versus parton- $x$ .

uum. The quark helicity polarization is shown in solid-blue, and the anti-quark helicity polarization is shown in solid-brown. The helicity distributions are comparable away from the end-points.

## VII. MESON DISTRIBUTION AMPLITUDES

In general, the distribution amplitudes (DAs) are the leading twist transition matrix elements between a pertinent hadron and the vacuum. Throughout, the DAs will be normalized to 1.

### A. Pseudoscalar meson distribution amplitude

The twist-2 DA of the pseudoscalar meson is defined as

$$\langle 0 | \bar{\psi}(0) \gamma^+ \gamma^5 \frac{\tau^a}{\sqrt{2}} W(0, \xi^-) \psi(\xi^-) | \pi^a(P) \rangle = i f_\pi P^+ \int_0^1 dx e^{-ixP^+ \xi^-} \phi_\pi^A(x) \quad (121)$$



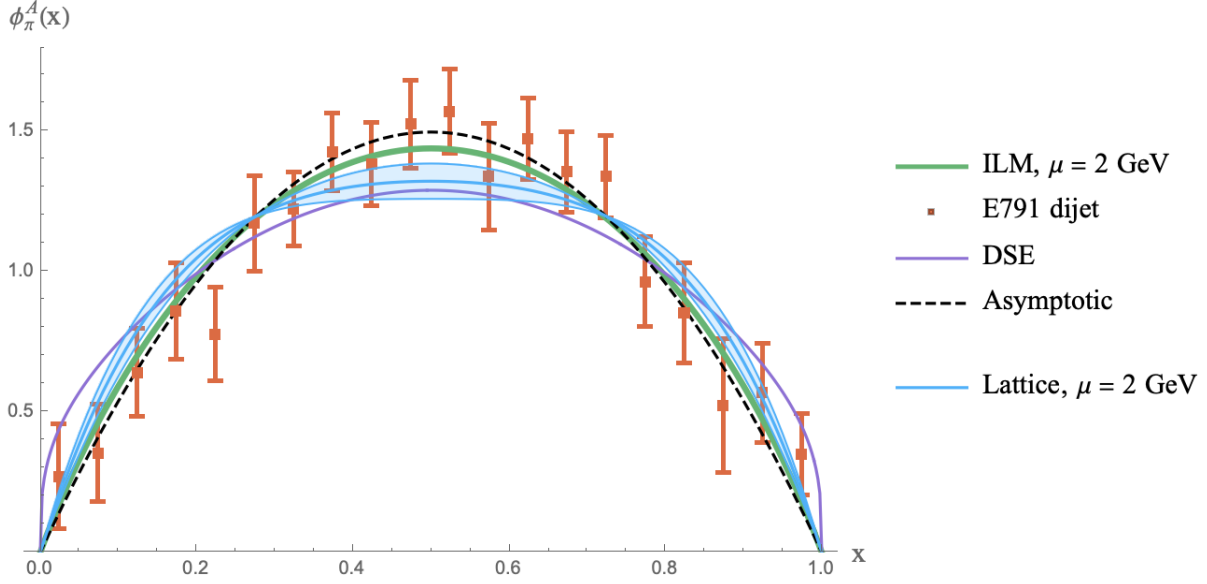


FIG. 14: The evolved pion DA using the NLO ERBL equation to  $\mu = 2$  GeV (solid-green), compared with the lattice calculation (RQCD) (shaded-blue) [65], Dyson-Schwinger result [66] (solid-purple) and the asymptotic QCD result (dashed-black). The experimental data points (red squared points) are extracted from  $\pi^-$  into di-jets via diffractive dissociation with invariant dijet mass 6 GeV [67] and normalized in [68].

where the pion decay constant is defined as

$$\langle 0 | \bar{\psi} \gamma^\mu \gamma^5 \frac{\tau^a}{\sqrt{2}} \psi | \pi^a(P) \rangle = i f_\pi P^\mu \quad (122)$$

For  $\pi^\mp$ , we have  $\tau^\pm = (\tau^1 \pm i\tau^2)/\sqrt{2}$  and for  $\pi^0$ , we have  $\tau^3$ . Hence, the twist-2 DA of the pseudoscalar meson can be expressed in terms of the light front pion wave function

$$\phi_\pi^A(x) = 4 \frac{\sqrt{2N_c}M}{f_\pi} \int \frac{d^2k_\perp}{(2\pi)^3} \frac{\phi_\pi(x, k_\perp)}{\sqrt{2x\bar{x}}} [x\mathcal{F}(P-k) + \bar{x}\mathcal{F}(k)] \quad (123)$$

Similarly, the decay constant can also be written in terms of the light front wave function.

$$f_\pi = 4\sqrt{2N_c}M \int_0^1 dx \int \frac{d^2k_\perp}{(2\pi)^3} \frac{\phi_\pi(x, k_\perp)}{\sqrt{2x\bar{x}}} [x\mathcal{F}(P-k) + \bar{x}\mathcal{F}(k)] \quad (124)$$

To enforce axial current conservation, it is natural to assume that

$$x\mathcal{F}(P-k) + \bar{x}\mathcal{F}(k) \approx \mathcal{F}\left(\frac{k_\perp}{2\lambda_S\sqrt{x\bar{x}}}\right)$$

Thus, the pion DA with the quark form factor is

$$\phi_\pi^A(x) = \frac{\sqrt{2N_c}M}{2\pi^2 f_\pi} C_\pi x\bar{x} \int_0^\infty dz \frac{z}{\frac{\rho^2}{4\lambda_S^2}(x\bar{x}m_\pi^2 - M^2) - x\bar{x}z^2} (zF'(z))^4 \quad (125)$$

and the pion decay constant with the quark form factor is

$$f_\pi = \frac{\sqrt{2N_c}M}{2\pi^2} C_\pi \int_0^1 dx \int_0^\infty dz x\bar{x} z \frac{1}{\frac{\rho^2}{4\lambda_S^2}(x\bar{x}m_\pi^2 - M^2) - x\bar{x}z^2} (zF'(z))^4 \quad (126)$$

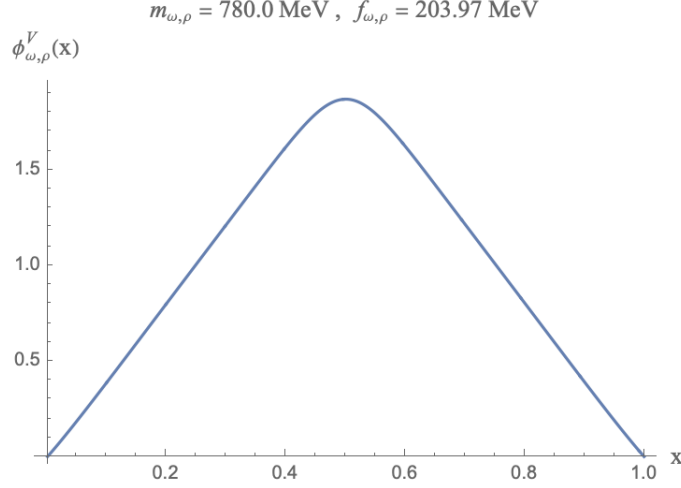


FIG. 15: Un-evolved longitudinal vector DA in the QCD instanton vacuum at low resolution with  $\mu \sim 1/2\rho$ .

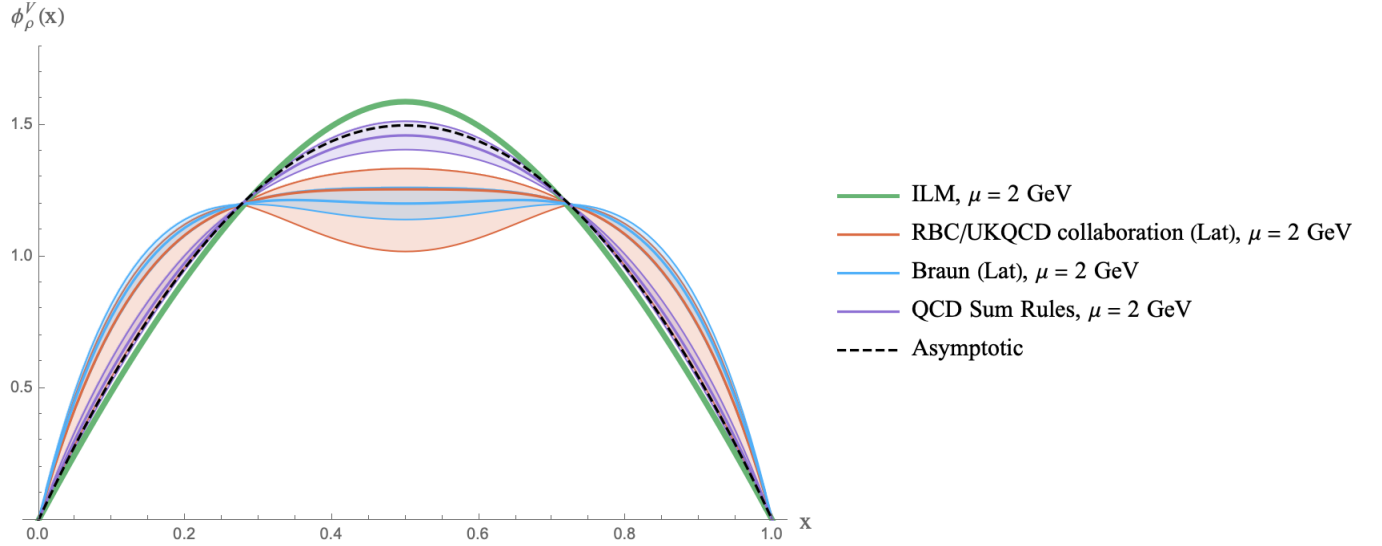


FIG. 16: Evolved longitudinal  $\rho$  DA to  $\mu = 2$  GeV in solid-green, compared with the lattice in RBC/UKQCD collaboration [69] in filled-red and the lattice [70] in filled-blue. The QCD asymptotic result of  $6x\bar{x}$  is in dashed-black and the QCD sum result [71] is in filled-purple.

The pion (axial) DA  $\phi^A(x)$  is normalized to 1

$$\int_0^1 dx \phi_\pi^A(x) = 1 \quad (127)$$

In Fig. 13 we show the un-evolved pion DA versus parton- $x$ , in the QCD instanton vacuum at low resolution. Our result for the evolved pion DA is shown in Fig. 14 in solid-blue, using the NLO ERBL equation to a scale of  $\mu = 2$  GeV. Our result is compared to the QCD asymptotic result in dashed-black, the lattice calculation from the RQCD collaboration [65] in shaded-purple, and the Dyson-Schwinger-Equation (DSE) in solid-green [66]. The empirical pion DA data points in brown, are extracted from  $\pi^-$  into di-jets via diffractive dissociation with invariant dijet mass 6 GeV [67], with the normalization discussed in [68].

### B. Longitudinally polarized vector meson distribution amplitude

The leading twist DA of the longitudinally polarized vector meson is defined as

$$\langle 0 | \bar{\psi}(0) \gamma^+ \frac{1}{\sqrt{2}} W(0, \xi^-) \psi(\xi^-) | \omega(\lambda, P) \rangle = f_\omega m_\omega \epsilon_\lambda^+(P) \int_0^1 dx e^{-ixP^+ \xi^-} \phi_\omega^V(x) \quad (128)$$

$$\langle 0 | \bar{\psi}(0) \gamma^+ \frac{\tau^a}{\sqrt{2}} W(0, \xi^-) \psi(\xi^-) | \rho(\lambda, P) \rangle = f_\rho m_\rho \epsilon_\lambda^+(P) \int_0^1 dx e^{-ixP^+ \xi^-} \phi_\rho^V(x) \quad (129)$$

where the vector meson decay constants are set by

$$\langle 0 | \bar{\psi} \gamma^\mu \frac{1}{\sqrt{2}} \psi | \omega(P, \lambda) \rangle = f_\omega m_\omega \epsilon_\lambda^\mu(P) \quad (130)$$

$$\langle 0 | \bar{\psi} \gamma^\mu \frac{\tau^a}{\sqrt{2}} \psi | \rho^a(P, \lambda) \rangle = f_\rho m_\rho \epsilon_\lambda^\mu(P) \quad (131)$$

The longitudinal meson distribution amplitude is related to the light front wavefunction through

$$\phi_{\omega, \rho}^V(x) = -\frac{2\sqrt{2N_c}}{f_{\omega, \rho} m_{\omega, \rho}} \int \frac{d^2 k_\perp}{(2\pi)^3} \frac{\phi_{\omega, \rho}(x, k_\perp)}{\sqrt{2x\bar{x}}} 2 [x\bar{x}m^2 + k_\perp^2 + M(k)M(P-k)] \quad (132)$$

To avoid the non-local effect of the emergent interactions [38, 72, 73], we will limit the analysis to the longitudinally polarized vector meson. We recall that the non-local vertices in this case are purely transverse, hence blind to the longitudinal polarization through minimal substitution. With this in mind, the longitudinally polarized vector meson contribution to the decay amplitude is

$$f_{\omega, \rho} = -\frac{2\sqrt{2N_c}}{m_{\omega, \rho}} \int_0^1 dx \int \frac{d^2 k_\perp}{(2\pi)^3} \frac{\phi_{\omega, \rho}(x, k_\perp)}{\sqrt{2x\bar{x}}} 2 [x\bar{x}m_{\omega, \rho}^2 + k_\perp^2 + M^2 \mathcal{F}(k) \mathcal{F}(P-k)] \quad (133)$$

To recover the Lorentz covariance and enforce current conservation, we remove the Lorentz violating term by approximating

$$x\bar{x}m_{\omega, \rho}^2 + k_\perp^2 + M(k)M(P-k) \approx 2(k_\perp^2 + M^2) \mathcal{F}^2\left(\frac{k_\perp}{2\lambda_V \sqrt{x\bar{x}}}\right)$$

which amounts to

$$f_{\omega, \rho} = -\frac{\sqrt{2N_c}}{4\pi^2 m_{\omega, \rho}} C_{\omega_L, \rho_L} \frac{4\lambda_V^2}{\rho^2} \int_0^1 dx \int_0^\infty dz z \frac{4x\bar{x} \left[ \frac{\rho^2 M^2}{4\lambda_V^2} + x\bar{x}z^2 \right]}{\left[ \frac{\rho^2}{4\lambda_V^2} (x\bar{x}m_{\omega, \rho}^2 - M^2) - x\bar{x}z^2 \right]} (zF'(z))^6 \quad (134)$$

hence the longitudinally polarized vector meson DA

$$\phi_{\omega, \rho}^V(x) = -\frac{\sqrt{2N_c}}{4\pi^2 f_{\omega, \rho} m_{\omega, \rho}} C_{\omega_L, \rho_L} \frac{4\lambda_V^2}{\rho^2} \int_0^\infty dz z \frac{4x\bar{x} \left[ \frac{\rho^2 M^2}{4\lambda_V^2} + x\bar{x}z^2 \right]}{\left[ \frac{\rho^2}{4\lambda_V^2} (x\bar{x}m_{\omega, \rho}^2 - M^2) - x\bar{x}z^2 \right]} (zF'(z))^6 \quad (135)$$

In Fig. 15 we show the un-evolved longitudinal vector meson DA versus parton- $x$ , in the QCD instanton vacuum at low resolution  $\mu \sim 1/2\rho$ . The evolved DA using NLO ERBL to  $\mu = 2 \text{ GeV}$ , is shown in Fig. 16 as solid-blue, and compared to the QCD asymptotic result  $6x\bar{x}$  as dashed-black, and the QCD sum rule result from [71] as filled-purple. The lattice results from [69] are in filled-brown, and the lattice from [70] are in filled-green.

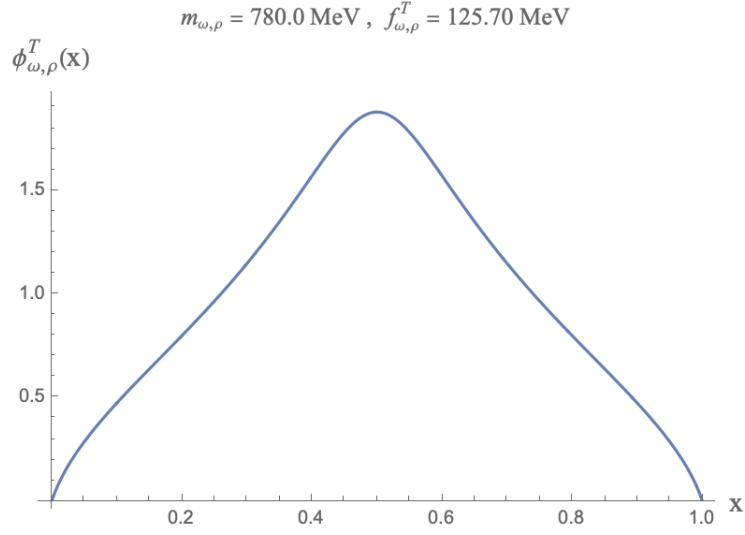


FIG. 17: Un-evolved transverse DA for a vector meson in the QCD instanton vacuum at a resolution  $\mu \sim 1/2\rho$ .

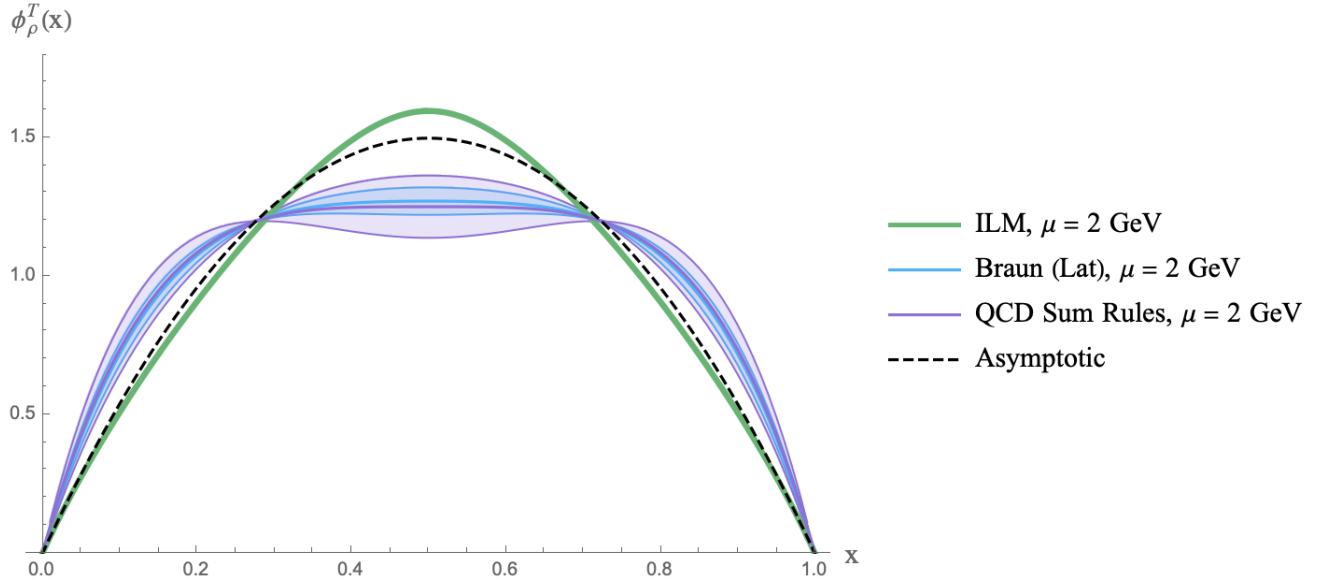


FIG. 18: Evolved transverse DA for the rho meson at  $\mu = 2 \text{ GeV}$  in solid-green, and compared with the lattice result at  $\mu = 2 \text{ GeV}$  [70] in filled-blue and the QCD sum rule result also at  $\mu = 2 \text{ GeV}$  [74] in filled-purple.

### C. Transversely polarized vector meson distribution amplitude

The general twist-2 DAs for the transversely polarized vector mesons are

$$\langle 0 | \bar{\psi}(0) i\gamma^+ \gamma_\perp^i \frac{1}{\sqrt{2}} W(0, \xi^-) \psi(\xi^-) | \omega(\lambda, P) \rangle = -i f_\omega^T P^+ \epsilon_\lambda^i(P) \int_0^1 dx e^{-ixP^+ \xi^-} \phi_\omega^T(x) \quad (136)$$

$$\langle 0 | \bar{\psi}(0) i \gamma^+ \gamma_\perp^a \frac{\tau^a}{\sqrt{2}} W(0, \xi^-) \psi(\xi^-) | \rho(\lambda, P) \rangle = -i f_\omega^T P^+ \epsilon_\lambda^i(P) \int_0^1 dx e^{-ixP^+ \xi^-} \phi_\rho^T(x) \quad (137)$$

where the transverse decay constants are defined as

$$\langle 0 | \bar{\psi} \sigma^{\mu\nu} \frac{1}{\sqrt{2}} \psi | \omega(P, \lambda) \rangle = i f_\omega^T (\epsilon_\lambda^\mu P^\nu - \epsilon_\lambda^\nu P^\mu) \quad (138)$$

$$\langle 0 | \bar{\psi} \sigma^{\mu\nu} \frac{\tau^a}{\sqrt{2}} \psi | \rho^a(P, \lambda) \rangle = i f_\rho^T (\epsilon_\lambda^\mu P^\nu - \epsilon_\lambda^\nu P^\mu) \quad (139)$$

Using the light front wave functions, we obtain

$$\phi_{\omega, \rho}^T(x) = -4 \frac{\sqrt{2N_c} M}{f_{\omega, \rho}^T} \int \frac{d^2 k_\perp}{(2\pi)^3} \frac{\phi_{\omega, \rho}(x, k_\perp)}{\sqrt{2x\bar{x}}} [x\mathcal{F}(P-k) + \bar{x}\mathcal{F}(k)] \quad (140)$$

with the vector meson decay constant

$$f_{\omega, \rho}^T = -4 \sqrt{2N_c} M \int_0^1 dx \int \frac{d^2 k_\perp}{(2\pi)^3} \frac{\phi_{\omega, \rho}(x, k_\perp)}{\sqrt{2x\bar{x}}} [x\mathcal{F}(P-k) + \bar{x}\mathcal{F}(k)] \quad (141)$$

following from the normalization of the DA to 1. Again, to enforce current conservation we approximate

$$x\mathcal{F}(P-k) + \bar{x}\mathcal{F}(k) \approx \mathcal{F}\left(\frac{k_\perp}{2\lambda_V \sqrt{x\bar{x}}}\right)$$

which yields the DA

$$\phi_{\omega, \rho}^T(x) = -\frac{\sqrt{2N_c} M}{2\pi^2 f_{\omega, \rho}^T} C_{\omega_T, \rho_T} \int_0^\infty dz x \bar{x} z \frac{1}{\frac{\rho^2}{4\lambda_V^2} (x\bar{x} m_{\omega, \rho}^2 - M^2) - x\bar{x} z^2} (zF'(z))^4 \quad (142)$$

and the transverse vector meson decay constant

$$f_{\omega, \rho}^T = -\frac{\sqrt{2N_c} M}{2\pi^2} C_{\omega_T, \rho_T} \int_0^1 dx \int_0^\infty dz x \bar{x} z \frac{1}{\frac{\rho^2}{4\lambda_V^2} (x\bar{x} m_{\omega, \rho}^2 - M^2) - x\bar{x} z^2} (zF'(z))^4 \quad (143)$$

The transverse decay constant  $f_{\omega, \rho}^T$  is scale-dependent due to the nonzero anomalous dimension of the tensor current [75],

$$f_{\omega, \rho}^T(\mu) = f_{\omega, \rho}^T(\mu_0) \left( \frac{\alpha_s(\mu)}{\alpha_s(\mu_0)} \right)^{C_F/\beta_0} \quad (144)$$

using the one-loop perturbative QCD result, with  $C_F = \frac{N_c^2 - 1}{2N_c}$  and  $\beta_0 = 11 - \frac{2}{3}N_f$ .

In Fig. 17 we show the un-evolved transverse DA versus parton- $x$ , in the QCD instanton vacuum at low resolution  $\mu \sim 1/2\rho$ . The evolved transverse DA using NLO ERBL to  $\mu = 2$  GeV, is shown in Fig. 18 in solid-blue, and compared to the QCD asymptotic result  $6x\bar{x}$  in dashed-black. The lattice results at  $\mu = 2$  GeV [70] are shown in filled-brown, and the QCD sum rule result also at  $\mu = 2$  GeV [74] are shown in filled-purple.

#### D. End-point behavior and ERBL evolution

The comparison between our results in the QCD instanton vacuum at low resolution  $\mu = 0.313$  GeV, and the data as well as the lattice results at higher resolution at  $\mu = 2$  GeV, required the use of the

Efremov-Radyushkin-Brodsky-Lepage (ERBL) evolution of the DA, briefly reviewed in Appendix E. Recall that the anomalous dimensions for  $\phi_\pi^A$  and  $\phi_{\omega, \rho}^V$  are the same (conserved currents, but only in the chiral limit for the former), while the anomalous dimension for  $\phi_{\omega, \rho}^T$  is different due to the running

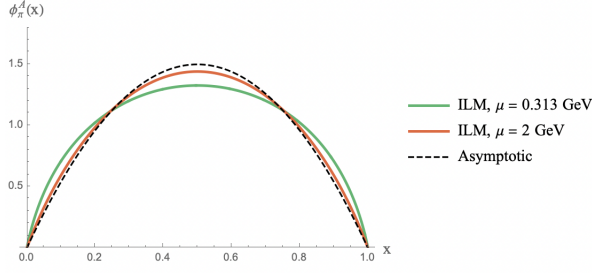


FIG. 19: The pion twist-2 distribution amplitude at  $\mu = 0.313$  GeV,  $\mu = 2$  GeV and  $\mu = \infty$  (asymptotic form)

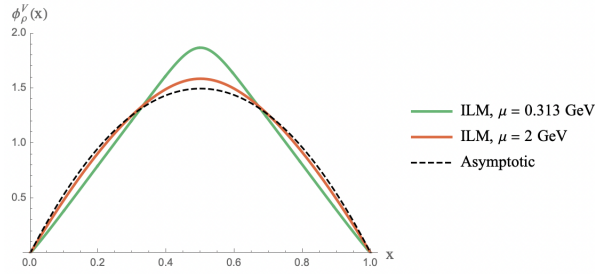


FIG. 20: The longitudinally polarized vector twist-2 distribution amplitude at  $\mu = 0.313$  GeV,  $\mu = 2$  GeV and  $\mu = \infty$  (asymptotic form)

of the quark tensor current. We now focus on the behavior of the end-points for the pseudoscalar and vector DAs.

In Fig. 19 we show the twist-2 pion DA versus parton- $x$  in the QCD instanton vacuum at low resolution with  $\mu = 0.313$  GeV in solid-green, the evolved DA with  $\mu = 2$  GeV in solid-red, and the QCD asymptotic result  $6x\bar{x}$  in dashed-black. We note that  $\phi_\pi^A(x \rightarrow 1, \mu = 0.313 \text{ GeV}) \sim 10.56(1-x)^{0.959}$  near the end point, and asymptotes the QCD result at

infinite resolution.

In Fig. 20 we show the longitudinally polarized vector twist-2 DA versus parton- $x$ , in the QCD instanton vacuum at low resolution with  $\mu = 0.313$  GeV in solid-green, the evolved DA with  $\mu = 2$  GeV in solid-red, and the QCD asymptotic result  $6x\bar{x}$  in dashed-black. The longitudinal vector DA at the end point scales as  $\phi_\rho^V(x \rightarrow 1, \mu = 0.313 \text{ GeV}) \sim 3.68(1-x)^{1.0067}$  asymptotically. The evolution broadens somewhat the DA.

In Fig. 21 we show the transversely polarized vector twist-2 DA versus parton- $x$ , in the QCD instanton vacuum at low resolution with  $\mu = 0.313$  GeV in solid-green, the evolved DA with  $\mu = 2$  GeV in solid-red, and the QCD asymptotic result  $6x\bar{x}$  in dashed-black. The end point behavior of the transversely polarized vector twist-2 distribution amplitude scales as  $\phi_\rho^T(x \rightarrow 1, \mu = 0.313 \text{ GeV}) \sim 6.37(1-x)^{0.9402}$  at the initial scale. The evolution depletes the DA near the end-points, by increasing the power and eventually the DA will approach its asymptotic form.

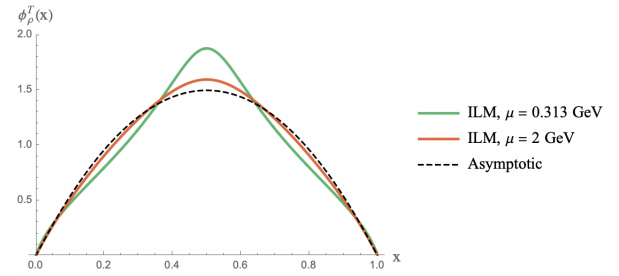


FIG. 21: The transversely polarized vector twist-2 distribution amplitude at  $\mu = 0.313$  GeV,  $\mu = 2$  GeV and  $\mu = \infty$  (asymptotic form)

solid-red, and the QCD asymptotic result  $6x\bar{x}$  in dashed-black. The end point behavior of the transversely polarized vector twist-2 distribution amplitude scales as  $\phi_\rho^T(x \rightarrow 1, \mu = 0.313 \text{ GeV}) \sim 6.37(1-x)^{0.9402}$  at the initial scale. The evolution depletes the DA near the end-points, by increasing the power and eventually the DA will approach its asymptotic form.

### E. Meson decay constants

In the QCD instanton vacuum with the fixed parameters detailed above, we obtain for the pseudoscalar and vector decay constants

$$f_\pi = 130.3 \text{ MeV} \quad f_\rho = 203.97 \text{ MeV} \quad f_\rho^T = 125.70 \text{ MeV} \quad f_\rho^T / f_\rho = 0.6163$$

Cata and Mateu [76] have argued that in the large  $N_c$  limit that  $f_\rho^T / f_\rho = 1/\sqrt{2} \simeq 0.707$ . Our result is consistent with this ratio. Our results are compared with the lattice calculations [70], and the values quoted by the Particle Data Group [77] in the table below. The transverse  $\rho$  decay constant  $f_\rho^T$  is evolved to 2 GeV starting from 0.313 GeV using (144) when compared with the lattice. We display the results at  $Q = 2$  GeV.

	$f_\pi$ (MeV)	$f_\rho$ (MeV)	$f_\rho^T$ (MeV)	$f_\rho^T/f_\rho$
ILM(this work)	130.3	203.97	92.48	0.453
Lattice (2GeV) [70]	-	199(4)(1)	124(4)(1)	0.629(8)
PDG (exp) [77]	$130.3 \pm 0.3$	$210 \pm 4$	-	-

### VIII. MESON ELECTROMAGNETIC FORM FACTORS

The electromagnetic form factor  $F_X(Q^2)$  in hadron-X, is given by the transition matrix element of the EM current

$$J_{EM}^\mu = \sum_f Q_f \bar{\psi}_f \gamma^\mu \psi_f \quad (145)$$

• **spin-0 meson electromagnetic form factor**

$$\langle X(P') | J_{EM}^\mu | X(P) \rangle = F_X(Q^2) (P + P')^\mu \quad (146)$$

• **spin-1 meson electromagnetic form factor**

$$\begin{aligned} \langle X(\lambda', P') | J_{EM}^\mu | X(\lambda, P) \rangle = & \left[ F_{1X}(Q^2) \epsilon_{\lambda'}^*(P') \cdot \epsilon_\lambda(P) - F_{2X}(Q^2) \frac{q \cdot \epsilon_\lambda(P) q \cdot \epsilon_{\lambda'}^*(P')}{2m_X^2} \right] (P + P')^\mu \\ & - F_{3X}(Q^2) [\epsilon_{\lambda'}^{\mu*}(P') q \cdot \epsilon_\lambda(P) - \epsilon_\lambda^\mu(P) q \cdot \epsilon_{\lambda'}^*(P')] \end{aligned} \quad (147)$$

with fixed momentum transfer  $q = P' - P$  and  $Q^2 = -q^2 = q_\perp^2$ . They capture the charge and current distributions inside the hadron. For spin-1 mesons, we have three-types of form factors  $F_{1X}$ ,  $F_{2X}$ ,  $F_{3X}$ . From these form factors one can define the three Sachs form factors [78, 79] for the spin-1 meson, namely, the charge  $G_C^X(Q^2)$ , the magnetic  $G_M^X(Q^2)$  and the quadrupole  $G_Q^X(Q^2)$  form factors. The relation between the Lorentz invariant form factors  $F_1^X$ ,  $F_2^X$ , and  $F_3^X$  and the Sachs form factors are

$$G_C^X(Q^2) = F_{1X}(Q^2) + \frac{Q^2}{6m_X^2} G_Q^X(Q^2) \quad (148)$$

$$G_M^X(Q^2) = F_{3X}(Q^2) \quad (149)$$

$$G_Q^X(Q^2) = F_{1X}(Q^2) + \left(1 + \frac{Q^2}{4m_X^2}\right) F_{2X}(Q^2) - F_{3X}(Q^2) \quad (150)$$

In the presence of non-local interactions, the Noether construction is more subtle, as additional contributions from the emerging non-local interactions are needed to enforce current conservation in general [38, 72, 73]. Fortunately, in the light front formalism, the contributions from the non-local vertices of the emerging effective action, do not contribute in the leading twist approximation [38]. Throughout, we will restrict our discussion of the EM form factors to the leading twist approximation.

The leading-twist form factor (charge form factor  $G_C^X$ ) can be evaluated by the plus component of the spin-averaged meson matrix element in the  $q^+ = 0$  frame,

• **spin-0 meson form factor**

$$F_X(Q^2) = \frac{1}{2P^+} \langle X(P') | J_{EM}^+ | X(P) \rangle \quad (151)$$

• **spin-1 meson form factor**

$$F_X(Q^2) = \frac{1}{2P^+} \left[ \frac{1}{3} \sum_\lambda \langle X(\lambda, P') | J_{EM}^+ | X(\lambda, P) \rangle \right] \quad (152)$$

If we choose a specific frame where  $q^+ = 0$ , with

$$P^\mu = \left( P^+, 0, \frac{m_X^2}{2P^+} \right), \quad P'^\mu = \left( P^+, q_\perp, \frac{m_X^2 + q_\perp^2}{2P^+} \right),$$

the meson form factor follows as

$$F_X(Q^2) = \int_0^1 dx \int \frac{d^2 k_\perp}{(2\pi)^3} \left[ \Phi_X^*(x, k_\perp + \bar{x}q_\perp, s'_1, s'_2) Q_{f_1} \frac{\bar{u}_{s'_1}(k+q) \gamma^+ u_{s_1}(k)}{2xP^+} \delta_{s'_2, s_2} \Phi_X(x, k_\perp, s_1, s_2) \right. \\ \left. - \Phi_X^*(x, k_\perp - xq_\perp, s'_1, s'_2) Q_{f_2} \frac{\bar{v}_{s'_2}(k) \gamma^+ v_{s'_2}(k+q)}{2\bar{x}P^+} \delta_{s'_1, s_1} \Phi_X(x, k_\perp, s_1, s_2) \right] \quad (153)$$

More specifically, in the pion channel it is given by

$$F_\pi(Q^2) = \int_0^1 dx \int \frac{d^2 k_\perp}{(2\pi)^3} \left[ Q_u \phi_\pi(x, k_\perp + \bar{x}q_\perp) \phi_\pi(x, k_\perp) 4 \left( \frac{k_\perp^2 + M^2 + \bar{x}k_\perp \cdot q_\perp}{x\bar{x}} \right) \right. \\ \left. - Q_d \phi_\pi(x, k_\perp - xq_\perp) \phi_\pi(x, k_\perp) 4 \left( \frac{k_\perp^2 + M^2 - xk_\perp \cdot q_\perp}{x\bar{x}} \right) \right] \quad (154)$$

while in the vector channel it reads

$$F_{\omega, \rho}(Q^2) = \int_0^1 dx \int \frac{d^2 k_\perp}{(2\pi)^3} \left[ Q_u \phi_{\omega, \rho}(x, k_\perp + \bar{x}q_\perp) \phi_{\omega, \rho}(x, k_\perp) \frac{8}{3} \left( \frac{k_\perp^2 + (1 + 2x\bar{x})M^2 + \bar{x}k_\perp \cdot q_\perp}{x\bar{x}} \right) \right. \\ \left. - Q_d \phi_{\omega, \rho}(x, k_\perp - xq_\perp) \phi_{\omega, \rho}(x, k_\perp) \frac{8}{3} \left( \frac{k_\perp^2 + (1 + 2x\bar{x})M^2 - xk_\perp \cdot q_\perp}{x\bar{x}} \right) \right] \quad (155)$$

To proceed, it is useful to parametrize the non-local form factor using

so that

$$\mathcal{F}_M(z, x, \theta) = (z_+ F'(z_+))^2 (z_- F'(z_-))^2$$

$$z_\pm = \left[ z^2 \pm \frac{\bar{x}\rho q_\perp}{2\lambda_X \sqrt{x\bar{x}}} z \cos \theta + \frac{\bar{x}^2 \rho^2 q_\perp^2}{16x\bar{x}\lambda_X^2} \right]^{1/2}$$

With this in mind, the pion form factor can be worked out

$$F_\pi(Q^2) = \frac{C_\pi^2}{2\pi^2} \int_0^{2\pi} \frac{d\theta}{2\pi} \int_0^1 dx \int_0^\infty dz x \bar{x} z \\ \times \left( \frac{2}{3} \left[ \frac{x\bar{x}z^2 + \frac{\rho^2 M^2}{4\lambda_S^2} - \frac{\bar{x}^2 \rho^2 q_\perp^2}{16\lambda_S^2}}{\left( x\bar{x}z^2 - \frac{\rho^2}{4\lambda_S^2} (x\bar{x}m_\pi^2 - M^2) + \frac{\bar{x}^2 \rho^2 q_\perp^2}{16\lambda_S^2} \right)^2 - \frac{\bar{x}^2 \rho^2 q_\perp^2}{4\lambda_S^2} x\bar{x}z^2 \cos^2 \theta} \right] \mathcal{F}_M(z, x, \theta) \right. \\ \left. + \frac{1}{3} \left[ \frac{x\bar{x}z^2 + \frac{\rho^2 M^2}{4\lambda_S^2} - \frac{x^2 \rho^2 q_\perp^2}{16\lambda_S^2}}{\left( x\bar{x}z^2 - \frac{\rho^2}{4\lambda_S^2} (x\bar{x}m_\pi^2 - M^2) + \frac{x^2 \rho^2 q_\perp^2}{16\lambda_S^2} \right)^2 - \frac{x^2 \rho^2 q_\perp^2}{4\lambda_S^2} x\bar{x}z^2 \cos^2 \theta} \right] \mathcal{F}_M(z, \bar{x}, \theta) \right) \quad (156)$$

The pion EM form factor in (156), accounts for only the coupling to the lowest Fock component of the pion on the light front. While it accounts properly for the charge normalization, it falls short from accounting for the rho-meson cloud at non-vanishing  $Q^2$ , which is a coherent multi-Fock component. For small  $Q^2$ , the pion sources a rho-meson, which is readily obtained by resumming the bubble chain in the t-channel in our light front formulation, in line with vector meson dominance (VMD) [80] (and references therein),

$$F_\pi^{\text{VDM}}(Q^2) = F_\pi(0) \frac{1}{1 + Q^2/m_{\omega, \rho}^2} \quad (157)$$



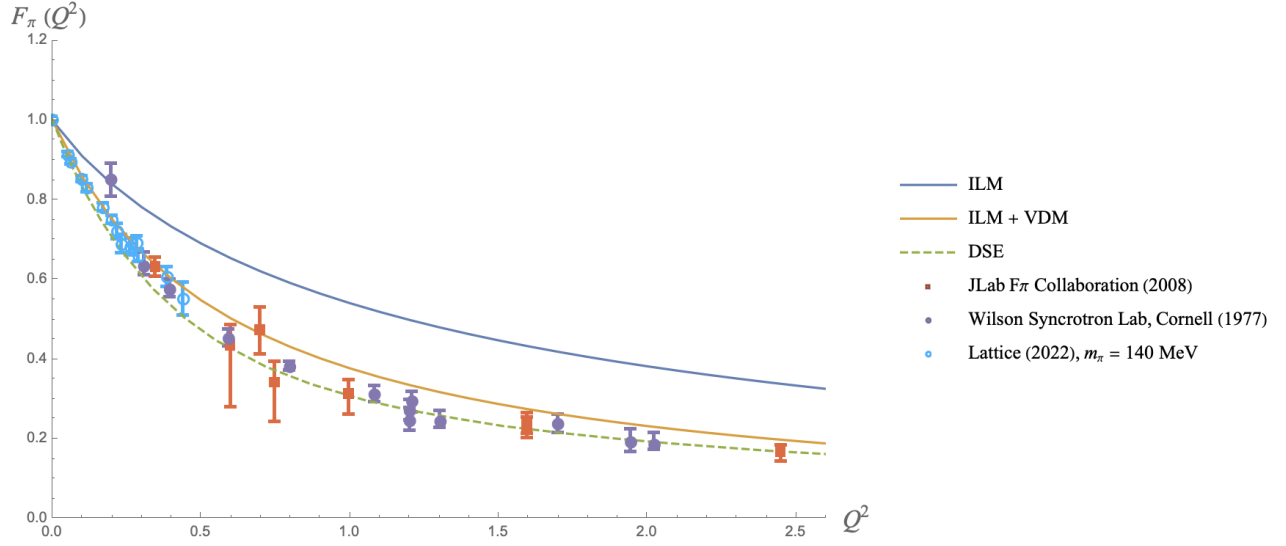


FIG. 22: Our results in solid-blue (undressed) and solid-orange (dressed) for the pion EM form factor, are compared with the JLab measurements in red-squares [81] and the Cornell measurements in purple-dots [82, 83]. The recent lattice calculations are shown in blue-triangles [84], and the Dyson-Schwinger results are shown in dashed-green [85].

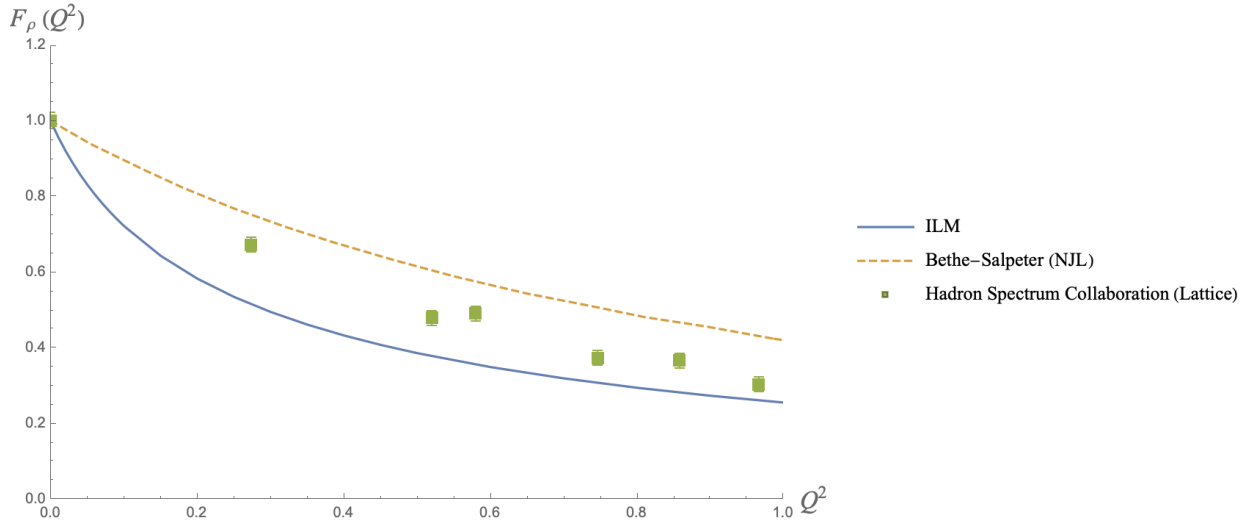


FIG. 23: Our calculations are compared with the recent lattice calculation [86], and the model analysis by Bethe-Salpeter equation using the random-phase approximation in the NJL model [78].

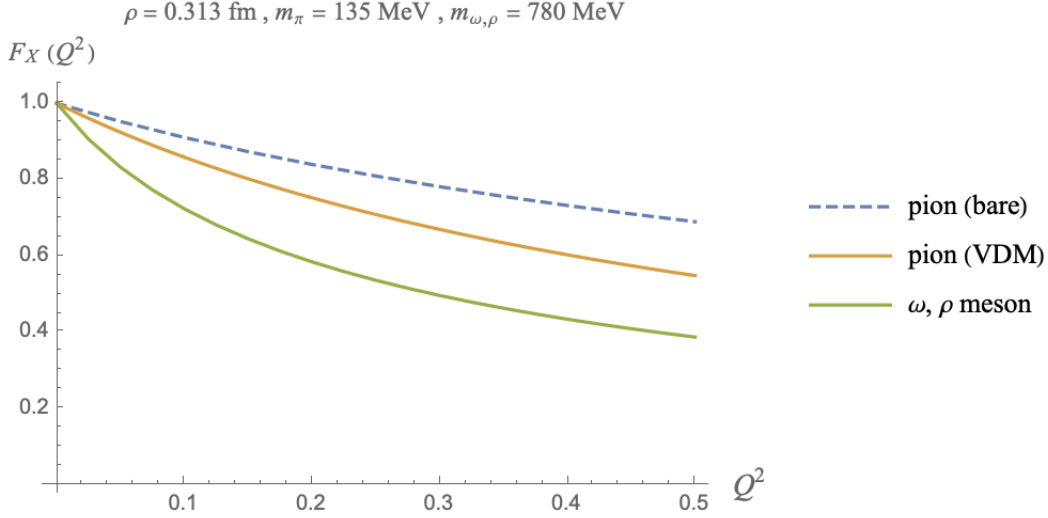


FIG. 24: Pion EM form factor in dashed-blue (undressed) and in solid-orange (dressed) in comparison to the vector EM form factor in solid-green.

The EM form factors of the vector mesons follow similarly

$$\begin{aligned}
 F_{\omega, \rho}(Q^2) = & \frac{C_{\omega, \rho}^2}{3\pi^2} \int_0^{2\pi} \frac{d\theta}{2\pi} \int_0^1 dx \int_0^\infty dz x \bar{x} z \\
 & \times \left( \frac{2}{3} \frac{x \bar{x} z^2 + \frac{\rho^2 M^2}{4\lambda_V^2} (1 + 2x \bar{x}) - \frac{\bar{x}^2 \rho^2 q_\perp^2}{16\lambda_V^2}}{\left[ \left( x \bar{x} z^2 - \frac{\rho^2}{4\lambda_V^2} (x \bar{x} m_{\omega, \rho}^2 - M^2) + \frac{\bar{x}^2 \rho^2 q_\perp^2}{16\lambda_V^2} \right)^2 - \frac{\bar{x}^2 \rho^2 q_\perp^2}{4\lambda_V^2} x \bar{x} z^2 \cos^2 \theta \right]} \mathcal{F}_M(z, x, \theta) \right. \\
 & \left. + \frac{1}{3} \frac{x \bar{x} z^2 + \frac{\rho^2 M^2}{4\lambda_V^2} (1 + 2x \bar{x}) - \frac{x^2 \rho^2 q_\perp^2}{16\lambda_V^2}}{\left[ \left( x \bar{x} z^2 - \frac{\rho^2}{4\lambda_V^2} (x \bar{x} m_{\omega, \rho}^2 - M^2) + \frac{x^2 \rho^2 q_\perp^2}{16\lambda_V^2} \right)^2 - \frac{x^2 \rho^2 q_\perp^2}{4\lambda_V^2} x \bar{x} z^2 \cos^2 \theta \right]} \mathcal{F}_M(z, \bar{x}, \theta) \right)
 \end{aligned} \tag{158}$$

In Fig. 22 we show the bare pion form factor (156) in solid-blue and the rho-meson dressed pion form factor (157) in solid-orange, versus  $Q^2$ . Our results in the QCD instanton vacuum are compared to the measurement using pion scattering from the reaction  $^1H(e, e'\pi^+)n$  by the JLab  $F_\pi$  collaboration in red-squares [81], the Cornell collaboration in purple-dots [82, 83], and the lattice results in blue-triangles [84]. The Dyson-Schwinger results with rainbow ladders, are shown in dashed-green [85]. Clearly, our lowest undressed Fock contribution fails to reproduce the pion EM form factor, while the dressed multi-Fock component agrees relatively well with the current measurements. This result underlies the collective character of the pion state.

In Fig. 23 we show the EM form factor of the rho meson in blue-solid versus  $Q^2$ , in comparison to the lattice data in green-squares from the Hadron Spectrum Collaboration [86]. The results from the Bethe-Salpeter in the NJL model are shown in dashed-orange. The fall off of the form factor is sharper in our case in comparison to the lattice results, reflecting on a larger charge radius for the rho. This fall off is sensitive to the value of  $\lambda_V$  in (79) fixed by the rho weak decay constants. A larger value of  $\lambda_V$  yields a smaller charge radius, at the expense of the weak decay constants. We note that the fall off of our rho form factor is slower than that reported in [51, 87–89], but about similar to the reported lattice results. In Fig. 24, we compare the EM form factors for the pion undressed in dashed-blue, dressed in solid-orange with the EM form factor of the vector mesons in solid-green.

On the light front, all hadrons are 2D Lorentz contracted. The light front radius  $r_X$  follows from

$$F_X(Q^2) = 1 - \frac{Q^2}{6} r_X^2 + \mathcal{O}(Q^4) \quad (159)$$

For the pion EM form factor, we have

$$\begin{aligned} r_\pi &= 0.489 \text{ fm} \\ r_\pi^{\text{VDM}} &= 0.620 \text{ fm} \\ r_\pi^{\text{exp}} &= 0.659 \pm 0.004 \text{ fm} \end{aligned} \quad (160)$$

The charge radius from other work can also be found in

Reference	$r_\pi$ (fm)
ILM (this work)	0.620
Faessler [41]	0.650
Hutauruk[40]	0.629

Without the rho-cloud, the bare EM size of the pion  $r_\pi$ , is slightly larger than the size of an instanton  $\rho = 0.313$  fm. Pions are collective Goldstone modes, strongly bound by single instantons (anti-instantons) of size  $\rho$ . In contrast, the EM size of the rho and omega  $r_{\omega,\rho} = 0.997$  fm is about twice the pion size. Vector mesons are bound by molecular configurations of size about  $2\rho$ . As we noted, the empirical value of the charge radius for the pion  $r_\pi^{\text{exp}}$  in [61, 90] compares well only with the dressed pion, in line with the VMD lore. For completeness, we compare our charge radius for the rho-meson with some model calculations in the table.

Reference	$r_\rho$ (fm)
ILM (this work)	0.997
de Melo[87]	0.608
Bhagwat[91]	0.735
Krutov[92]	0.748
Carrillo-Serrano[78]	0.819
Owen[93]	0.819

## IX. CONCLUSIONS

We presented a detailed analysis of the emerging 't Hooft non-local interactions on the light front, in the light scalar and pseudoscalar channels. These interactions include not only the standard single instanton and anti-instanton chirality flipping contributions, but also the molecular chirality preserving

contributions. The diluteness of the instanton tunneling rates in the QCD vacuum, makes the molecular contributions parametrically small. Their contribution is subleading in the spontaneous breaking of chiral symmetry, yet leading in the formation of the light vector mesons.

Our analysis focused on the light front formulation, where the light quark fields are split into a good plus bad component. The elimination of the bad component generates additional multi-fermion interactions. Using the  $1/N_c$  book-keeping analysis, we have shown that in leading order these additional interactions are tadpole-like and can be resummed to renormalize the non-local interactions between the good components. They are at the origin of the non-trivial vacuum structure on the light front, as initially observed in the NJL model with local interactions [56–58]. Contrary to common lore, the vacuum is non-trivial on the light front.

The light front Hamiltonian associated to the emerging non-local effective action, was used to define the eigenvalue problem for the light scalar and vector meson states, limited to their lowest Fock component. The explicit breaking of Lorentz symmetry, yields apparently different equations for the longitudinally and transversely polarized rho and omega vector mesons. Fortunately, a thorough analysis of the longitudinal equation shows that the difference is emanable to the ratio of the vector to scalar interaction strengths, which is parametrically small in the QCD instanton vacuum.

Our light front results for the light scalar and vector mesons PDFs and DAs, are evaluated at a low renormalization point of about  $1/2\rho \sim 0.31$  GeV. A comparison to existing measurements and lattice simulations at a scale of  $\mu = 2$  GeV requires evolution. For simplicity, we have assumed that factorization holds at this relatively low scale, and used perturbative QCD evolution. Our results were shown to be remarkably consistent with most measurements. Yet a more appropriate evolution from this low renormalization scale, should perhaps make use of non-perturbative effects [16]. This will be discussed elsewhere.

Finally, we have used the light front wavefunctions in the QCD instanton vacuum, to analyze the EM form factors of the pions and rho and omega vector mesons. The leading Fock state in the rho meson, yields a rho EM form factor in good agreement with the recently reported lattice simulations. This is not the case of the pion, when limited to its lowest Fock

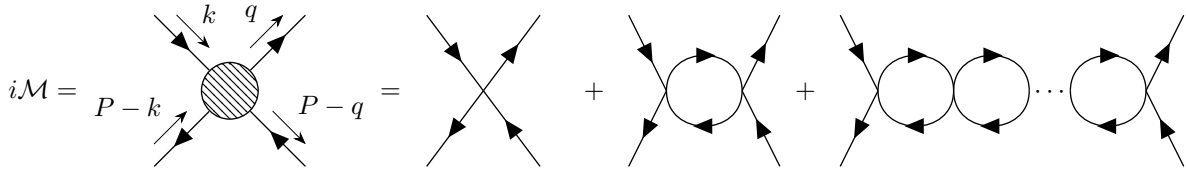
component, a well known shortcoming. This is readily fixed by resumming the leading rho contribution to the pion EM form factor, in line with the tenets of vector dominance.

**Acknowledgements** This work is supported by the Office of Science, U.S. Department of Energy

under Contract No. DE-FG-88ER40388.

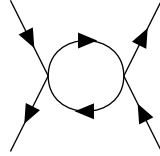
### Appendix A: Lorentz covariant formalism: Bethe-Salpeter equation

To investigate the meson structures in a covariant frame, we can organize the Bethe-Salpeter kernel in  $1/N_c$ . In leading order (LO), the vacuum polarization function contributes to the 4-point function through the bubble-chain



The next-to-leading order (NLO) is more involved [94]. Using our emerging action for the light quarks with non-local interactions, the vacuum polarization function  $\Pi^{\alpha\beta}$  is given by

$$\Pi^{\alpha\beta} = -i \int \frac{d^4k}{(2\pi)^4} \frac{\text{tr}[\Gamma^\alpha(\not{k} + M(k))\Gamma^\beta(\not{P} - \not{k} - M(P-k))]}{[k^2 - M^2(k)][(P-k)^2 - M^2(P-k)]} \mathcal{F}(k)\mathcal{F}(P-k) \quad (\text{A1})$$



where  $\Gamma^\alpha = 1, i\gamma^5, \tau^a, i\gamma^5\tau^a, \gamma^\mu, \gamma^\mu\tau^a, \gamma^\mu\gamma^5, \gamma^\mu\gamma^5\tau^a$  for  $\sigma, \eta', a_0, \pi, \omega, \rho, f_1, a_1$  respectively. In the low momentum limit ( $k \ll 1/\rho$ ), similar to the approximation we imposed in the gap equation, we approximate the momentum-dependent constituent mass  $M(k)$  in the fermionic bubble functions by  $M(0)$ , the emergent constituent mass at zero momentum.

$$\int \frac{d^4k}{(2\pi)^4} \Pi_X(M(k), M(P-k)) \approx \int \frac{d^4k}{(2\pi)^4} \Pi_X(M, M)$$

The vacuum polarization function  $\Pi$  in the low momentum limit, simplifies

$$\Pi_X^{\alpha\beta} = -i \int \frac{d^4k}{(2\pi)^4} \frac{\text{tr}[\Gamma^\alpha(\not{k} + M)\Gamma^\beta(\not{P} - \not{k} - M)]}{(k^2 - M^2)((P-k)^2 - M^2)} \mathcal{F}(k)\mathcal{F}(P-k) \quad (\text{A2})$$

#### 1. Scalar channel

In the scalar channel and close to the pole, the resummation of the vacuum polarizations gives

$$i\mathcal{M} = \bar{u}_{s'_1}(q)v_{s'_2}(P-q)\sqrt{\mathcal{F}(q)\mathcal{F}(P-q)}D_\sigma(P^2)\sqrt{\mathcal{F}(k)\mathcal{F}(P-k)}\bar{v}_{s_2}(P-k)u_{s_1}(k) \quad (\text{A3})$$

$$i\mathcal{M} = \bar{u}_{s'_1}(q)\tau^a v_{s'_2}(P-q)\sqrt{\mathcal{F}(q)\mathcal{F}(P-q)}D_{a_0}(P^2)\sqrt{\mathcal{F}(k)\mathcal{F}(P-k)}\bar{v}_{s_2}(P-k)\tau^a u_{s_1}(k) \quad (\text{A4})$$

with the scalar propagator

$$D_{\sigma,a_0}(P^2) = \frac{iG_{\sigma,a_0}}{1 - G_{\sigma,a_0}\Pi_{SS}(P^2)} \quad (\text{A5})$$

The scalar vacuum polarization function is

$$\begin{aligned} \Pi_{SS} &= -2iN_c \int \frac{d^4k}{(2\pi)^4} \frac{\text{tr}[(\not{k} + M)(\not{P} - \not{k} - M)]}{(k^2 - M^2)((P - k)^2 - M^2)} \mathcal{F}(k)\mathcal{F}(P - k) \\ &= -2iN_c \int \frac{d^4k}{(2\pi)^4} \frac{4k \cdot (P - k) - 4M^2}{(k^2 - M^2)((P - k)^2 - M^2)} \mathcal{F}(k)\mathcal{F}(P - k) \end{aligned} \quad (\text{A6})$$

## 2. Pseudoscalar channel

In the pseudoscalar channel, the resummation gives

$$i\mathcal{M} = \bar{u}_{s'_1}(q) i\gamma^5 v_{s'_2}(P - q) \sqrt{\mathcal{F}(q)\mathcal{F}(P - q)} D_{\eta'}(P^2) \sqrt{\mathcal{F}(k)\mathcal{F}(P - k)} \bar{v}_{s_2}(P - k) i\gamma^5 u_{s_1}(k) \quad (\text{A7})$$

$$i\mathcal{M} = \bar{u}_{s'_1}(q) i\gamma^5 \tau^a v_{s'_2}(P - q) \sqrt{\mathcal{F}(q)\mathcal{F}(P - q)} D_{\pi}(P^2) \sqrt{\mathcal{F}(k)\mathcal{F}(P - k)} \bar{v}_{s_2}(P - k) i\gamma^5 \tau^a u_{s_1}(k) \quad (\text{A8})$$

with the pseudoscalar propagator

$$D_{\pi,\eta'}(P^2) = \frac{iG_{\pi,\eta'}}{1 - G_{\pi,\eta'}\Pi_{PP}(P^2)} \quad (\text{A9})$$

The pseudoscalar vacuum polarization is

$$\begin{aligned} \Pi_{PP} &= -2iN_c \int \frac{d^4k}{(2\pi)^4} \frac{\text{tr}[(\not{k} + M)i\gamma^5(\not{P} - \not{k} - M)i\gamma^5]}{(k^2 - M^2)((P - k)^2 - M^2)} \mathcal{F}(k)\mathcal{F}(P - k) \\ &= -2iN_c \int \frac{d^4k}{(2\pi)^4} \frac{4k \cdot (P - k) + 4M^2}{(k^2 - M^2)((P - k)^2 - M^2)} \mathcal{F}(k)\mathcal{F}(P - k) \end{aligned} \quad (\text{A10})$$

We have neglected the pseudoscalar-axial mixing as higher order in  $g_V/g_S$ .

## 3. Vector channel

In the vector channel, the vacuum polarization function can be rearranged through

$$\begin{aligned} \Pi_{VV}^{\mu\nu} &= -2iN_c \int \frac{d^4k}{(2\pi)^4} \frac{\text{tr}[(\not{k} + M)\gamma^\mu(\not{P} - \not{k} - M)\gamma^\nu]}{(k^2 - M^2)((P - k)^2 - M^2)} \mathcal{F}(k)\mathcal{F}(P - k) \\ &= -\Pi_{VV}(P^2) \left( g^{\mu\nu} - \frac{P^\mu P^\nu}{P^2} \right) \end{aligned} \quad (\text{A11})$$

with manifest current conservation  $P_\mu \Pi_{\omega,\rho}^{\mu\nu} = 0$ . The resummation of the fermionic chains, gives

$$i\mathcal{M} = \bar{u}_{s'_1}(q) \gamma_\mu v_{s'_2}(P - q) \sqrt{\mathcal{F}(q)\mathcal{F}(P - q)} D_{\omega}^{\mu\nu}(P^2) \sqrt{\mathcal{F}(k)\mathcal{F}(P - k)} \bar{v}_{s_2}(P - k) \gamma_\nu u_{s_1}(k) \quad (\text{A12})$$

$$i\mathcal{M} = \bar{u}_{s'_1}(q) \gamma_\mu \tau^a v_{s'_2}(P - q) \sqrt{\mathcal{F}(q)\mathcal{F}(P - q)} D_{\rho}^{\mu\nu}(P^2) \sqrt{\mathcal{F}(k)\mathcal{F}(P - k)} \bar{v}_{s_2}(P - k) \gamma_\nu \tau^a u_{s_1}(k) \quad (\text{A13})$$

with the vector propagator

$$D_{\omega,\rho}^{\mu\nu}(P^2) = \frac{-iG_{\omega,\rho}}{1 - G_{\omega,\rho}\Pi_{\omega,\rho}(P^2)} \left( g^{\mu\nu} - G_{\omega,\rho}\Pi_{VV}(P^2) \frac{P^\mu P^\nu}{P^2} \right) \quad (\text{A14})$$

where

$$\Pi_{VV} = -2iN_c \frac{4}{3} \int \frac{d^4k}{(2\pi)^4} \frac{2k \cdot (P - k) + 4M^2}{(k^2 - M^2)((P - k)^2 - M^2)} \mathcal{F}(k)\mathcal{F}(P - k) \quad (\text{A15})$$

---

The scattering amplitude develops poles at the location of the bound states, whenever

$$G_X \Pi_X(m_X^2) = 1 \quad (\text{A16})$$

with  $P^2 = m_X^2$ . This fixes the mass eigenvalue equation. If we only consider the 't Hooft Lagrangian, the single instanton and anti-instanton interactions for  $\sigma$

and  $\pi$  are attractive, while those for  $\eta'$  and  $a_0$  are repulsive. The molecular interactions  $\omega$ ,  $\rho$ , and  $a_1$  are attractive within a certain range, but repulsive in the  $f_1$  channel.

## Appendix B: Bound State Equation of Longitudinal Vector Meson

The bound state equation for the longitudinal meson on the light front, is not only more involved than that of its transverse counterpart, but apparently different. Here, we detail its derivation, and show that the differences can be removed thanks to a number of identities. More specifically, the longitudinally bound state equation can be readily cast in the form

$$\begin{aligned} m_{\omega,\rho}^2 \left( 1 + \frac{k_\perp^2 + M^2}{m_{\omega,\rho}^2 x\bar{x}} \right) \phi_{\omega,\rho}(x, k_\perp) &= \frac{k_\perp^2 + M^2}{x\bar{x}} \left( 1 + \frac{k_\perp^2 + M^2}{m_{\omega,\rho}^2 x\bar{x}} \right) \phi_{\omega,\rho}(x, k_\perp) \\ &- \frac{8g_{\omega,\rho}}{\sqrt{2x\bar{x}}} \sqrt{\mathcal{F}(k) \mathcal{F}(P-k)} \int \frac{dy d^2 q_\perp}{\sqrt{2y\bar{y}} (2\pi)^3} \left[ \frac{q_\perp^2 + M^2}{y\bar{y}} - 4g_{\omega,\rho} w_-(P^+)(P^+)^2 \right] \left( y\bar{y} + \frac{q_\perp^2 + M^2}{m_{\omega,\rho}^2} \right) \phi_{\omega,\rho}(y, q_\perp) \sqrt{\mathcal{F}(q) \mathcal{F}(P-q)} \\ &- \frac{8g_{\omega,\rho}}{\sqrt{2x\bar{x}}} \sqrt{\mathcal{F}(k) \mathcal{F}(P-k)} \left[ \frac{k_\perp^2 + M^2}{x\bar{x}} - 4g_{\omega,\rho} w_-(P^+)(P^+)^2 \right] \int \frac{dy d^2 q_\perp}{\sqrt{2y\bar{y}} (2\pi)^3} \left( y\bar{y} + \frac{q_\perp^2 + M^2}{m_{\omega,\rho}^2} \right) \phi_{\omega,\rho}(y, q_\perp) \sqrt{\mathcal{F}(q) \mathcal{F}(P-q)} \end{aligned} \quad (\text{B1})$$

The tadpole resummation involved in the bound state equation of the longitudinal mode can be rearranged as

$$\begin{aligned} w_-(P^+) &= \int \frac{dk^+ d^2 k_\perp}{(2\pi)^3} \frac{(k_\perp^2 + M^2) \epsilon(k^+)}{2(k^+)^2 (P^+ - k^+)} \mathcal{F}(k) \mathcal{F}(P-k) \\ &= \frac{1}{(P^+)^2} \int \frac{dx d^2 k_\perp}{(2\pi)^3} \frac{(k_\perp^2 + M^2) \epsilon(x)}{2x^2 \bar{x}} \mathcal{F}(k) \mathcal{F}(P-k) \\ &= \frac{1}{(P^+)^2} \int_0^1 dx \int \frac{d^2 k_\perp}{(2\pi)^3} \frac{(k_\perp^2 + M^2)}{2x\bar{x}} \mathcal{F}(k) \mathcal{F}(P-k) \\ &= \frac{m_{\omega,\rho}^2}{2(P^+)^2} \end{aligned} \quad (\text{B2})$$

Remarkably the complicated result (B1), can be considerably simplified by noting that it is composed of three integrals

$$\begin{aligned} H_1 &= \int \frac{dy}{\sqrt{2y\bar{y}}} \int \frac{d^2 q_\perp}{(2\pi)^3} (y\bar{y} m_{\omega,\rho}^2 + q_\perp^2 + M^2) \phi_{\omega,\rho}(y, q_\perp) \sqrt{\mathcal{F}(q) \mathcal{F}(P-q)} \\ H_2 &= \int \frac{dy}{\sqrt{2y\bar{y}}} \int \frac{d^2 q_\perp}{(2\pi)^3} (y\bar{y} m_{\omega,\rho}^2 + q_\perp^2 + M^2) \left( \frac{q_\perp^2 + M^2}{y\bar{y} m_{\omega,\rho}^2} \right) \phi_{\omega,\rho}(y, q_\perp) \sqrt{\mathcal{F}(q) \mathcal{F}(P-q)} \\ \eta &= \int \frac{dy d^2 q_\perp}{(2\pi)^3} \frac{q_\perp^2 + M^2}{m_{\omega,\rho}^2 y\bar{y}} \mathcal{F}(q) \mathcal{F}(P-q) \end{aligned}$$

The integrals  $H_1$  and  $H_2$  are not independent of each other. Indeed, if we multiply (B1) by  $\sqrt{2x\bar{x}}$  and  $\sqrt{\mathcal{F}(q) \mathcal{F}(P-q)}$ , and integrate the result over the momentum phase space, we have

$$H_2 = \frac{H_1}{1 - 4g_{\omega,\rho} \int \frac{dy d^2 q_\perp}{(2\pi)^3} \mathcal{F}(q) \mathcal{F}(P-q)} + 4g_{\omega,\rho} \eta H_1 \quad (\text{B3})$$

Inserting (B3) in (B1), the equation simplifies

$$\begin{aligned}
& \left( m_{\omega,\rho}^2 - \frac{k_\perp^2 + M^2}{x\bar{x}} \right) \phi_{\omega,\rho}(x, k_\perp) \\
&= -8g_{\omega,\rho} \left[ 1 - 4g_{\omega,\rho} \int \frac{dy d^2 q_\perp}{(2\pi)^3} \mathcal{F}(q) \mathcal{F}(P-q) \right]^{-1} \left[ 1 - 4g_{\omega,\rho} \left( \int \frac{dy d^2 q_\perp}{(2\pi)^3} \mathcal{F}(q) \mathcal{F}(P-q) \right) \left( \frac{k_\perp^2 + M^2}{m_{\omega,\rho}^2 x\bar{x} + k_\perp^2 + M^2} \right) \right] \\
& \quad \times \frac{1}{\sqrt{2x\bar{x}}} \sqrt{\mathcal{F}(k) \mathcal{F}(P-k)} \int \frac{dy}{\sqrt{2y\bar{y}}} \int \frac{d^2 q_\perp}{(2\pi)^3} (y\bar{y} m_{\omega,\rho}^2 + q_\perp^2 + M^2) \phi_{\omega,\rho}(y, q_\perp) \sqrt{\mathcal{F}(q) \mathcal{F}(P-q)} \\
& \simeq -\frac{8g_{\omega,\rho}}{\sqrt{2x\bar{x}}} \frac{\sqrt{\mathcal{F}(k) \mathcal{F}(P-k)}}{1 - 4g_{\omega,\rho} \int \frac{dy d^2 q_\perp}{(2\pi)^3} \mathcal{F}(q) \mathcal{F}(P-q)} \int \frac{dy}{\sqrt{2y\bar{y}}} \int \frac{d^2 q_\perp}{(2\pi)^3} (y\bar{y} m_{\omega,\rho}^2 + q_\perp^2 + M^2) \phi_{\omega,\rho}(y, q_\perp) \sqrt{\mathcal{F}(q) \mathcal{F}(P-q)}
\end{aligned} \tag{B4}$$

where we dropped the higher order terms in  $\mathcal{O}(g_{\omega,\rho}^2)$  in the third equality. As we argued in the main text, the QCD instanton vacuum is dilute, with the contributions  $g_{\omega,\rho}/g_S$  parametrically small. We have only kept them in leading order in the vector channels, as their keeping at next to leading order involves a more complex book-keeping procedure. With this in mind, we can further simplify (B4) by multiplying it by  $\sqrt{2x\bar{x}}$  and  $\sqrt{\mathcal{F}(q) \mathcal{F}(P-q)}$  again, and integrating over  $x$  and  $k_\perp$ . The result is

$$\begin{aligned}
& \int \frac{dx d^2 k_\perp}{(2\pi)^3} \sqrt{2x\bar{x}} \sqrt{\mathcal{F}(k) \mathcal{F}(P-k)} \left( m_{\omega,\rho}^2 - \frac{k_\perp^2 + M^2}{x\bar{x}} \right) \phi_{\omega,\rho}(x, k_\perp) \\
&= -8g_{\omega,\rho} \int \frac{dy d^2 q_\perp}{(2\pi)^3} \mathcal{F}(q) \mathcal{F}(P-q) \int \frac{dx d^2 k_\perp}{(2\pi)^3} \sqrt{2x\bar{x}} \sqrt{\mathcal{F}(k) \mathcal{F}(P-k)} \left( \frac{k_\perp^2 + M^2}{x\bar{x}} \right) \phi_{\omega,\rho}(x, k_\perp)
\end{aligned} \tag{B5}$$

hence the bound state equation

$$\left( m_{\omega,\rho}^2 - \frac{k_\perp^2 + M^2}{x\bar{x}} \right) \phi_{\omega,\rho}(x, k_\perp) \simeq -\frac{16g_{\omega,\rho}}{\sqrt{2x\bar{x}}} \sqrt{\mathcal{F}(k) \mathcal{F}(P-k)} \int \frac{dy}{\sqrt{2y\bar{y}}} \int \frac{d^2 q_\perp}{(2\pi)^3} (q_\perp^2 + M^2) \phi_{\omega,\rho}(y, q_\perp) \sqrt{\mathcal{F}(q) \mathcal{F}(P-q)} \tag{B6}$$

### Appendix C: Light front wave functions with $P_\perp \neq 0$

To obtain the off-diagonal hadronic matrix elements, we need to generalize the light front wave functions to a frame with  $P_\perp \neq 0$ . In this frame, the hadronic momentum is

$$P^\mu = \left( P^+, P_\perp, \frac{P_\perp^2 + m_X^2}{2P^+} \right)$$

The quark  $k_1$  and anti-quark  $k_2$  momenta can be parameterized by

$$\begin{aligned}
k_1^\mu &= \left( xP^+, xP_\perp + k_\perp, \frac{(xP_\perp + k_\perp)^2 + M^2}{2xP^+} \right) \\
k_2^\mu &= \left( \bar{x}P^+, \bar{x}P_\perp - k_\perp, \frac{(\bar{x}P_\perp - k_\perp)^2 + M^2}{2\bar{x}P^+} \right)
\end{aligned}$$

For the spin-1 meson, the polarization vector  $\epsilon_\lambda^\mu(P)$  is defined as

$$\begin{aligned}
\epsilon_\pm^\mu(P) &= \frac{1}{\sqrt{2}} \left( 0, 1, \pm i, \frac{P^1 \pm iP^2}{P^+} \right) \\
\epsilon_0^\mu(P) &= \frac{1}{m_X} \left( P^+, \frac{P^1}{2}, \frac{P^2}{2}, \frac{P_\perp^2 - m_X^2}{2P^+} \right)
\end{aligned}$$

With this symmetric parameterization, the light front wave functions have the same form. The spin-independent wave functions are

$$\phi_X(x, k_\perp) = \frac{C_X}{\sqrt{2x\bar{x}}(m_X^2 - \frac{k_\perp^2 + M^2}{x\bar{x}})} \sqrt{\mathcal{F}(k) \mathcal{F}(P-k)} \tag{C1}$$

### scalar channels

$$\Phi_\sigma(x, k_\perp, s_1, s_2) = \frac{1}{\sqrt{N_c}} \phi_\sigma(x, k_\perp) \bar{u}_{s_1}(k) v_{s_2}(P-k) \tag{C2}$$

$$\Phi_{a_0}(x, k_\perp, s_1, s_2) = \frac{1}{\sqrt{N_c}} \phi_{a_0}(x, k_\perp) \bar{u}_{s_1}(k) \tau^a v_{s_2}(P - k) \quad (C3)$$

**pseudoscalar channels**

$$\Phi_{\eta'}(x, k_\perp, s_1, s_2) = \frac{1}{\sqrt{N_c}} \phi_{\eta'}(x, k_\perp) \bar{u}_{s_1}(k) i\gamma^5 v_{s_2}(P - k) \quad (C4)$$

$$\Phi_\pi(x, k_\perp, s_1, s_2) = \frac{1}{\sqrt{N_c}} \phi_\pi(x, k_\perp) \bar{u}_{s_1}(k) i\gamma^5 \tau^a v_{s_2}(P - k) \quad (C5)$$

**vector channels**

$$\Phi_\omega^\lambda(x, k_\perp, s_1, s_2) = \frac{1}{\sqrt{N_c}} \phi_\omega(x, k_\perp) \epsilon_\lambda^\mu(P) \bar{u}_{s_1}(k) \gamma_\mu v_{s_2}(P - k) \quad (C6)$$

$$\Phi_\rho^\lambda(x, k_\perp, s_1, s_2) = \frac{1}{\sqrt{N_c}} \phi_\rho(x, k_\perp) \epsilon_\lambda^\mu(P) \bar{u}_{s_1}(k) \gamma_\mu \tau^a v_{s_2}(P - k) \quad (C7)$$

#### Appendix D: Spin-dependent Wave Functions on the Light Front

The spin-dependent wave functions denotes the spin states in the creation of a quark-anti-quark pair. The wave functions for each channels are

**scalar**

$$\bar{u}_{s_1}(k) v_{s_2}(P - k) = \frac{1}{\sqrt{x\bar{x}}} \chi_{s_1}^\dagger [M(\bar{x} - x) \sigma_z - k_\perp \cdot \sigma_\perp] \eta_{s_2} \quad (D1)$$

**pseudoscalar**

$$\bar{u}_{s_1}(k) i\gamma^5 v_{s_2}(P - k) = \frac{i}{\sqrt{x\bar{x}}} \chi_{s_1}^\dagger [M - k_\perp \cdot \sigma_\perp \sigma_z] \eta_{s_2} \quad (D2)$$

**vector**

$$\epsilon_+^\mu(P) \bar{u}_{s_1}(k) \gamma_\mu v_{s_2}(P - k) = -\frac{1}{\sqrt{x\bar{x}}} \chi_{s_1}^\dagger \left[ \sqrt{2} M \sigma^+ + \left( \bar{x} \frac{1 + \sigma_z}{\sqrt{2}} + x \frac{1 - \sigma_z}{\sqrt{2}} \right) k_R \right] \eta_{s_2} \quad (D3)$$

$$\epsilon_-^\mu(P) \bar{u}_{s_1}(k) \gamma_\mu v_{s_2}(P - k) = -\frac{1}{\sqrt{x\bar{x}}} \chi_{s_1}^\dagger \left[ \sqrt{2} M \sigma^- - \left( \bar{x} \frac{1 - \sigma_z}{\sqrt{2}} + x \frac{1 + \sigma_z}{\sqrt{2}} \right) k_L \right] \eta_{s_2} \quad (D4)$$

$$\epsilon_0^\mu(P) \bar{u}_{s_1}(k) \gamma_\mu v_{s_2}(P - k) = -\frac{m_X}{2P^+} \left( 1 + \frac{k_\perp^2 + M^2}{x\bar{x}m_X^2} \right) \frac{1}{\sqrt{x\bar{x}}} \chi_{s_1}^\dagger 2x\bar{x}P^+ \sigma_z \eta_{s_2} \quad (D5)$$

where  $\sigma^\pm = (\sigma_x \pm i\sigma_y)/2$  and  $k_{L,R} = k^1 \pm ik^2$

---

#### Appendix E: ERBL Evolution

At the leading twist, we have three types of distribution amplitudes (DA) defined by vector, axial vector and tensor currents. In this work, the pion axial DA, vector DA of  $\omega$  and  $\rho$  and their tensor DA are discussed. Without loss of generality, we only display the isovector states for the ERBL evolution.



$$\langle 0 | \bar{\psi}(0) \gamma^+ \gamma^5 \frac{\tau^a}{\sqrt{2}} W(0, \xi^-) \psi(\xi^-) | \pi(P) \rangle = i f_\pi P^+ \int_0^1 dx e^{-ixP^+ \xi^-} \phi_\pi^A(x) \quad (E1)$$

$$\langle 0 | \bar{\psi}(0) \gamma^+ \frac{\tau^a}{\sqrt{2}} W(0, \xi^-) \psi(\xi^-) | \rho(\lambda, P) \rangle = f_\rho m_\rho \epsilon_\lambda^+(P) \int_0^1 dx e^{-ixP^+ \xi^-} \phi_\rho^V(x) \quad (E2)$$

$$\langle 0 | \bar{\psi}(0) i \gamma^+ \gamma_\perp^i \frac{\tau^a}{\sqrt{2}} W(0, \xi^-) \psi(\xi^-) | \rho(\lambda, P) \rangle = -i f_\rho^T P^+ \epsilon_\lambda^i(P) \int_0^1 dx e^{-ixP^+ \xi^-} \phi_\rho^T(x) \quad (E3)$$

The DA's can be expanded in terms of Gegenbauer polynomials  $C_n^{3/2}(x - \bar{x})$ . This expansion is around the asymptotic form  $6x(1-x) = 6x\bar{x}$  predicted by perturbative QCD in the Bjorken limit

$$\phi^{A,V,T}(x, \mu) = 6x\bar{x} \sum_{n=0}^{\infty} C_n^{3/2}(x - \bar{x}) a_n^{A,V,T}(\mu) \quad (E4)$$

Due to the orthogonality of the Gegenbauer polynomials, the coefficient can be obtained by

$$a_n^{A,V,T}(\mu) = \frac{2(2n+3)}{3(n+1)(n+2)} \int_0^1 dy C_n^{3/2}(y - \bar{y}) \phi^{A,V,T}(y, \mu) \quad (E5)$$

Using the Gegenbauer polynomial basis  $C_n^m(z)$ , we can convert the integro-differential equation of the evolution into an infinite set of differential equation in terms of  $a_n$ .

$$\mu \frac{d}{d\mu} a_n^{A,V,T}(\mu) = -\frac{\alpha_s(\mu)}{2\pi} \gamma_n^{A,V,T} a_n^{A,V,T}(\mu) \quad (E6)$$

with the anomalous dimension [59, 70]

$$\gamma_n^A = C_F \left[ -3 + 4 \sum_{j=1}^{n+1} \frac{1}{j} - \frac{2}{(n+1)(n+2)} \right] \quad (E8)$$

$$\gamma_n^V = C_F \left[ -3 + 4 \sum_{j=1}^{n+1} \frac{1}{j} - \frac{2}{(n+1)(n+2)} \right] \quad (E9)$$

$$\gamma_n^T = C_F \left( -4 + 4 \sum_{j=1}^{n+1} \frac{1}{j} \right) \quad (E10)$$

Now the hard evolution can be readily solved in terms of the Gegenbauer coefficients  $a_n$ .

where  $C_F = \frac{N_c^2 - 1}{2N_c}$ ,

$$a_n^{A,V,T}(Q) = a_n^{A,V,T}(Q_0) \left( \frac{\alpha_s(Q)}{\alpha_s(Q_0)} \right)^{\frac{\gamma_n^{A,V,T}}{\beta_0}} \quad (E7) \quad \text{and } \Lambda_{QCD} = 226 \text{ MeV.}$$

$$\alpha_s(Q) = \frac{4\pi}{\beta_0 \ln \left( \frac{Q^2}{\Lambda_{QCD}^2} \right)}$$

$$\beta_0 = \frac{11}{3} N_c - \frac{2}{3} n_f$$

[1] G. R. Farrar and D. R. Jackson, *Phys. Rev. Lett.* **43**, 246 (1979).

[2] X. Ji, *Phys. Rev. Lett.* **110**, 262002 (2013),

arXiv:1305.1539 [hep-ph].

[3] J.-H. Zhang, J.-W. Chen, X. Ji, L. Jin, and H.-W. Lin, *Phys. Rev. D* **95**, 094514 (2017),

- arXiv:1702.00008 [hep-lat].
- [4] A. V. Radyushkin, *Phys. Rev. D* **95**, 056020 (2017), arXiv:1701.02688 [hep-ph].
  - [5] S.-i. Nam, *Mod. Phys. Lett. A* **32**, 1750218 (2017), arXiv:1704.03824 [hep-ph].
  - [6] M. C. Chu, J. M. Grandy, S. Huang, and J. W. Negele, *Phys. Rev. D* **49**, 6039 (1994), arXiv:hep-lat/9312071.
  - [7] D. Diakonov and V. Y. Petrov, *Nucl. Phys. B* **272**, 457 (1986).
  - [8] E. V. Shuryak, *Nucl. Phys. B* **319**, 541 (1989).
  - [9] M. A. Nowak, J. J. M. Verbaarschot, and I. Zahed, *Nucl. Phys. B* **325**, 581 (1989).
  - [10] M. Kacir, M. Prakash, and I. Zahed, *Acta Phys. Polon. B* **30**, 287 (1999), arXiv:hep-ph/9602314.
  - [11] T. Schäfer and E. V. Shuryak, *Rev. Mod. Phys.* **70**, 323 (1998), arXiv:hep-ph/9610451.
  - [12] E. Shuryak and I. Zahed, (2021), arXiv:2110.15927 [hep-ph].
  - [13] E. Shuryak and I. Zahed, (2021), arXiv:2111.01775 [hep-ph].
  - [14] E. Shuryak and I. Zahed, (2021), arXiv:2112.15586 [hep-ph].
  - [15] E. Shuryak and I. Zahed, (2022), arXiv:2202.00167 [hep-ph].
  - [16] E. Shuryak and I. Zahed, (2022), arXiv:2208.04428 [hep-ph].
  - [17] L. Chang, I. C. Cloet, J. J. Cobos-Martinez, C. D. Roberts, S. M. Schmidt, and P. C. Tandy, *Phys. Rev. Lett.* **110**, 132001 (2013), arXiv:1301.0324 [nucl-th].
  - [18] C. Chen, L. Chang, C. D. Roberts, S. Wan, and H.-S. Zong, *Phys. Rev. D* **93**, 074021 (2016), arXiv:1602.01502 [nucl-th].
  - [19] M. Ding, K. Raya, D. Binosi, L. Chang, C. D. Roberts, and S. M. Schmidt, *Phys. Rev. D* **101**, 054014 (2020), arXiv:1905.05208 [nucl-th].
  - [20] E. Ruiz Arriola and W. Broniowski, *Phys. Rev. D* **66**, 094016 (2002), arXiv:hep-ph/0207266.
  - [21] A. E. Dorokhov, W. Broniowski, and E. Ruiz Arriola, *Phys. Rev. D* **84**, 074015 (2011), arXiv:1107.5631 [hep-ph].
  - [22] W. Broniowski and E. Ruiz Arriola, *Phys. Lett. B* **773**, 385 (2017), arXiv:1707.09588 [hep-ph].
  - [23] W. Broniowski and E. Ruiz Arriola, *PoS Hadron2017*, 174 (2018), arXiv:1711.09355 [hep-ph].
  - [24] M. Praszalowicz and A. Rostworowski, in *37th Rencontres de Moriond on QCD and Hadronic Interactions* (2002) pp. 283–286, arXiv:hep-ph/0205177.
  - [25] D. G. Dumm, S. Noguera, N. N. Scoccola, and S. Scopetta, *Phys. Rev. D* **89**, 054031 (2014), arXiv:1311.3595 [hep-ph].
  - [26] V. Y. Petrov and P. V. Pobylitsa, (1997), arXiv:hep-ph/9712203.
  - [27] V. Y. Petrov, M. V. Polyakov, R. Ruskov, C. Weiss, and K. Goeke, *Phys. Rev. D* **59**, 114018 (1999), arXiv:hep-ph/9807229.
  - [28] A. E. Dorokhov, *Nuovo Cim. A* **109**, 391 (1996).
  - [29] A. E. Dorokhov and L. Tomio, (1998), arXiv:hep-ph/9803329.
  - [30] I. V. Anikin, A. E. Dorokhov, and L. Tomio, *Phys. Atom. Nucl.* **64**, 1329 (2001).
  - [31] A. E. Dorokhov and L. Tomio, *Phys. Rev. D* **62**, 014016 (2000).
  - [32] S.-i. Nam, H.-C. Kim, A. Hosaka, and M. M. Musakhanov, *Phys. Rev. D* **74**, 014019 (2006), arXiv:hep-ph/0605259.
  - [33] A. V. Radyushkin, in *Workshop on Continuous Advances in QCD* (1994) arXiv:hep-ph/9406237.
  - [34] S. J. Brodsky, F.-G. Cao, and G. F. de Teramond, *Phys. Rev. D* **84**, 033001 (2011), arXiv:1104.3364 [hep-ph].
  - [35] S. J. Brodsky, G. F. de Teramond, H. G. Dosch, and J. Erlich, *Phys. Rept.* **584**, 1 (2015), arXiv:1407.8131 [hep-ph].
  - [36] S. Jia and J. P. Vary, *Phys. Rev. C* **99**, 035206 (2019), arXiv:1811.08512 [nucl-th].
  - [37] J. Lan, C. Mondal, S. Jia, X. Zhao, and J. P. Vary, *Phys. Rev. Lett.* **122**, 172001 (2019), arXiv:1901.11430 [nucl-th].
  - [38] W.-Y. Liu, E. Shuryak, and I. Zahed, *Phys. Rev. D* **107**, 094024 (2023), arXiv:2302.03759 [hep-ph].
  - [39] P. Maris and P. C. Tandy, *Phys. Rev. C* **62**, 055204 (2000), arXiv:nucl-th/0005015.
  - [40] P. T. P. Hutaauruk, I. C. Cloet, and A. W. Thomas, *Phys. Rev. C* **94**, 035201 (2016), arXiv:1604.02853 [nucl-th].
  - [41] A. Faessler, T. Gutsche, M. A. Ivanov, V. E. Lyubovitskij, and P. Wang, *Phys. Rev. D* **68**, 014011 (2003), arXiv:hep-ph/0304031.
  - [42] A. Bashir, L. Chang, I. C. Cloet, B. El-Bennich, Y.-X. Liu, C. D. Roberts, and P. C. Tandy, *Commun.*

- Theor. Phys. **58**, 79 (2012), arXiv:1201.3366 [nucl-th].
- [43] M. Chen, Chin. Phys. C **45**, 123104 (2021), arXiv:2106.08782 [hep-ph].
- [44] M. A. Ivanov, J. G. Körner, J. N. Pandya, P. Santorelli, N. R. Soni, and C.-T. Tran, Front. Phys. (Beijing) **14**, 64401 (2019), arXiv:1904.07740 [hep-ph].
- [45] D. Ebert, R. N. Faustov, and V. O. Galkin, Phys. Lett. B **635**, 93 (2006), arXiv:hep-ph/0602110.
- [46] D. Ebert, R. N. Faustov, and V. O. Galkin, Eur. Phys. J. C **47**, 745 (2006), arXiv:hep-ph/0511029.
- [47] H.-M. Choi, Phys. Rev. D **75**, 073016 (2007), arXiv:hep-ph/0701263.
- [48] E. P. Biernat and W. Schweiger, Phys. Rev. C **89**, 055205 (2014).
- [49] R. M. Moita, J. P. B. C. de Melo, K. Tsushima, and T. Frederico, Phys. Rev. D **104**, 096020 (2021), arXiv:2104.02787 [hep-ph].
- [50] T. M. Aliev, A. Ozpineci, and M. Savci, Phys. Lett. B **678**, 470 (2009), arXiv:0902.4627 [hep-ph].
- [51] J. P. B. C. De Melo, Phys. Lett. B **788**, 152 (2019), arXiv:1810.11478 [hep-ph].
- [52] D. Melikhov and S. Simula, Phys. Rev. D **65**, 094043 (2002), arXiv:hep-ph/0112044.
- [53] W. Jaus, Phys. Rev. D **67**, 094010 (2003).
- [54] A. I. Vainshtein, V. I. Zakharov, V. A. Novikov, and M. A. Shifman, Sov. Phys. Usp. **25**, 195 (1982).
- [55] T. Schäfer, E. V. Shuryak, and J. J. M. Verbaarschot, Phys. Rev. D **51**, 1267 (1995), arXiv:hep-ph/9406210.
- [56] W. Bentz, T. Hama, T. Matsuki, and K. Yazaki, Nucl. Phys. A **651**, 143 (1999), arXiv:hep-ph/9901377.
- [57] K. Itakura and S. Maedan, Phys. Rev. D **62**, 105016 (2000), arXiv:hep-ph/0004081.
- [58] K. Naito, S. Maedan, and K. Itakura, Physical Review D **70** (2004), 10.1103/physrevd.70.096008.
- [59] A. Kock, Y. Liu, and I. Zahed, Phys. Rev. D **102**, 014039 (2020), arXiv:2004.01595 [hep-ph].
- [60] A. Kock and I. Zahed, Phys. Rev. D **104**, 116028 (2021), arXiv:2110.06989 [hep-ph].
- [61] K. Olive, Chinese Physics C **38**, 090001 (2014).
- [62] P. Faccioli and E. V. Shuryak, Phys. Rev. D **64**, 114020 (2001), arXiv:hep-ph/0106019.
- [63] D. Ebert and H. Reinhardt, Nuclear Physics B **271**, 188 (1986).
- [64] C. Schüren, F. Döring, E. Ruiz Arriola, and K. Goeke, Nuclear Physics A **565**, 687 (1993).
- [65] G. S. Bali, V. M. Braun, S. Bürger, M. Göckeler, M. Gruber, F. Hutzler, P. Korcyl, A. Schäfer, A. Sternbeck, and P. Wein (RQCD), JHEP **08**, 065 (2019), [Addendum: JHEP **11**, 037 (2020)], arXiv:1903.08038 [hep-lat].
- [66] C. Shi, C. Chen, L. Chang, C. D. Roberts, S. M. Schmidt, and H.-S. Zong, Phys. Rev. D **92**, 014035 (2015), arXiv:1504.00689 [nucl-th].
- [67] E. M. Aitala *et al.* (E791), Phys. Rev. Lett. **86**, 4768 (2001), arXiv:hep-ex/0010043.
- [68] W. Broniowski, E. R. Arriola, and K. Golec-Biernat, Phys. Rev. D **77**, 034023 (2008).
- [69] P. A. Boyle, D. Brommel, M. A. Donnellan, J. M. Flynn, A. Jüttner, and C. T. Sachrajda (RBC, UKQCD), PoS LATTICE2008, 165 (2008), arXiv:0810.1669 [hep-lat].
- [70] V. M. Braun *et al.*, JHEP **04**, 082 (2017), arXiv:1612.02955 [hep-lat].
- [71] N. G. Stefanis and A. V. Pimikov, Nucl. Phys. A **945**, 248 (2016), arXiv:1506.01302 [hep-ph].
- [72] R. S. Plant and M. C. Birse, Nucl. Phys. A **628**, 607 (1998), arXiv:hep-ph/9705372.
- [73] R. D. Bowler and M. C. Birse, Nucl. Phys. A **582**, 655 (1995), arXiv:hep-ph/9407336.
- [74] P. Ball and V. M. Braun, Phys. Rev. D **54**, 2182 (1996), arXiv:hep-ph/9602323.
- [75] Q. Chang, X.-N. Li, X.-Q. Li, and F. Su, Chin. Phys. C **42**, 073102 (2018), arXiv:1805.00718 [hep-ph].
- [76] O. Cata and V. Mateu, Phys. Rev. D **77**, 116009 (2008), arXiv:0801.4374 [hep-ph].
- [77] M. Tanabashi *et al.* (Particle Data Group), Phys. Rev. D **98**, 030001 (2018).
- [78] M. E. Carrillo-Serrano, W. Bentz, I. C. Cloët, and A. W. Thomas, Phys. Rev. C **92**, 015212 (2015), arXiv:1504.08119 [nucl-th].
- [79] P. L. Chung, F. Coester, B. D. Keister, and W. N. Polyzou, Phys. Rev. C **37**, 2000 (1988).
- [80] H. B. O'Connell, B. C. Pearce, A. W. Thomas, and A. G. Williams, Prog. Part. Nucl. Phys. **39**, 201 (1997), arXiv:hep-ph/9501251.
- [81] G. M. Huber *et al.* (Jefferson Lab), Phys. Rev. C **78**, 045203 (2008), arXiv:0809.3052 [nucl-ex].
- [82] C. J. Bebek, C. N. Brown, S. D. Holmes, R. V.

- Kline, F. M. Pipkin, S. Raither, L. K. Sisterson, A. Browman, K. M. Hanson, D. Larson, and A. Silverman, *Phys. Rev. D* **17**, 1693 (1978).
- [83] V. A. Nesterenko and A. V. Radyushkin, *Phys. Lett. B* **115**, 410 (1982).
- [84] X. Gao, N. Karthik, S. Mukherjee, P. Petreczky, S. Syritsyn, and Y. Zhao, *Phys. Rev. D* **104**, 114515 (2021), [arXiv:2102.06047 \[hep-lat\]](#).
- [85] L. Chang, I. C. Cloët, C. D. Roberts, S. M. Schmidt, and P. C. Tandy, *Phys. Rev. Lett.* **111**, 141802 (2013), [arXiv:1307.0026 \[nucl-th\]](#).
- [86] C. J. Shultz, J. J. Dudek, and R. G. Edwards, *Phys. Rev. D* **91**, 114501 (2015), [arXiv:1501.07457 \[hep-lat\]](#).
- [87] J. P. B. C. de Melo and T. Frederico, *Phys. Rev. C* **55**, 2043 (1997), [arXiv:nucl-th/9706032](#).
- [88] H.-M. Choi and C.-R. Ji, *Phys. Rev. D* **70**, 053015 (2004), [arXiv:hep-ph/0402114](#).
- [89] H. L. L. Roberts, A. Bashir, L. X. Gutierrez-Guerrero, C. D. Roberts, and D. J. Wilson, *Phys. Rev. C* **83**, 065206 (2011), [arXiv:1102.4376 \[nucl-th\]](#).
- [90] Z.-F. Cui, D. Binosi, C. D. Roberts, and S. M. Schmidt, *Phys. Lett. B* **822**, 136631 (2021), [arXiv:2108.04948 \[hep-ph\]](#).
- [91] M. S. Bhagwat and P. Maris, *Phys. Rev. C* **77**, 025203 (2008), [arXiv:nucl-th/0612069](#).
- [92] A. F. Krutov, R. G. Polezhaev, and V. E. Troitsky, *Phys. Rev. D* **93**, 036007 (2016), [arXiv:1602.00907 \[hep-ph\]](#).
- [93] B. Owen, W. Kamleh, D. Leinweber, B. Menadue, and S. Mahbub, *Phys. Rev. D* **91**, 074503 (2015), [arXiv:1501.02561 \[hep-lat\]](#).
- [94] M. Oertel, M. Buballa, and J. Wambach, *Nucl. Phys. A* **676**, 247 (2000), [arXiv:hep-ph/0001239](#).